

GASOLINE SYSTEMS



Sensitivity Analysis and Offline Parameter Identification for Induction Machines using an Automated Measurement Procedure

Masterthesis
<Milo De Soricellis>, GS/EH-ESS3

18.03.2015

– DIPLOMAND –

Contents

List of Figures	v
List of Tables	ix
1 Introduction	1
2 Brief overview on induction machines modeling	3
2.1 Zero Leakage Inductance Models of Induction Machines	6
2.2 Machine model with leakage inductances	7
2.3 Universal IRTF based model	8
2.4 Universal Field Oriented model	12
2.5 Rotor Flux Oriented Model	14
3 Parameters sensitivity analysis	17
3.1 Stator resistance	17
3.2 Rotor resistance	18
3.3 Main inductance	26
3.4 Stray inductances	29
4 Test Bench measurements definition	31
4.1 DC test	34
4.2 Drag torque test	34
4.3 No load test	36
4.4 Short circuit test	38
4.5 DQ-map test	40
4.6 Rotor resistance detection	46
4.7 nTq-map	48
5 Test Bench automated measurement system	49
5.1 Interface	51
5.2 Real time plotting	53
5.3 Gui development	54
6 Documentation of the results	57

Appendix	93
A Motor plate data	93
Nomenclature	95
Bibliography	99

List of Figures

1.1	Model of electrical drive for vehicle applications.	1
2.1	Typical geometry of an induction machine.[DDPV11]	4
2.2	Simplest model of an induction machine.	6
2.3	Induction machine model with leakage inductances.	7
2.4	Universal <i>IRTF</i> model with scale factor for transformation.	8
2.5	Inductances transformation system.	9
2.6	Vector diagram: at the left before transformation, at the right included the scale factor a	10
2.7	Universal <i>IRTF</i> model without scaling module.	10
2.8	Model with rotor transformed in the stator reference system.	12
2.9	Vector diagram with d-q reference system.	13
2.10	Complete vector model in d-q reference system.	13
2.11	Vectorial representation of the rotor flux oriented model.	14
2.12	d-axis representation of rotor flux model.	15
2.13	q-axis representation of rotor flux model.	15
3.1	Typical cross-section shape of a rotor bar.	18
3.2	Model for the study of a skin effect in a rotor bar.	19
3.3	Distribution of density current inside rotor bar varying the operative conditions.[Kab+97]	22
3.4	Influence of the frequency on the resistance and inductance linked to a rectangular rotor slot.	23
3.5	Trend of the slip frequency on a d-q reference system.	24
3.6	Influence of a wrong rotor resistance on the stator current vector.	25
3.7	Influence of rotor resistance variation on the torque taking into account a 10% of increment in the absolute value.	25
3.8	Magnetic characteristic of the iron.	26
3.9	Influence of the main inductance variation on the torque produced to the shaft; the value has to be incremented of the 10%.	28
3.10	Close rotor slot shape (right) and open rotor slot shape (left).	29
3.11	Influence of the rotor leakage inductance variation on the torque produced to the shaft; the value has to be incremented of the 10%.	30
4.1	Accuracy of measurements linked to the number of measured points.	32
4.2	Scheme of the test bench used for the test.	32

4.3	Measure of stator phase resistance.	34
4.4	Theoretically gear losses calculation estimated in Watt above torque and speed axes.	35
4.5	Universal induction motor model in no load condition.	36
4.6	Universal induction motor model in short circuit condition.	38
4.7	A couple of points in motoring and generating d-q map.	41
4.8	Optimization algorithm for the rotor resistance.	44
4.9	Trend of the voltages response.	47
4.10	Dependency of maximum torque available from voltage.	48
5.1	Automation system development.	50
5.2	A computer network diagram of clients communicating with a server via network.	51
5.3	Server interface receiving measurements by the client.[Bosb]	52
5.4	Real time plotting example.	53
5.5	Gui framework for the automation system.	54
5.6	Abstract of the GUI.	55
5.7	Check set points through the gui.	56
5.8	Interface for analyze the results in the post-processing.	56
6.1	Results of drag torque measurements with the data fitting.	58
6.2	Magnetizing curve from No Load test.	59
6.3	Stator inductance calculated from No Load test.	60
6.4	Stator-rotor stray inductance calculated from Short Circuit test.	61
6.5	Rotor resistance calculated from Short Circuit test.	61
6.6	Stator-rotor stray inductance at 50Hz.	62
6.7	Different views of parameter set in the machine's model.	63
6.8	Main inductance identified from No Load and Short Circuit test.	64
6.9	Example of DQ set points at 3000 rpm generated by the tool.	66
6.10	Measured DQ-map at 3000 rpm after importing and filtering invalid values.	67
6.11	Effect of the non linearity of the inverter on the reference signal.	68
6.12	Main inductance calculated from the DQ-map.	69
6.13	Leakage inductance of rotor calculated from the DQ-map.	69
6.14	Simulated compensation of the inverter voltage drop and time shifting.	70
6.15	Voltage responses to the impulses for the rotor resistance identification.	71
6.16	Zoom for the response with $R_r = 5.6 \text{ m}\Omega$	72
6.17	Zoom for the response with $R_r = 7 \text{ m}\Omega$	72
6.18	Zoom for the response with $R_r = 6.4 \text{ m}\Omega$	72
6.19	Comparison between measured and calculated torque at 500 rpm with $R_r = 6.4 \text{ m}\Omega$	73
6.20	Results of the rotor resistance optimization.	74

6.21 Comparison between skin effect parametrization optimized from measurements (black) and analytical (red).	75
6.22 Main inductance after optimization.	76
6.23 Main inductance merged with the original one.	77
6.24 Behaviour of the gear losses on the two different operation of the motor. . .	77
6.25 Torque error after parameters updating at 500 rpm.	78
6.26 Map of the torque error neglecting the gear losses taking into account the average value between motoring and generating at 500 rpm.	79
6.27 Map of the torque error taking into account the average value between motoring and generating at 3000 rpm.	81
6.28 Torque error at 6000 rpm with mean values.	82
6.29 Torque error at 9000 rpm with mean values.	83
6.30 Torque error at 3000 rpm.	84
6.31 Torque error due to the asymmetrical losses.	85
6.32 Asymmetrical losses in terms of Watt.	86
6.33 Estimation of total iron losses from simulation.	87
6.34 Calculation of pure gear losses.	87
6.35 Mechanical power above the map.	88
6.36 Overall gear efficiency.	88
6.37 Example of a nTq-map generated by the gui.	89
6.38 Efficiency of the overall E-drive at 260V in motor operation.	90
6.39 Comparison between reference torque and the mechanical response of the motor.	90

List of Tables

4.1	Sorting of dq operative points example.	41
6.1	Volt-ampere measurements.	57

1 Introduction

Electrical machines, at this time, are used in several applications, from the industrial sector to private home purposes. In this way much research has been done about motors and their appliance, also because the necessity of the marked increase. We need more complex systems to fulfill the increasing of requirements on the drive's torque and speed accuracy. Regarding this, the work focuses on electrical and hybrid vehicles. Those technologies get more and more attention in the society, hence also in the research; in fact the tendency is to move on electrical transports, reducing the contribution to the atmospheric pollution due to the exhausts emissions. For an electrical motor embedded on a vehicle is even more so important to design an electrical drive which is able to control the torque very accurately, in order to guarantee safety for the driver. Just as an example, a typical electrical drive for vehicle application is shown in *Fig. 1.1*.

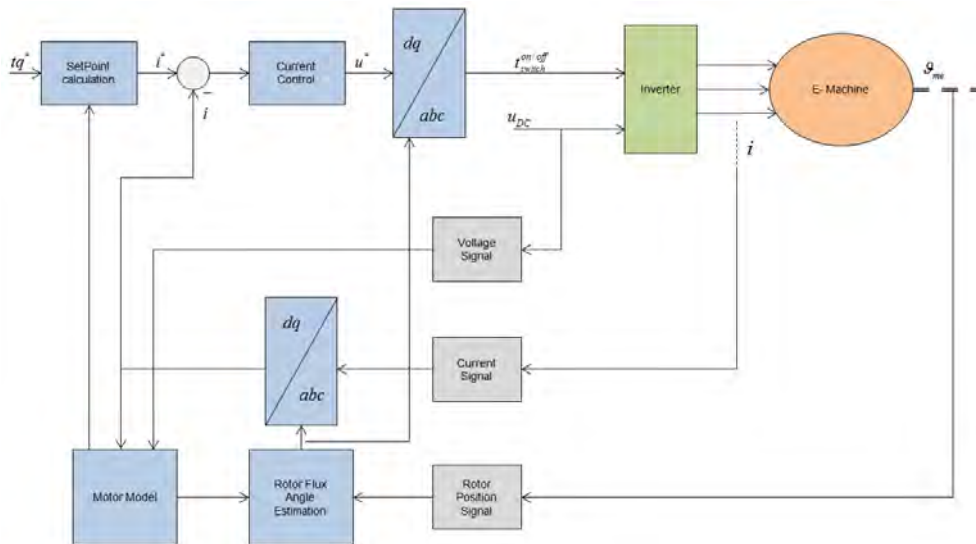


Figure 1.1: Model of electrical drive for vehicle applications.

Basically, a torque is given as input by the driver and the controller, taking into account the feedback signals from the motor, has to be able to elaborate an output, supplied then to the motor, that fits well with the reference given, in order to reach as fast as possible the desired speed.

The latter statement has some critical points inside which are the purpose of this thesis. The achievement of the reference by the motor is strictly linked to the parameters detected

from the software, in fact if there is an error in their estimation, there will be an error also in the output value. This is an important issue about electrical drives and motor control: the parameters detection. At this point it is necessary to distinguish two situations:

- Online detection.
- Offline detection.

Speaking about the first point, the problem is not easy to tackle due to the lack of sensors in the car for economic reasons, instead for the offline detection the situation is different. The offline detection, normally, is necessary when it is wanted to study the electrical characteristics of a prototype and for example, test the electrical drives response. And moreover, is necessary for the thermal and acoustic analysis.

In this thesis, we are going to take into account this kind of detection.

In particular, besides the definition of a standard procedure for machine's analysis and parameter's detection, another important goal is to implement automation, as far as possible, inside the process of measuring. This is another important fact: since the development of the electronics and software engineering is became stronger in these last decades, in the industrial sector is arose the necessity of automation in order to decrease the time of working procedures and increase consequently the volume of working per time unit. In a research division is very important to have this feature, because thanks to it is possible to:

- decrease the necessary time from development to verification of a prototype;
- create general and standard analysis protocols;
- make easy the comprehension and the use of test bench by the side of different kind of users and workers.

Therefore, this thesis will try to take into account these latter considerations in order to develop an efficient and automated system for asynchronous motor measurements. In the second chapter is introduced the modeling system of the induction motor used in all the thesis. In the third chapter the sensitivity of model parameters is discussed in detail. Further, in the fourth chapter, taking into account the non linearity of parameters, will be defined the test to conduce on the Test Bench in order to identify and understand completely the parameters. In the fifth chapter a brief introduction to the idea of automation of the measurement process will be shown and at the end all the results of the test conducted are presented in the last chapter.

2 Brief overview on induction machines modeling

Electrical drives with induction machines remain the dominant market leader in the field of automotive. The combination of a robust low cost squirrel-cage machine, high power density converter, and versatile controller yields a highly adaptable drive for wide ranging rugged industrial applications. We want in this chapter to give some notions about this kind of motor in according with the common literature [DDPV07] and, in particular, we want to show the mathematical link between real machine and the model adopted further in the next chapters. Initially, a brief review of the induction machine with squirrel-cage rotor is given in terms of a cross-sectional view and simplified symbolic and generic models. As a platform for introducing field-oriented models, first models without leakage inductances are derived showing the essence of torque production of the machine. Central to this chapter is the introduction of a universal flux linkage model which allows a three-to-two inductances transformation leading to a simplified IRTF (*Ideal Rotating Transformer*) machine model. This universal model is the stepping stone to the Universal Field-Oriented (UFO) machine model which gives a basic understanding of the transient behavior of induction machines. Furthermore, this model is the basis for the development of field-oriented control [DDPV11]. It is meant that the reader of this paper has already got basis about electrical machines.

Induction Machine with Squirrel-Cage Rotor

Fig. 2.1 shows the cross-section of a induction machine with a so-called squirrel-cage rotor. The squirrel cage consists of a set of conductors (shown in red), which are short-circuited at both ends by a conductive ring. The cage is embedded in the rotor lamination as may be observed from *Fig. 2.1*. A three phase two-layer winding is housed in the stator of a four-pole machine. A rotating field created by the stator winding is penetrating the rotor. If the rotor is rotating asynchronously to the stator field (which means it is rotating at a different speed), alternating currents are induced in the squirrel cage. These currents, together with the stator field, are responsible for the torque production of the machine. This is why asynchronous machines are also known as induction machines. If stator field and rotor were rotating synchronously, no currents would be induced and no torque could be produced. Note, that, regardless of the rotor speed, the rotor field and stator field are still rotating synchronously with a phase shift. The difference between the speed of the rotor and the fields is compensated by the frequency of the rotor currents, the so-called rotor slip frequency. The asynchronous nature of the machine is the reason why for the control of

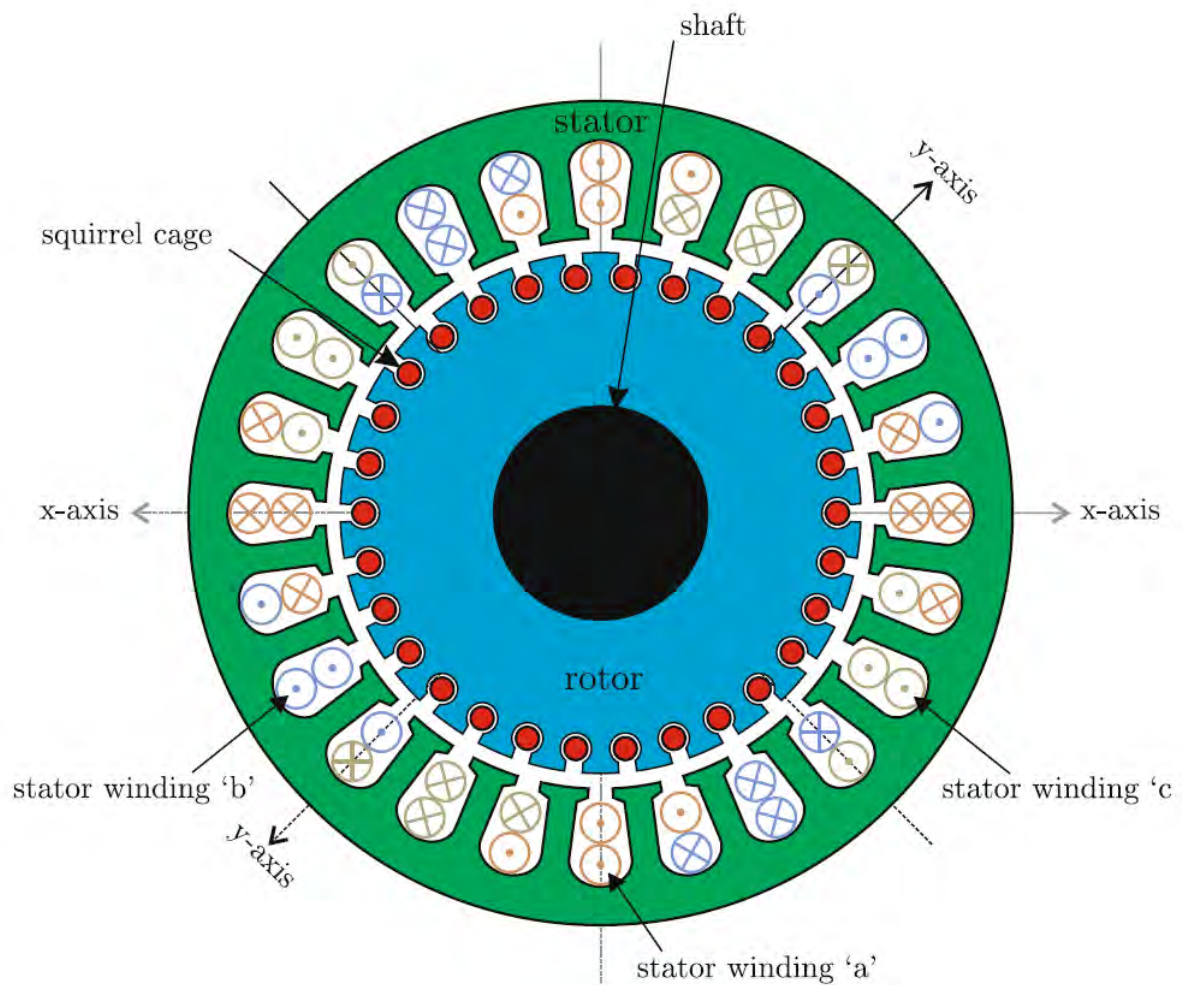


Figure 2.1: Typical geometry of an induction machine.[DDPV11]

induction machines, only the position of stator field and rotor field are required and not the absolute rotor position.

2.1 Zero Leakage Inductance Models of Induction Machines

As first introduction we are going to present the basis and most simple model of asynchronous motor, which does not take into account the leakage induction of the stator and the rotor. In this context is considered an ideal machine with two poles. The model is shown in *Fig. 2.2* and the variables of the circuit are expressed in a general way as vectors in a general reference system. It might be possible to show the completely derivation of this vector model beginning from real machine with three phase circuit on the stator, but this is not the aim of this thesis and for this reason we start directly from the model expressed with space vectors, which represent the real machine taking into account the vector transformation of the parameters.

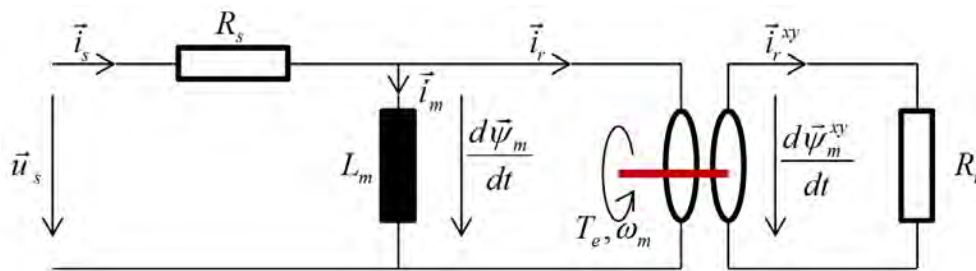


Figure 2.2: Simplest model of an induction machine.

$$\vec{u}_s = R_s \vec{i}_s + \frac{d\vec{\psi}_m}{dt} \quad (2.1)$$

$$\vec{\psi}_m = L_m (\vec{i}_s - \vec{i}_r) \quad (2.2)$$

$$0 = -R_r \vec{i}_r^{xy} + \frac{d\vec{\psi}_m^{xy}}{dt} \quad (2.3)$$

The first two equations are bounded to the point of view of the stator, that is also called “stationary reference”; instead the third equation is referred to the rotor and due to this the current and flux vectors are expressed in a different vector system, since that the rotor turn with a certain speed. Moreover, we can add the general equation for the torque generated by the motor, which is valid in each kind of model.

$$T_e = \vec{\psi}_m \times \vec{i} \quad (2.4)$$

It is possible to understand, therefore, that the torque will be at its maximum value when the vector of main flux and the current are perfectly at 90° degrees.

In this model we have represented the windings resistance of stator (R_s), the resistance of

the rotor bar (R_r) and the main inductance (L_m) which is the responsible of the motor's excitation and to whom we link the magnetization flux at the air gap. This parameters might be enough for describe the power transfer and conversion from electrical to mechanical, but, unfortunately is far from the real behavior of the motor. For example, in *Fig. 2.2* it seems that stator and rotor are completely coupled and all the flux generated in the stator is transferred to the rotor, but, actually this is not possibly because, we should take into account the leakage of the flux, in fact some flux's lines of the flux generated by the stator windings are not coupled with the rotor bars and this phenomenon is very important because influence the behavior and the performance of the machine.

2.2 Machine model with leakage inductances

After the consideration made in the previous section, we are going to introduce in the model two new parameters, which have the intention to consider the leakage flux on the stator and rotor side. Those parameters are respectively $L_{\sigma s}$ and $L_{\sigma r}$. The extended model is shown

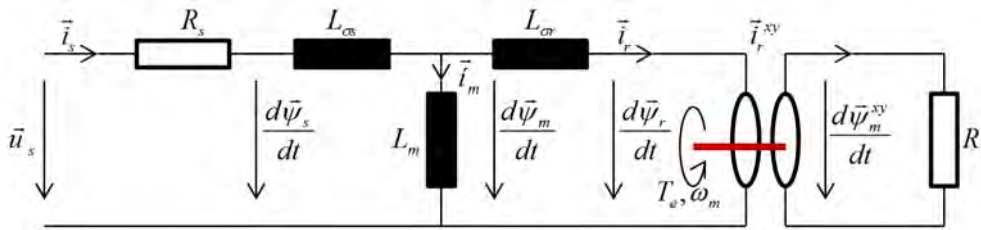


Figure 2.3: Induction machine model with leakage inductances.

in *Fig. 2.3* with both side leakage inductance, and the new equation set is:

$$\vec{u}_s = R_s \vec{i}_s + \frac{d\vec{\psi}_m}{dt} \tag{2.5}$$

$$\vec{\psi}_s = \vec{\psi}_m + L_{\sigma s} \vec{i}_s \tag{2.6}$$

$$\vec{\psi}_r = \vec{\psi}_m - L_{\sigma r} \vec{i}_r \tag{2.7}$$

$$\vec{\psi}_m = L_m (\vec{i}_s - \vec{i}_r) \tag{2.8}$$

$$0 = -R_r \vec{i}_r^{xy} + \frac{d\vec{\psi}_r^{xy}}{dt} \tag{2.9}$$

As we will see further in the next chapters the introduction of these two parameters create not few problems, mainly because it is very difficult to estimate their value; moreover for the squirrel cage induction motors, where the rotor parameters are not accessible.

2.3 Universal IRTF based model

This section is the heart of this chapter, because we are going to show the mathematical transformation which allowed us to derive the *Universal Field Oriented* model; the model that is currently used for the control techniques. The universal IRTF based model take into account the previous model with leakage inductance, but add also a parameter a , which assign a determinate value is able to simplify the model from, for example, three inductance to two. We start from the *Fig. 2.3* and add a new section which take into account the transformation factor, as seen in *Fig. 2.4*.

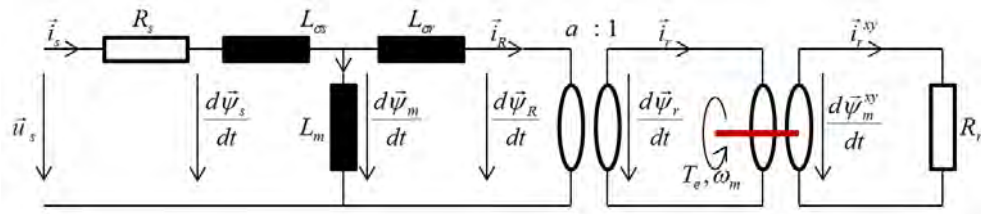


Figure 2.4: Universal *IRTF* model with scale factor for transformation.

The transformation process is initiated considering the previous equation set and rearranging the stator and rotor flux equations in this manner:

$$\vec{\psi}_s = L_s \vec{i}_s - L_m \vec{i}_r - a L_m \vec{i}_s + a L_m \vec{i}_s \quad (2.10)$$

with $L_s = L_m + L_{\sigma s}$.

This expression may be written as

$$\vec{\psi}_s = \underbrace{(L_s - a L_m)}_{L_{\sigma s}} \vec{i}_s + \underbrace{a L_m}_{L_M} (\vec{i}_s - \vec{i}_r) \quad (2.11)$$

where the parameters $L_{\sigma s}$ and L_M are introduced, representing a generalized leakage inductance and magnetizing inductance. Furthermore, a scaled rotor current vector i_R is introduced, which along with the scaled rotor flux linkage vector ψ_R is defined as

$$\vec{i}_R = \frac{\vec{i}_r}{a} \quad (2.12)$$

$$\vec{\psi}_R = a \vec{\psi}_r \quad (2.13)$$

The introduction of this parameter transformation with scaling factor a is necessary, in order that the product of the current and flux linkage vectors remains unaffected by the scaling. Now considering the elaboration done on the stator equation, by *Fig. 2.3*, the

transformation is also transferred to the rotor, as follow

$$\vec{\psi}_R = aL_m\vec{i}_s - a^2L_r\vec{i}_R - aL_m\vec{i}_R + aL_m\vec{i}_R \quad (2.14)$$

with $L_r = L_m + L_{\sigma r}$.

This expression may also be rewritten as

$$\vec{\psi}_R = aL_m(\vec{i}_s - \vec{i}_R) - \underbrace{(a^2L_r - aL_m)}_{L_{\sigma R}}\vec{i}_R \quad (2.15)$$

where a second leakage parameter $L_{\sigma R}$ is introduced. Finally, grouping the equations, we obtain

$$\vec{\psi}_s = L_{\sigma S}\vec{i}_s + L_M\vec{i}_M \quad (2.16)$$

$$\vec{\psi}_R = L_M\vec{i}_M - L_{\sigma R}\vec{i}_R \quad (2.17)$$

where $\vec{i}_M = \vec{i}_s - \vec{i}_R$ represents the scaled magnetizing current vector. The universal model is created and paying attention to the equation just written, is possible to deduce the transformation system of the motor's parameters, which underline the linkage between the real and the scaled parameters:

$$L_{\sigma S} = L_m\left(\frac{L_s}{L_m} - a\right) \quad (2.18)$$

$$L_{\sigma R} = aL_m\left(a - \frac{L_m}{L_r}\right) \quad (2.19)$$

$$L_M = aL_m \quad (2.20)$$

Figure 2.5: Inductances transformation system.

From the transformation system equation observation, the domain of a is clear:

$$\frac{L_m}{L_r} < a < \frac{L_s}{L_m} \quad (2.21)$$

Just for clarify the ideas of the transformation, before go further and show the advantages of this mathematical work, in *Fig. 2.6* is showed the step from the original model to the universal one, by vector diagram for an arbitrarily chosen set of currents \vec{i}_s and \vec{i}_r and a set of inductances L_m , $L_{\sigma s}$, and $L_{\sigma r}$. It shows an a -axis which is a line defined by the endpoints of the vectors $\vec{\psi}_s$ and $\vec{\psi}_m$ respectively. This line is significant because it represents the locus of the vector $\vec{\psi}_M$ endpoint as function of the transformation variable a .

The next step is to delete the transformation module present in *Fig. 2.4*, in order to re-assembly the model and can write the equation set. Avoid the module keeping the

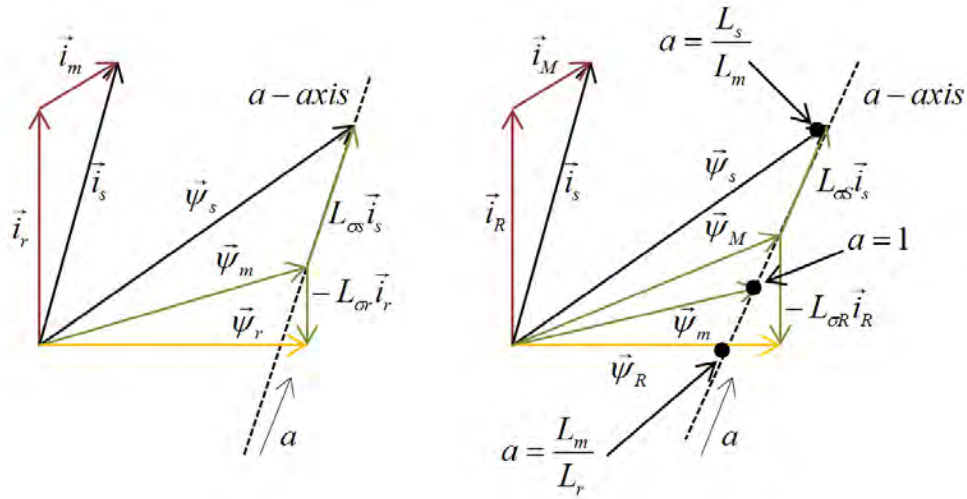


Figure 2.6: Vector diagram: at the left before transformation, at the right included the scale factor a .

transformation factor valid with the introduction of the scaled parameters is possible, and this will not affect the torque, but the rotor resistance has to be calculated as follow

$$R_R = a^2 R_r \tag{2.22}$$

The resultant universal IRTF based symbolic machine model is shown in Fig. 2.7

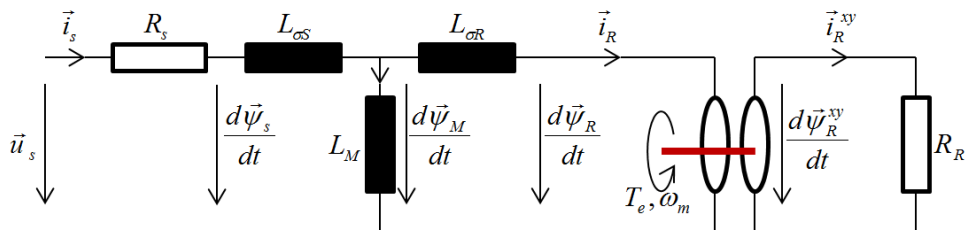


Figure 2.7: Universal IRTF model without scaling module.

and the corresponding equation set is

$$\vec{u}^s = R_s \vec{i}_s + \frac{d\vec{\psi}_m}{dt} \quad (2.23)$$

$$\vec{\psi}_s = \vec{\psi}_M + L_{\sigma s} \vec{i}_s \quad (2.24)$$

$$\vec{\psi}_R = \vec{\psi}_M - L_{\sigma r} \vec{i}_R \quad (2.25)$$

$$\frac{\vec{\psi}_m}{L_M} = \vec{i}_s - \vec{i}_R \quad (2.26)$$

$$0 = -R_R \vec{i}_R + \frac{d\vec{\psi}_R^{xy}}{dt} \quad (2.27)$$

Now is possible to show the real importance of this universal model and this is done starting considering those three cases:

- $a = \frac{L_m}{L_r}$: with this condition, the model showed in *Fig. 2.4* is reduced to only two inductance, $L_{\sigma s}$ and L_m , because, applying the transformation seen in *Fig. 2.5*, the $L_{\sigma r} = 0$. This model will be called to the *rotor flux based IRTF*;
- $a = 1$: The universal model is reduced to the original five parameter model as given in *Fig. 2.3*;
- $a = \frac{L_s}{L_m}$: with this third condition, the universal model is reduced to another alternative two inductances, since that applying the transformation seen in *Fig. 2.5*, the $L_{\sigma s} = 0$. This model will be called to the *stator flux based IRTF*;

Therefore, is comprehensible, as the model can be simplified and exploited then to be implemented in the software of the electrical drives for the machine's control.

2.4 Universal Field Oriented model

As last improvement of the model, we want to reach the most important and useful model in the electrical drives field. For obtain this there are two intermediate steps, which are very important:

- Since that the equation which govern the rotor behavior is fixed to its speed, we need to transform that in the *stationary reference system*, which rotate at the stator angular frequency ω_s , in order to make homogeneous the stator and rotor vectors. The general space vector conversion required for this task is of the form $A^{xy} = A^{stat}e^{j\theta}$. The revised rotor based equation in stationary coordinates is of the form

$$0 = -R_R \vec{i}_R + \frac{d\vec{\psi}_R}{dt} - j\omega_m \vec{\psi}_R \quad (2.28)$$

in *Fig. 2.8* is shown the model with the rotor on the side of the stator as was the intention of the transformation;

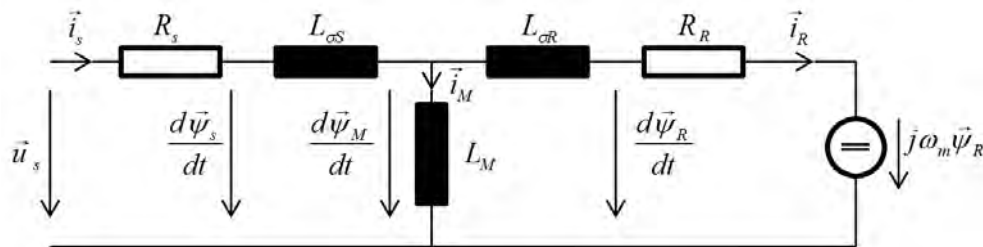


Figure 2.8: Model with rotor transformed in the stator reference system.

- Second step consists of another transformation in a more convenient reference system, which is the *synchronous reference system*. This is very useful in order to tie strictly the stator and rotor based space equations to the flux linkage vector $\vec{\psi}_M$ and get the so-called field oriented transformation.

With the latter step we are able to generate the *Universal Field-Oriented model*, considering the reference frame called *direct* and *quadrature*, i.e. $\vec{x}^{dq} = x_d + jx_q$. Since that the direct axis is aligned for definition with the flux linkage vector $\vec{\psi}_M$, that vector will have only the d-component ($\vec{\psi}_M = \psi_{Md}$ and $\psi_{Mq} = 0$). The situation can be observed in *Fig. 2.9*. The

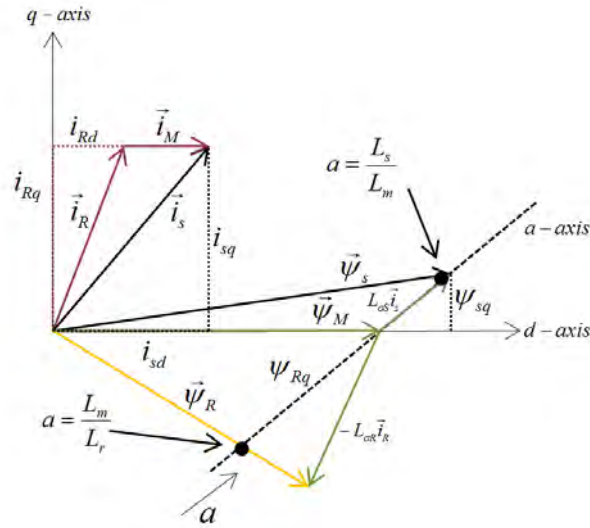


Figure 2.9: Vector diagram with d-q reference system.

final equation set is

$$\vec{u}_s^{dq} = R_s \vec{i}_s + \frac{d\vec{\psi}_s^{dq}}{dt} + j\omega_s \vec{\psi}_s^{dq} \tag{2.29}$$

$$\vec{\psi}_s^{dq} = \vec{\psi}_M + L_{\sigma S} \vec{i}_s^{dq} \tag{2.30}$$

$$\vec{\psi}_R^{dq} = \vec{\psi}_M - L_{\sigma R} \vec{i}_R^{dq} \tag{2.31}$$

$$\frac{\vec{\psi}_M^{dq}}{L_M} = \vec{i}_s^{dq} - \vec{i}_R^{dq} \tag{2.32}$$

$$\frac{d\vec{\psi}_R^{dq}}{dt} = R_R \vec{i}_R^{dq} - j(\omega_s - \omega_m) \vec{\psi}_R^{dq} \tag{2.33}$$

Those are the vector equation which govern the so-called *UFO* model, shown in his complex form in *Fig. 2.10*.

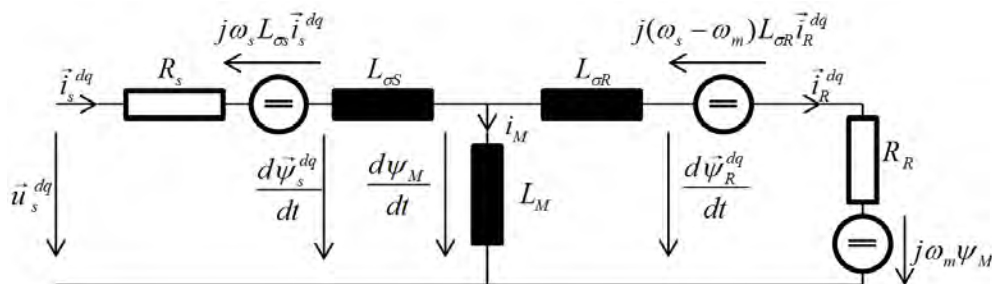


Figure 2.10: Complete vector model in d-q reference system.

2.5 Rotor Flux Oriented Model

In this last section, we are going to take into account a modified model, by scaling factor, which is one of the most exploited model in the controlling techniques and in fact is the reference model of the induction motor for all the next chapters. For the generation of this model, is necessary to put $a = \frac{L_m}{L_r}$ considering the domain of the scaling factor in equation (2.21). In this case the rotor flux $\vec{\psi}_R$ is aligned with d -axis and since that $L_{\sigma R} = 0$, the rotor flux is coincident with the magnetization flux $\vec{\psi}_M$. The situation is represented in *Fig. 2.11*. An important benefit of a rotor-oriented flux model is that there is a complete

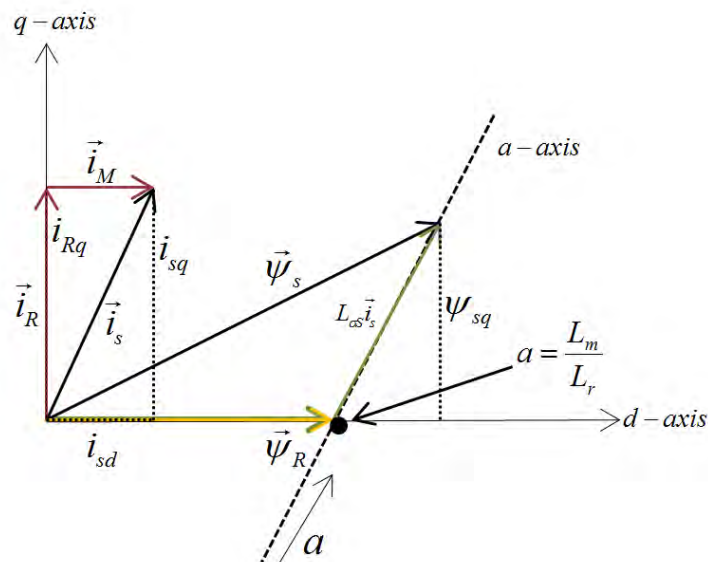


Figure 2.11: Vectorial representation of the rotor flux oriented model.

decoupling between the direct and quadrature currents. It means that we are able to control the torque only varying the q-current and the main flux only varying the d-current. This is very important and makes the control system simple and robust. As a final note, below is shown the complete dynamical model divided in the d and q components and related equations; this is obtained taking the set equation referred to *Fig. 2.10*, separating d-q terms and neglecting the rotor leak inductance.

$$u_{sd} = R_s i_{sd} - \omega_s L_{\sigma S} i_{sq} + L_{\sigma S} \frac{di_{sd}}{dt} + \frac{d\psi_M}{dt} \quad (2.34)$$

$$\psi_M = L_M (i_{sd} - i_{Rd}) \quad (2.35)$$

$$\frac{d\psi_M}{dt} = R_R i_{sd} \quad (2.36)$$

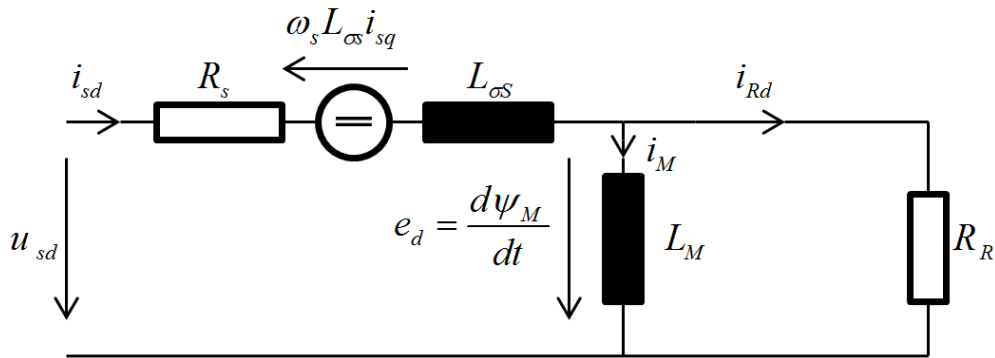


Figure 2.12: d-axis representation of rotor flux model.

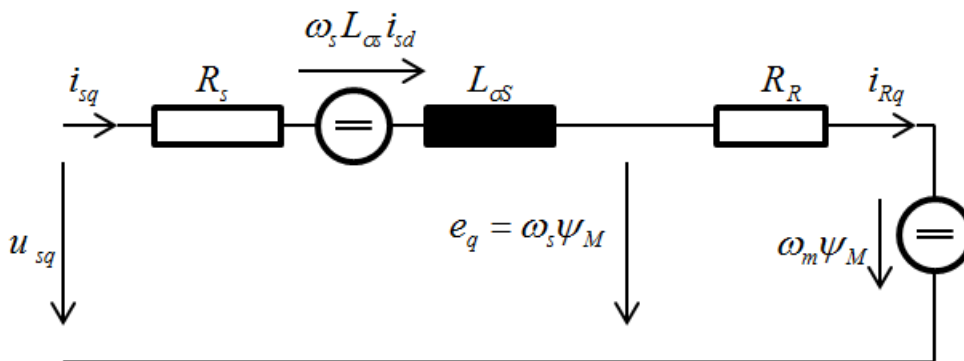


Figure 2.13: q-axis representation of rotor flux model.

$$u_{sq} = R_s i_{sq} - \omega_s L_{\sigma S} i_{sd} + L_{\sigma S} \frac{di_{sq}}{dt} + \omega_s \psi_M \quad (2.37)$$

$$\omega_s \psi_M = R_R i_{sq} + \omega_m \psi_M \quad (2.38)$$

$$\omega_{slip} = \frac{R_R i_{sq}}{\psi_M} \quad (2.39)$$

$$(2.40)$$

The torque expression can be shown through a power balance on (2.34) and (2.37):

$$\begin{aligned} u_{sd} \cdot i_{sd} &= R_s i_{sd} \cdot i_{sd} - \omega_s L_{\sigma S} i_{sq} \cdot i_{sd} + L_{\sigma S} \frac{di_{sd}}{dt} \cdot i_{sd} + R_R \cdot i_{sd} \cdot i_{sd} \\ u_{sq} \cdot i_{sq} &= R_s i_{sq} \cdot i_{sq} + \omega_s L_{\sigma S} i_{sd} \cdot i_{sq} + L_{\sigma S} \frac{di_{sq}}{dt} \cdot i_{sq} + (R_R \cdot i_{sq} + \omega_m \psi_M) \cdot i_{sq} \\ u_{sd} i_{sd} + u_{sq} i_{sq} &= \underbrace{(R_s + R_R)(i_{sd}^2 + i_{sq}^2)}_{P_j} + \underbrace{\left(\frac{d\psi_{sd}}{dt}\right) i_{sd} + \left(\frac{d\psi_{sq}}{dt}\right) i_{sq}}_{P_m} + \underbrace{\omega_m \psi_M i_{sq}}_{P_{me}} \end{aligned}$$

The only one term linked to the transfer from electrical power to mechanical is the last one and taking into account the d-q transformation (which it has been done counting the power conservation), $P_{me} = tq\Omega_m$, we obtain:

$$tq = 3\left(\frac{\omega_m}{\Omega_m}\right)\psi_M i_{sq} = 3p\psi_M i_{sq} \quad (2.41)$$

with $\Omega_m = \frac{\omega_m}{p}$, where p are the pole pair of the motor.

3 Parameters sensitivity analysis

In this chapter, considering the motor's model presented previously we are going to investigate the dependence of the parameters from physical variables as temperature, saturation and speed. The induction machine model seen in *Sec. 2.4* and *Sec. 2.5*, naturally includes only constant parameters. Such a model is sufficient to describe the fundamental-wave characteristics of the induction machine model in a certain operating point. In fact the main point when a motor has to be controlled is that the parameters of the motor which describe its performance, changes and has to be known completely above all the operative range, because they are not linear and constant. Declaring and investigating this no-linearity, further we will be able to define the test has to be done to the machine in order to estimate completely the parameters. Considering the general model presented in *Sec. 2.2* with real and not scaled parameters, for the definition of the machine we have:

- Stator resistance (R_s);
- Stray stator inductance ($L_{\sigma s}$);
- Magnetization inductance (L_m);
- Stray rotor inductance ($L_{\sigma r}$);
- Rotor resistance (R_r).

For a more accurate description of the physical machine we should also include the iron losses, represented by a resistance (R_{fe}) in the model, but for matter of time regards experimentation on the test bench, we are not going to consider that parameter for the moment.

3.1 Stator resistance

This resistance consists of all the stator copper coils and for its nature it does not suffer much as the rotor bar, of the skin effect and we can neglect this phenomenon, but, clearly, the temperature afflicts its value. The most part of metals, in fact are inclined to increase their resistance with the temperature. This is due to the enhancement of the entropy inside the atomic structure of the material to which we associate a major probability of collision between electrons and since that they are the charge carrier, they have more difficulties to transfer the energy inside the conductor and this is seen as an increasing of resistance. Said

that, the general equation for the non linear behavior of resistance towards temperature is:

$$R_{T_x} = R_{T_0} \cdot (1 + \alpha_0(T_x - T_0)) \quad (3.1)$$

with:

T_0 = reference temperature that normally is 20°;

T_x = over temperature expressed in Celsius degrees;

α_0 = temperature coefficient specific for the material, for example $\alpha_0^{copper} = 0.0043 \frac{1}{C}$.

Then, know the resistance at the standard temperature is possible to estimate its value for different values of temperature. In this way, we understand that is important to take into account this dependence, because in normal operative condition of an asynchronous motor, temperatures can reach also 100°, that means for copper, an increasing in the value, about 35%.

3.2 Rotor resistance

This parameter is associated to the rotor bars. Conventionally, in electrical vehicles application the rotor is configured as seen in the introduction of chapter 2, that means in a squirrel cage with single bars. In *Fig. 2.1* there is a representation, but in the reality the cross section of a rotor bar is much different from circular conductor and is more like the shape showed in *Fig. 3.1*. The bars has the same dependence from temperature of the

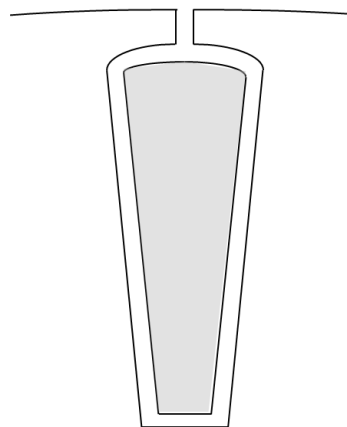


Figure 3.1: Typical cross-section shape of a rotor bar.

stator windings, therefore the equation (3.1) is still valid, but considering the real shape of the rotor conductors, is possible to understand how the skin effect can play an important role in this case. When the asynchronous machine is working in steady-state at a certain

speed that we call n , in the rotor bar the current induced beats at the slip frequency and this frequency variate in the operative field of the motor. Normally, the slip frequency is low till the motor reaches the base speed, but after that, at high speed the motor is controlled in flux weakening and the slip frequency increase again in order to keep constant the power. Therefore, the rotor resistance is strictly linked to this frequency, because the distribution of the current into the bar section change and changing the equivalent useful section, the value of the resistance is modified.

Detailed analysis of the not uniform current distribution in the rotor's bars

For studying and understand the phenomenon, clearly, we need to take a simple model which represents the rotor bar and for this reason we base the analysis on the model showed in *Fig. 3.2*. All the variables are extended in the 3-dimensions and for starting the consideration

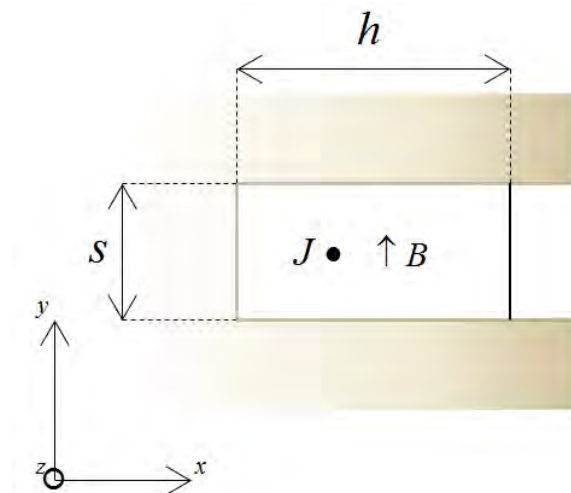


Figure 3.2: Model for the study of a skin effect in a rotor bar.

are exploited two Maxwell equations: the one referred to the Faraday's law and the other referred to the Ampere's law:

$$\begin{aligned}
 \nabla \times \vec{H} &= \vec{J} \\
 \nabla \times \vec{E} &= -\frac{\partial \vec{B}}{\partial t} \\
 \vec{B} &= \mu \vec{H} \\
 \vec{J} &= \sigma \vec{E}
 \end{aligned}$$

Before to go further is necessary to state some simplifying hypothesis:

1. \vec{J} is supposed to be distributed only along the z-axis; that means:

$$J_x = 0, J_y = 0 \implies H_z = 0$$

2. The field \vec{B} has only a component along y-axis, that means:

$$B_x = 0, B_z = 0 \implies H_x = 0$$

3. The variables have a sinusoidal behavior, which imply:

$$\frac{df(t)}{dt} = j\omega f_t$$

Taking into account those latter considerations we can review the Maxwell's equations as follow:

$$\frac{\partial H_y}{\partial x} = J_x \quad (3.2)$$

$$\frac{\partial J_z}{\partial x} = j\omega\sigma\mu H_y \quad (3.3)$$

$$\frac{\partial J_z}{\partial y} = j\omega\sigma\mu H_x \quad (3.4)$$

We define also $a = \sqrt{j\omega\varepsilon\mu} = (1 + j)\sqrt{\frac{\omega\varepsilon\mu}{2}}$ and rearranging the Eq. 3.2-3.3, is possible to write:

$$\frac{\partial^2 J_z}{\partial x^2} - a^2 J_z = 0 \quad (3.5)$$

We have found out a differential equation of second order which define the electromagnetic behavior of the current inside the rotor bar. A general solution of this equation is:

$$J_{z(x)} = c_1 e^{ax} + c_2 e^{-ax}$$

Therefore, in order to find a solution, is necessary to put boundary's conditions:

1. The first consists in to put the y-component of magnetic field to zero for $x = 0$, that is:

$$H_y |_{x=0} = 0 \implies \frac{\partial J_z}{\partial x} |_{x=0} = 0 \implies c_1 a - c_2 a = 0 \implies c_1 = c_2$$

2. The second is to consider the total current which flow in the section of the bar

$$I = s \int_0^h J_{z(x)} dx :$$

$$\begin{aligned} \frac{I}{s} &= c_1 \int_0^h (e^{ax} + e^{-ax}) dx \\ &= \frac{c_1}{a} [(e^{ah} - 1) - (e^{-ah} - 1)] \\ &= \frac{c_1}{a} (e^{ah} - e^{-ah}) \\ &= \frac{c_1}{a} \sinh(ah) \cdot 2 \end{aligned}$$

Finally we obtain:

$$c_1 = \frac{a I}{2 s \sinh(ah)}$$

Applying the two boundary's conditions we have found the values of two constant terms and we can finally write the expression for the \vec{J}_z :

$$J_{z(x)} = a \frac{I}{s} \left(\frac{e^{ax} + e^{-ax}}{2} \right) \frac{1}{\sinh(ah)} \quad (3.6)$$

$$= a \frac{I \cosh(ax)}{s \sinh(ah)} \quad (3.7)$$

At this point we need to introduce the main parameter which describe the skin effect, that is the *penetration depth*:

$$\delta = \sqrt{\frac{2}{\omega \mu \sigma}} \quad (3.8)$$

Considering, therefore, the factor a and the variable δ , is possible to write

$$a = (1 + j) \sqrt{\frac{\omega \varepsilon \mu}{2}} = (1 + j) \frac{1}{\delta}$$

Looking to the hyperbolic terms in the $J_{z(x)}$ expression (3.7), we can substitute the argument as follow

$$\cosh(ax) = \cosh\left(\frac{x}{\delta} + j \frac{x}{\delta}\right) = \cos\left(\frac{x}{\delta}\right) \cosh\left(\frac{x}{\delta}\right) + j \sin\left(\frac{x}{\delta}\right) \sinh\left(\frac{x}{\delta}\right)$$

$$\sinh(ax) = \sinh\left(\frac{h}{\delta} + j \frac{h}{\delta}\right) = \cos\left(\frac{h}{\delta}\right) \cosh\left(\frac{h}{\delta}\right) - j \sin\left(\frac{h}{\delta}\right) \sinh\left(\frac{h}{\delta}\right)$$

Knowing that $\cosh(jz) = \cos(z)$ and $\sinh(jz) = j \sin(z)$.

With this last substitution we are able to obtain the final form of the *Eq.3.7*:

$$J_z(x) = J_{0z} \frac{\cos(\frac{x}{\delta}) \cosh(\frac{x}{\delta}) + j \sin(\frac{x}{\delta}) \sinh(\frac{x}{\delta})}{\cos(\frac{h}{\delta}) \cosh(\frac{h}{\delta}) - j \sin(\frac{h}{\delta}) \sinh(\frac{h}{\delta})} \quad (3.9)$$

with $J_{0z} = a \frac{I}{s}$.

If now we display graphically the *Eq. 3.9* varying the factor δ which depend directly from the frequency, we obtain a trend equal to one shown in *Fig. 3.3*. Is been introduced the

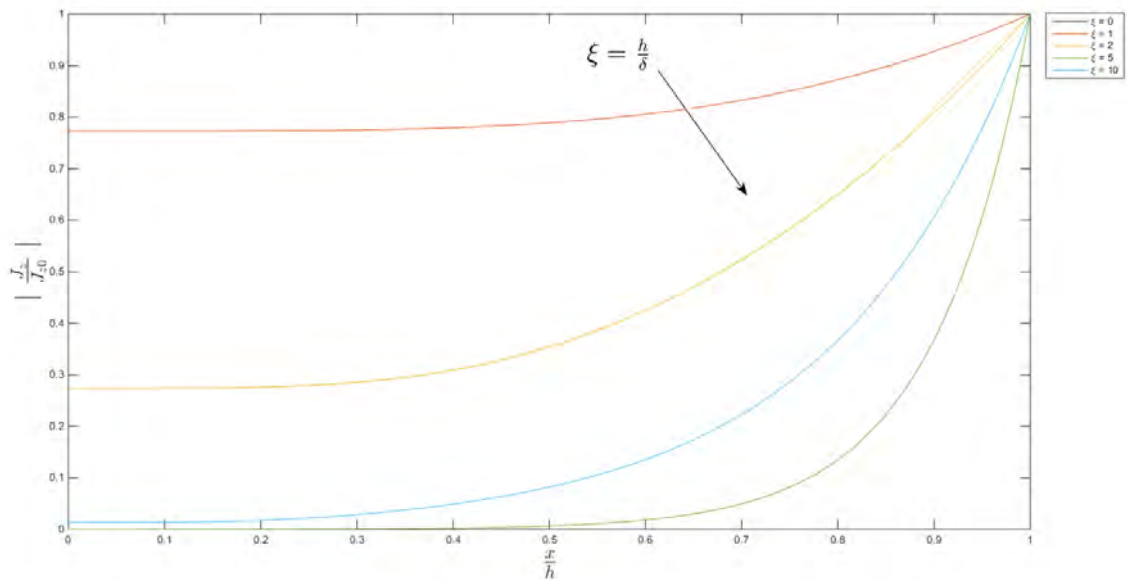


Figure 3.3: Distribution of density current inside rotor bar varying the operative conditions.[Kab+97]

parameter $\xi = \frac{h}{\delta}$ and it has been substituted opportunely in the *Eq. 3.9*; moreover the graph is been normalized to the stationary amplitude J_{0z} on y-axis and to the depth of the cave on x-axis. By the graph and the skin effect analysis we can understand how change the current distribution inside the rotor bars during the dynamical work of the motor; in fact, as the extreme cases we have that when the slip and the rotor frequency are maximum, the current is all concentrated in the upper part of the bar, near the air gap, instead when the motor is at nominal condition the distribution can be considered uniform. In this range of work, the rotor resistance variate much and we need to understand this variations in order to adjust the value in each operative condition and control correctly the motor. Clearly this current density no-linearity if on one side modify the resistance, on the other side acts also on the inductance linked to the slot, since that both the phenomenon arise with a current flowing in the slot. Having said that, from the equation 3.9 is possible to show respectively

the dependence of the resistance and of the inductance from the frequency:

$$R_\xi = R_0 \xi \frac{\sinh(2\xi) + \sin(2\xi)}{\cosh(2\xi) - \cos(2\xi)} \tag{3.10}$$

$$L_\xi = L_0 \frac{3 \sinh(2\xi) - \sin(2\xi)}{2\xi \cosh(2\xi) - \cos(2\xi)} \tag{3.11}$$

with:

$$R_0 = \frac{\rho l}{sh};$$

$$L_0 = \frac{2}{3} \mu_0 \frac{hl}{s}$$

An interesting thinking can be done taking into account the motor with the power elec-

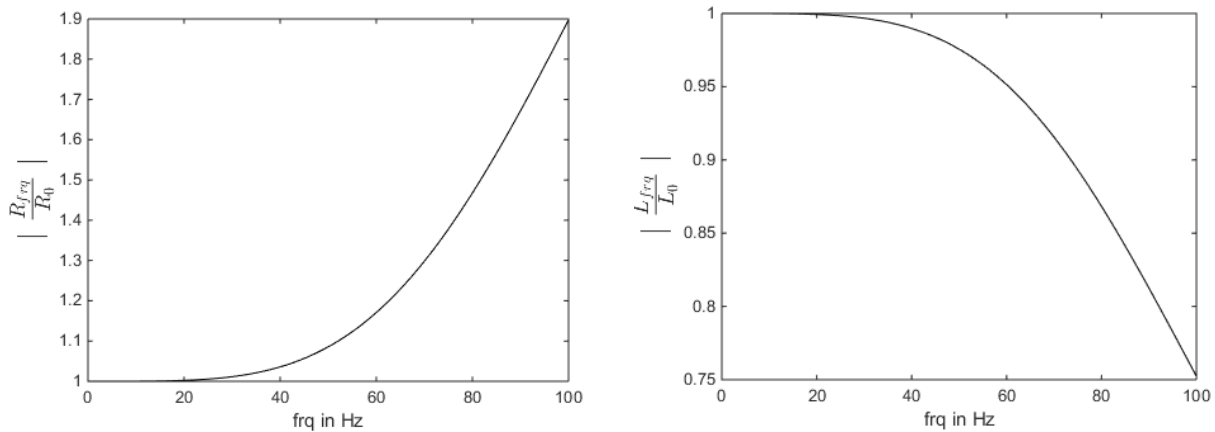


Figure 3.4: Influence of the frequency on the resistance and inductance linked to a rectangular rotor slot.

tronics inside a power train system; in fact having an inverter which control the motor, the operative conditions are imposed by the requirements of the vehicle. In this case the high slip frequency appears heavily during the flux weakening has it was explained at the beginning of the chapter and an idea of what it means in terms of d-q reference system is showed in *Fig. 3.5* The rotor resistance of induction machines plays an important role for the accuracy of the torque. If the software rotor resistance deviates from the real machine resistance (e.g. due to temperature, skin effect,...) the software estimated torque is different compared to the real machine torque. The torque error is mainly caused by an error in the set slip frequency, which is a calculated using the software rotor resistance as follow

$$\omega_{sl} = \frac{R_r}{L_M} \frac{i_q}{i_d} \tag{3.12}$$

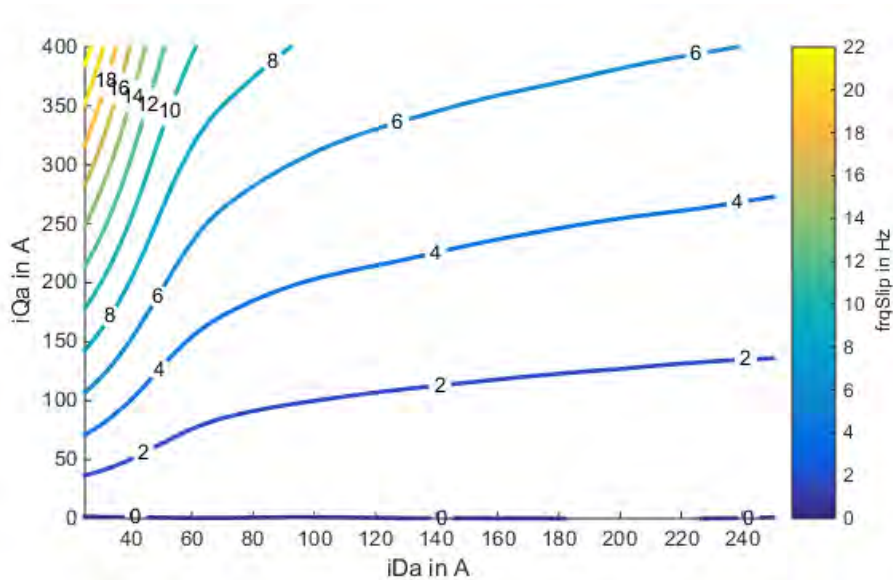


Figure 3.5: Trend of the slip frequency on a d-q reference system.

The equation is obtained from Eq. 2.39 in steady-state conditions. From this equation is comprehensible that a wrong rotor resistance generate a wrong imposition of operative condition, since that the slip frequency is fixed by the inverter; in detail we can write

$$\tan \theta = \frac{i_q}{i_d}$$

$$\theta = \arctan \frac{\omega_{sl} R_r}{L_M}$$

In Fig. 3.6 the phenomenon is showed and is possible to understand which the not correct identification of the rotor resistance creates a shifting of the stator current vector and consequently the generation of an error in the torque. This shifting of the angle cause clearly the error in the torque delivered on the shaft and for understand which is the influence of a not correct identification of the rotor resistance on the motor's operative area in the synchronous reference we have tried to compare the calculated torque from the software considering a 10% increase of the resistance. In according to the Fig. 3.7 the working area with high q-current and low d-current seems to be more sensible to the rotor resistance and this leads to think that an accurate parametrization of the skin effect is very important for the motor control.

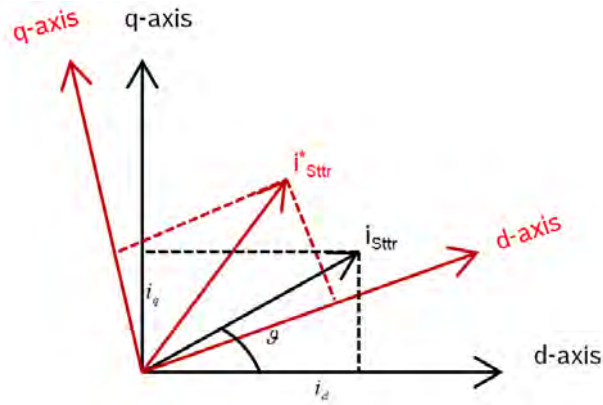


Figure 3.6: Influence of a wrong rotor resistance on the stator current vector.

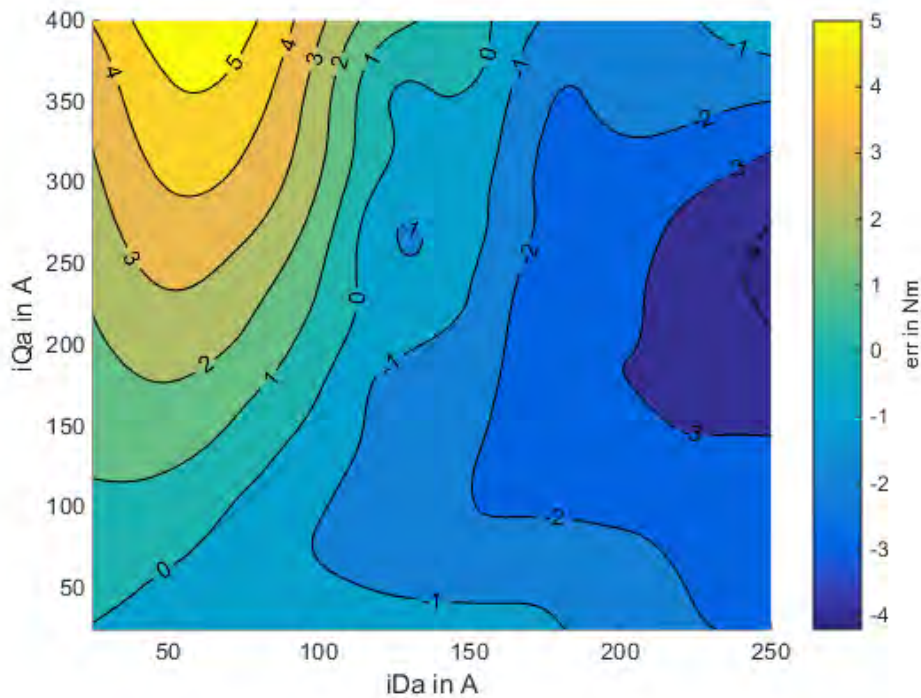


Figure 3.7: Influence of rotor resistance variation on the torque taking into account a 10% of increment in the absolute value.

3.3 Main inductance

This parameter is created in order to give reason to the magnetic flux that pass through the iron and allowed the excitation of the motor, in fact:

$$\psi_M = L_M(i_{sd} - i_{Rd}) = L_M i_M$$

But, as we well know, the inductance is strictly influenced by the saturation of the iron and since the magnetization characteristic of the iron is not linear, the behavior of the main inductance above the operative range of the motor is not linear. Looking *Fig. 3.8*, which represent a typical magnetic characteristic of iron, is easy to understand that increasing the current, the flux in the iron grows and when it overcomes a certain threshold, typical of the material considered, the iron loses its magnetic properties and the characteristic becomes rather flat. In those condition the magnetic behavior of the iron becomes similar to the magnetic behavior of the air and the phenomena observed is a sort of expulsion of flux lines from the iron. Since that the inductance trend is linked to the slope of the function in the figure, its value drops down strongly. When the iron is saturated the inductance associated becomes very small and the flux decrease suddenly. Normally, the stator and rotor teeth have the highest flux density and are the parts where saturation mainly occurs; instead, the flux density in the yoke is lower, but saturation might occur also in this part. Now we

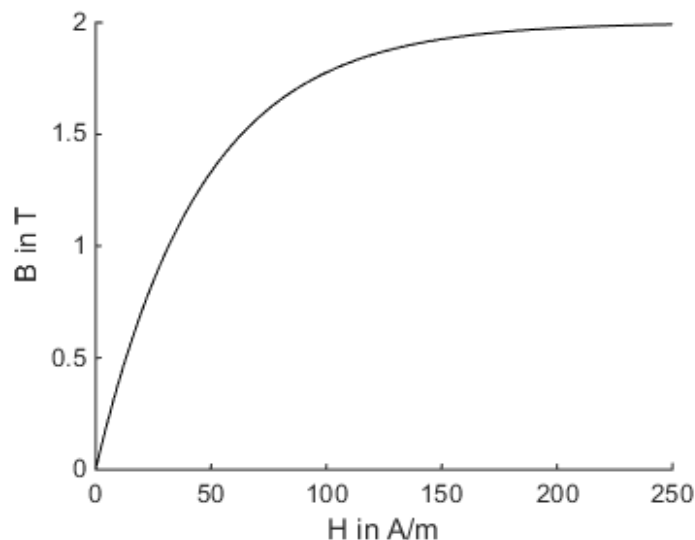


Figure 3.8: Magnetic characteristic of the iron.

want to understand the dependence of this parameter from the currents in the d-q system;

therefore considering the *rotor flux oriented model* seen in 2.5, we can write:

$$\begin{aligned}\vec{i}_s &= \vec{i}_\mu + \vec{i}_r = \vec{i}_M + \vec{i}_R \\ \vec{i}_\mu &= \vec{i}_M + \vec{i}_R - \vec{i}_r\end{aligned}$$

and considering the equation 2.12, results:

$$\vec{i}_\mu = \vec{i}_M + \vec{i}_R(1 - a)$$

Think to the model in steady-state condition we can substitute i_M with i_d and i_R with i_q , obtaining a direct dependence of the magnetizing current from the d and q component.

$$i_\mu = \sqrt{i_d^2 + i_q^2(1 - a)}$$

The direct consequence is that the main inductance itself depends thus from d and q current. An important fact has to be highlighted is the influence which has the deviation from the real value of this parameter on the motor control. In fact looking to the Eq. 2.35-2.41, is possible to notice that there is a direct correspondence between main inductance and the produced torque at the shaft. The equation 2.41 in steady state condition can be also written as

$$tq = 3pL_M i_{sd} i_{sq} \quad (3.13)$$

and this form leads us immediately to understand which can be the influence of a wrong parametrization of the inductance, on the torque produced, but considering also, as for the rotor resistance, the impact on the calculation of the slip frequency, which determines the imposed operative condition by the controller (Eq. 3.12). This effect has been calculated and displayed in Fig. 3.9. It is very interesting to notice which a variation of the main inductance value in the not saturated area, completely does not affect the torque produced.

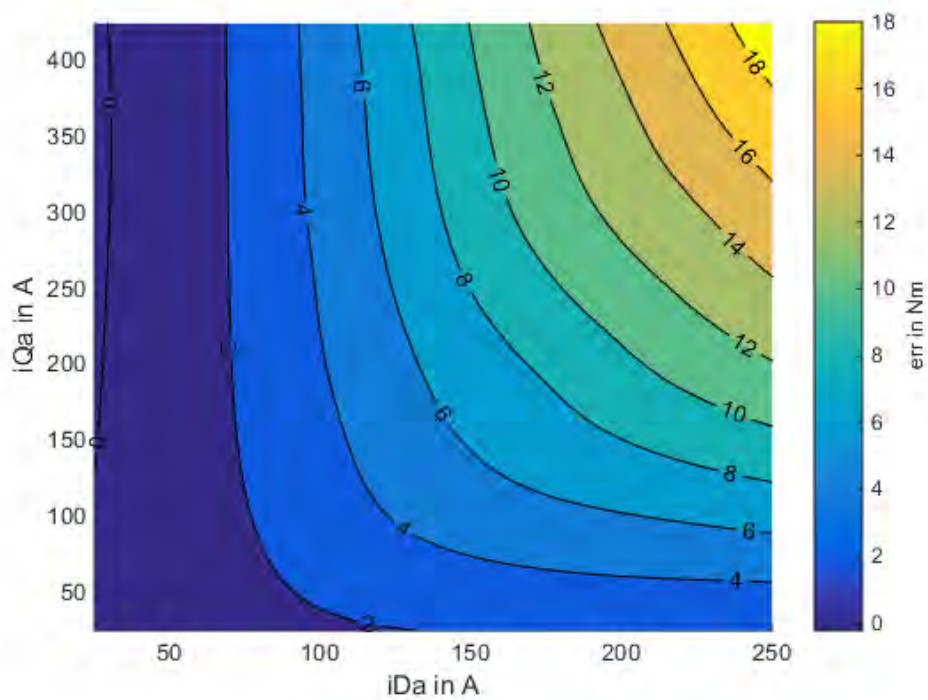


Figure 3.9: Influence of the main inductance variation on the torque produced to the shaft; the value has to be incremented of the 10%.

3.4 Stray inductances

Those parameters are linked to the leakage flux in stator and rotor slots; they are affected by the saturation as well as the main inductance, but is very hard to determine their behavior and dependence during the operative condition. Moreover, the rotor leakage inductance is also influenced by the skin effect in the bars, especially if the rotor is made by a squirrel cage with deep bars. The reasons for using closed and smooth slots are different:

- Hold firmly the bars in place;
- Allows accurate manufacturing of the rotor surface;
- Make easy the process of die-casting of the aluminum;
- Reduces the flux pulsations caused by rotor slotting, resulting in lower surface losses and attenuation of acoustic noise.

At the contrary the drawback is that on the top of the rotor, close the surface and the air gap, in correspondence to the bars there is a layer of iron which acts as a bridge, connecting all the rotor teeth. Being this layer very thin the flux which flows inside can easily be very high and this might lead the bridge to the saturation, giving a considerable contribute at the increasing of the rotor leakage inductance during operative condition of the motor. Thus, both the magnetizing inductance and the stray rotor inductance depends from the rotor current. In *Fig. 3.10* is showed the difference between closed and open rotor slots. At this



Figure 3.10: Close rotor slot shape (right) and open rotor slot shape (left).

point, as it has been done for the rotor resistance and the main inductance, we want to understand the effect of a not correct identification of the leakage inductance on the torque control and for doing this we deserve of the equation 3.13 in which appear the model L_M .

We know that it is calculated starting from the scaling factor a and considering the *rotor flux oriented model* is

$$a = \frac{L_m}{L_r}$$

Is clear that in this case the stray inductance of rotor plays a role in the identification of the correct reference system and in the calculation of the torque; taking into account an increment of 10% of the stray inductance of rotor we are able to display the torque error, which is showed in *Fig. 3.11* As is possible to see here, the torque error is not relevant

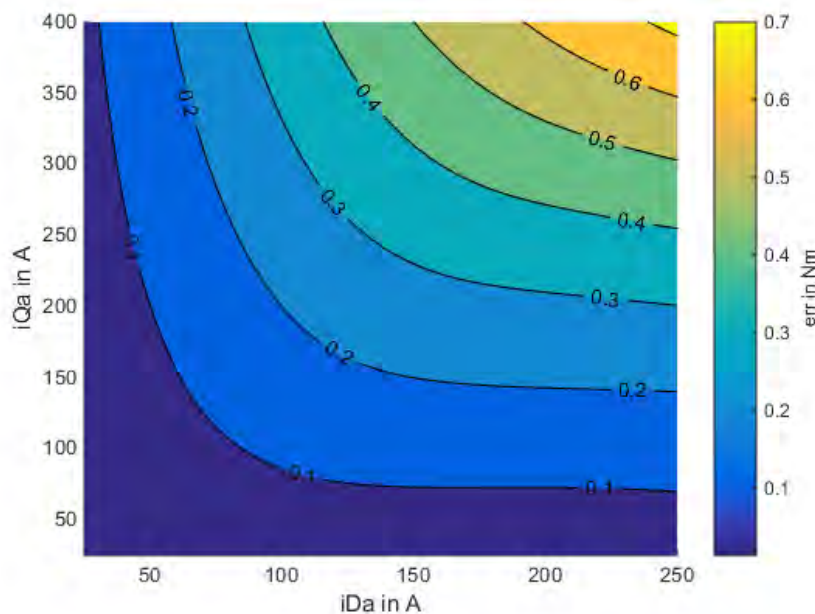


Figure 3.11: Influence of the rotor leakage inductance variation on the torque produced to the shaft; the value has to be incremented of the 10%.

compared to the error seen in *Fig. 3.7* and *Fig. 3.9* and for this reason our research on the correct parameter identification can be focused mainly on the rotor resistance and the main inductance which can be defined the main characters in the control of the induction machine. For what concern the stray inductance of stator, it influences the time constant of dynamic current path. Therewith, the stray inductance affects the current ripple. Thus, it does not directly influence the torque in a current controlled system.

4 Test Bench measurements definition

In this chapter we are going to discuss about the test analysis of the motor. The induction machine is well known, because it has more than one century of studies and applications since the end of XIX century. For this reason the challenge now is to try to overcome the standard models and control schemes, implementing always more accurate and complex models which take into account the skin effect, the iron losses, the gear losses etc. For get this, before is important to understand how is possible to investigate and measure directly those phenomenons in order to later create a good prediction system that is able to correct the parameters in each operative condition. Taking into account what is been presented till here, the next step is to define the test have to be conduced at the test bench in order to define completely the motor. Two important features have to be considered, are:

- the measured point;
- the time.

The time, clearly, as it has been said in the introduction is relevant, in fact optimizing this kind of procedure allowed to save several hours in the analysis and this optimization not only concern the automation of the process but also the definition of the test analysis and moreover the measurements points given in input to the test bench. Usually, is necessary to have several measured points in order to increase the accuracy of the results, but is also known that instead to measure much points, statistically is obtained the same results taking less points in a random order, in fact the trend of accuracy linked to the measured points is similar to the line showed in *Fig. 4.1*. For this analysis we have at disposition of a test bench equipped with a resolver, for the speed measurement, power analyzer, oscilloscope, thermal sensors embedded in several points inside the motor sample and a software for the control of the motor. In fact the motor can be tested in open loop, but also in close loop and exploiting the model seen in 2.5 the rotor flux oriented control scheme is implemented. For control the motor are necessary the default parameters values and at the beginning in the software are put the resistance and inductance values taken by the simulation; there is, in fact, a software called *ASMfeldor* [Bosa], which contains a complete model of the motor and the values of parameters are calculated by the design model of the motor. Later those values are updated with new measurements. The parameters dependence is managed completely by look up tables, which can be updated and improved test by test. A simplified scheme of the test bench used is presented in *Fig. 4.2*. All the variables measured are accessible, both the electrical signals and the values which stand in the inverter software. After a measurement, all the values are registered and saved in an excel file from which is

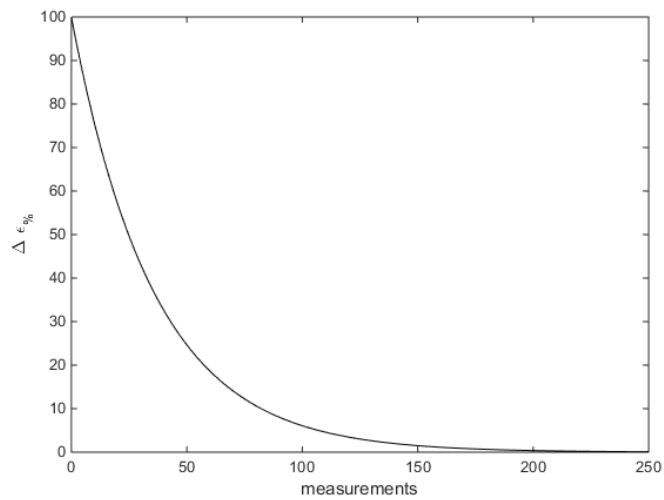


Figure 4.1: Accuracy of measurements linked to the number of measured points.

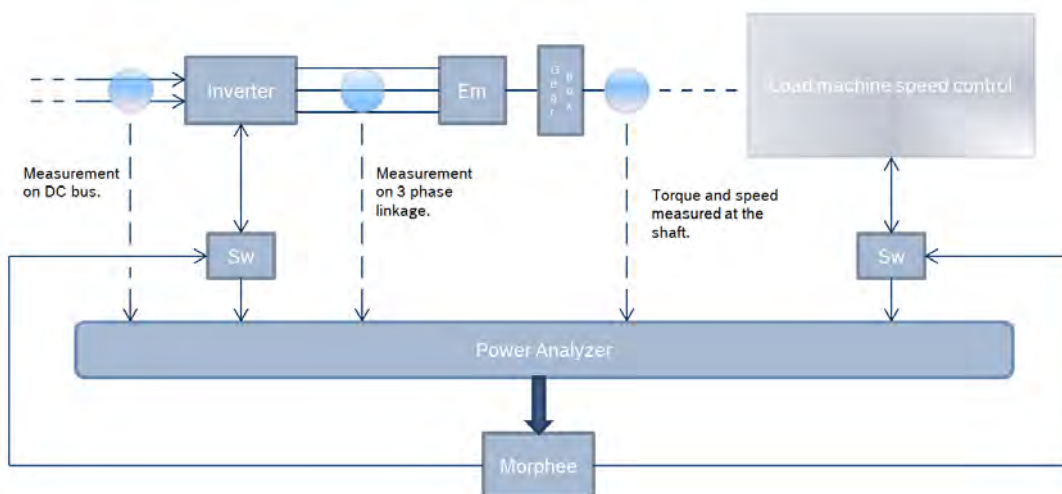


Figure 4.2: Scheme of the test bench used for the test.

possible to import the data in Matlab and elaborate the values for plotting or calculation. When a new sample has to be tested, the first operation is to measure the drag torque due to the gear box between the motor and the load machine, because the value estimated will be used further for correct the torque of the motor during other measurements. As far, after this simple test, the motor is processed to the no load and short circuit test, which are in literature the most important test for definition. The problem is that they are not able to characterize with enough accuracy the machine's parameters and their sensitivity above all the operative range of the motor and for this reason in this chapter we are going to discuss about some new test to conduce on the asynchronous motor in order to improve the accuracy of the off-line parameters detection and generate less error in the torque control.

4.1 DC test

This test is very simple and consist in the direct measurement of the stator resistance at the standard temperature of 20° with a multimeter. Is measured the voltage and the current which flow through two phases, as seen in *Fig. 4.3* and then the value is divided by factor two for get the resistance value of one phase. Moreover is measured the resistance of the cable from the inverter to the motor because the system see also this contribute of resistance and not only the contribute of the stator copper windings.

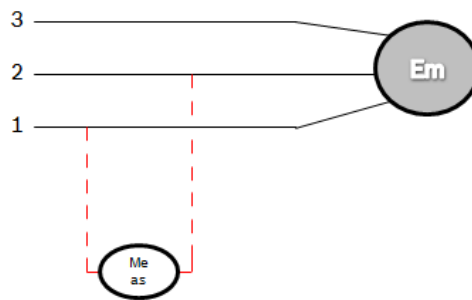


Figure 4.3: Measure of stator phase resistance.

4.2 Drag torque test

There is a difference between the electromagnetic torque (tq_{Em}) of the machine and the measured torque at the shaft (tq_{Emag}) and this difference is caused by the friction and the drag of the gears and the mechanical components, since that the torque sensor is put after the gear box, as is showed in *Fig. 4.2*. For conduce this test is given to the test bench a speed range from 0 rpm to the maximum speed, according to the motor data written in the appendix; in this case is 18000 rpm. The test bench measure the pure drag torque due to the gear and the machine (tq_{Drag}). This drag torque depend on the speed and therefore the trend is saved in the software in order to correct the torque measured with the motor loaded during the following test (*Eq. 4.1*). Normally for each speed step are done several measurements and then is taken an average value.

$$tq_{Em} = tq_{Emag} + tq_{Drag} \quad (4.1)$$

Unfortunately, this test does not give us all the information we need for correct the calculated torque in the software during the running of the motor, in fact the gear losses depends from the speed but also from the load conditions at a certain speed and since that is not possible to predict very well the losses due to the gears, this phenomenon will be cause of torque error at high speed. In *Fig. 4.4* is presented the analytical calculation of the gear losses

depending on torque and speed; as is possible to see the losses have a consistent variation above the torque axes for a rated speed.

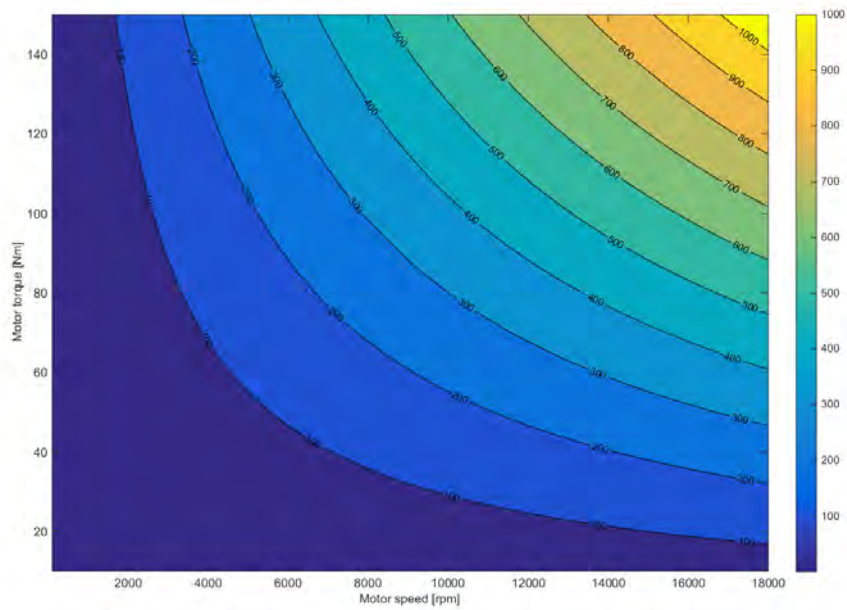


Figure 4.4: Theoretically gear losses calculation estimated in Watt above torque and speed axes.

4.3 No load test

For this test the electrical machine is operated at no load. A voltage is applied to the machine, while setting the slip frequency to zero (synchronous speed). In order to guarantee this condition, is exploited the load machine attached to the shaft of the sample motor on the test bench and it forces the rotor to turn at the same speed of the stator rotating field; this is the real condition of no load and the torque produced to the shaft is equal to zero. Working with the motor in this condition we ensure any induced current in the rotor bars, that means all the current supplied to the motor, flows inside the stator and in particular through the magnetizing branch, as we can deduce neglecting the rotor current from the universal model seen in chapter 2.4 (*Fig. 2.8*):

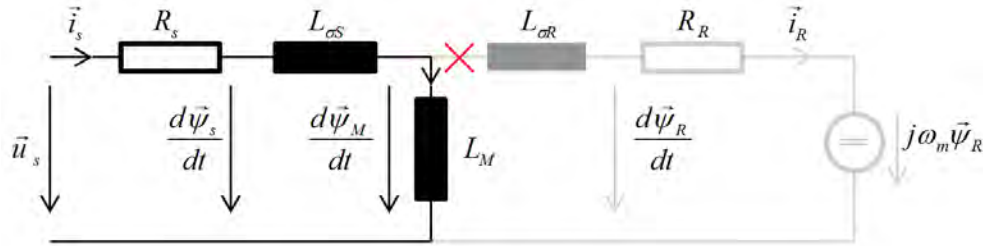


Figure 4.5: Universal induction motor model in no load condition.

In no load condition, thus, results simple to estimate the stator inductance, in fact referring on the stator voltage and stator current, we can write:

$$i_R = 0 \quad (4.2)$$

$$\psi_s = \int (u_s - R_s i_s) dt = \frac{u_s - R_s i_s}{\omega_s} \quad (4.3)$$

$$\psi_s = (L_{\sigma_s} + L_m) i_s = L_s i_s \quad (4.4)$$

$$L_s = \frac{\psi_s}{i_s} = \left(\frac{u_s}{i_s} \right) \left(\frac{\sin \varphi}{\omega_s} \right) \quad (4.5)$$

with φ = phase shift between stator voltage and current vectors.

The test is conducted for an increasing value of stator current, in order to estimate the dependence of the main inductance from iron saturation, as seen in Sec. 3.3 and display the trend. However, has to be noticed the limit of this test: due to the saturation the magnetizing inductance is also affected by the rotor current particularly when the rotor slots are closed or skewed. Therefore, the results obtained using the No Load test can be considered good only at light loads, that means when the rotor current is close to zero. As the load increases, and thus the rotor current increases, the magnetizing inductance and the rotor leakage inductance will change. To obtain a value of the magnetizing inductance with

a good accuracy, the inductance needs to be identified during the operation of the motor above all the operative area.

4.4 Short circuit test

Short circuit operation condition of the machine describes a test at standstill; it means that the shaft is kept locked and a voltage source is supplied to the motor. At zero speed, the back e.m.f. is zero. Depending on the frequency of the applied voltage, the current flows through the main inductance or the rotor stray inductance and the rotor resistance. As the value of the main inductance is much higher than the value of the rotor stray inductance, the amount of current through the main inductance reduces with increasing frequency because, as we well know, a general inductive impedance is in the shape of $Z_l = j\omega_s L$. So, is possible to exploit this phenomenon in short circuit in order to determine the value of the stray inductances and the rotor resistance. Has to be chosen a frequency which allowed to neglect the derivative branch of the main inductance. In *Fig. 4.6* is shown the simplification in short circuit.

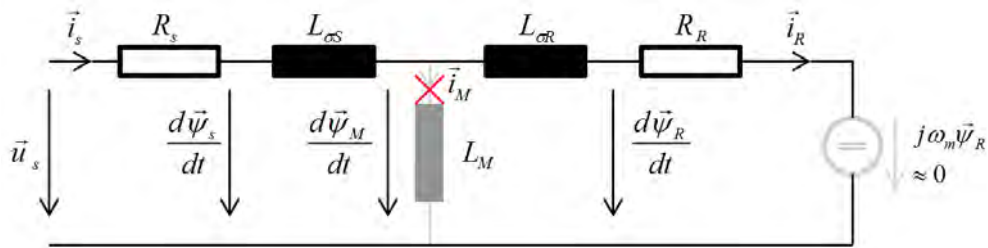


Figure 4.6: Universal induction motor model in short circuit condition.

In this situation, since that $i_M \sim 0$ is valid, we can write:

$$u_s = ((R_s + R_R) + j\omega(L_{\sigma s} + L_{\sigma r}))i_s \quad (4.6)$$

and therefore:

$$R_{sr} = R_s + R_R = \Re\left(\frac{u_s}{i_s}\right) \quad (4.7)$$

$$L_{sr} = L_{\sigma s} + L_{\sigma r} = \Im\left(\frac{u_s}{i_s}\right) = \left[\frac{u_s}{i_s}\right] \frac{\sqrt{(1 - \cos^2 \varphi)}}{\omega_s} \quad (4.8)$$

$$R_R = \left(\frac{u_s}{i_s}\right) \cos \varphi - (R_s + R_{wire}) \quad (4.9)$$

Normally this test is repeated at different level of frequency and the data collected are elaborated together with the data from No Load test and Dc test in order to calculate all the parameters. However with only those data, it would not be possible to distinguish the rotor stray inductance from the stator inductance and therefore is necessary to add a new value, which come from the hystorical data of production process. This value is the ratio between $L_{\sigma s}$ and $L_{\sigma r}$. For example, in this case the ratio is equal to 1.56. Unfortunately

as to be mentioned that detecting the leakage inductances with this method, does not lead us to get the values with high accuracy, in fact as is been defined the locked rotor test, the frequency of the signals has to be considerably high compared to the nominal condition and this affect the rotor stray inductance by the skin effect of the bars, as seen in *Sec. 3.2*; in fact besides the rotor resistance, it affects also the inductance associated to the current which flows in the bars.

4.5 DQ-map test

In this section we are going to introduce an experimental test which permits to analyze completely the machine. This test has the feature to be conducted exploiting the induction motor model showed in *Sec. 2.5* and therefore the d - q reference system. In input to the motor are given couples of current signals in d - q reference in order to test the motor in the same motoring and generating operative point. For define motoring and generating operative condition in d - q reference system is enough to fix the sign, as positive, of the d current and switch the sign of the q current in order to change the sign of the power. In *Fig. 4.7* is showed an example. Therefore in input is created a map of set points on dq-axis and the motor is feed with the points. But those points has to be evaluated carefully, because there are some physical constrains to take into account. The most important issue is the maximum stator flux, which is linked to the maximum voltage supplied from the DC bus and the speed of the motor during the test, as seen here below in *Eq.*. So, for each level of voltage and speed on which is made the test, has to be considered the maximum flux and the dq-map has to be re-shaped conveniently.

$$\psi_s^{max} = \frac{60}{2\pi n p} u_s^{max} = \frac{u_s^{max}}{\omega_s} \quad (4.10)$$

with:

u_s^{max} = maximum voltage applied on the stator side;

n = speed in rpm;

p = pole pairs.

Moreover, in order to increase the test speed and do not increase much the temperature, the motor is feed with not ordered couples of points, but considering maximum current values and minimum current values each time, as is showed in *Tab. 4.1*.

Implementing this kind of test and considering the model of the motor in *Fig. 2.12* and *Fig. 2.13* is possible to calculate directly all the inductances neglecting the resistance on the stator side (stator and cable resistance with their joints), as follow:

$$L_s = \frac{u_{sq}^{mot} + u_{sq}^{gen}}{\omega_s^{mot} \cdot i_{sd}^{mot} + \omega_s^{gen} \cdot i_{sd}^{gen}} \quad L_{\sigma S} = \frac{u_{sd}^{gen} - u_{sd}^{mot}}{\omega_s^{mot} \cdot i_{sq}^{mot} - \omega_s^{gen} \cdot i_{sq}^{gen}} \quad (4.11)$$

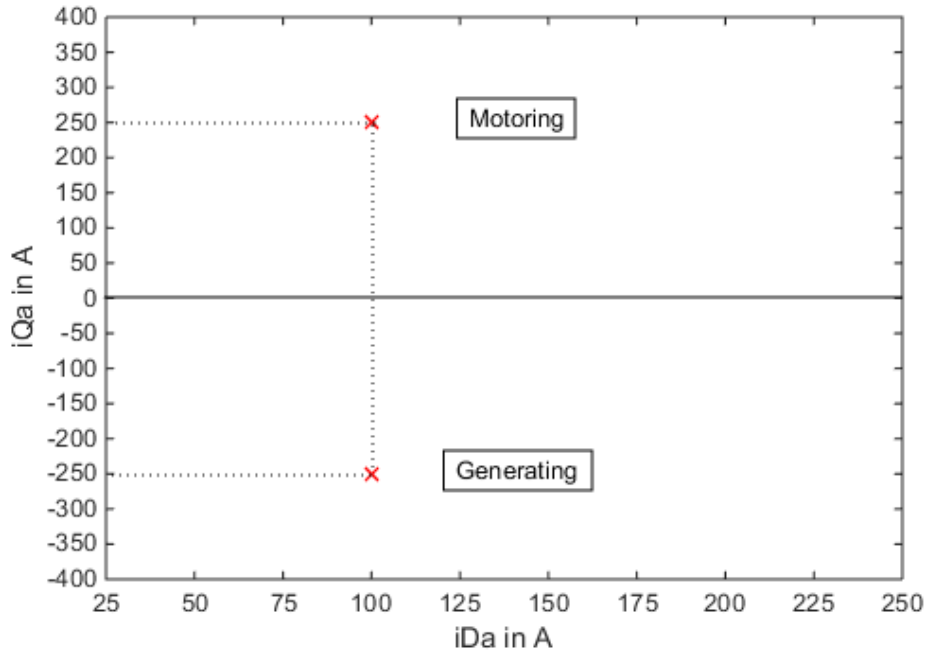


Figure 4.7: A couple of points in motoring and generating d-q map.

id [A]	iq [A]
50	+400
50	- 400
50	+50
50	- 50
50	+350
50	- 350
50	+100
50	- 100
50	+300
50	- 300
...	...

Table 4.1: Sorting of dq operative points example.

The equation are take out from *Eq. 2.34* and *Eq. 2.37* in steady-state condition. Considering, then, this system of equations:

$$L_{\sigma S} = L_m \cdot \left(\frac{L_s}{L_m} - a \right) \quad (4.12)$$

$$L_s = L_{\sigma s} + L_m \quad (4.13)$$

$$L_r = L_{\sigma r} + L_m \quad (4.14)$$

$$a = \frac{L_m}{L_r} \quad (4.15)$$

We can evaluate the real leakage inductance of stator as follow:

$$L_{\sigma S} = L_m \cdot \left(\frac{L_s}{L_m} - a \right)$$

$$L_{\sigma S} = L_m \cdot \left(\frac{L_s}{L_m} - \frac{L_m}{L_r} \right)$$

$$L_{\sigma S} = L_s - \frac{L_m^2}{L_r}$$

$$L_{\sigma S} = L_{\sigma s} + L_m - \frac{L_m^2}{L_r}$$

$$L_{\sigma s} = L_{\sigma S} - L_m + \frac{L_m^2}{L_r}$$

$$L_{\sigma s} = L_{\sigma S} - L_m \left(1 - \frac{L_m}{L_r} \right)$$

$$L_{\sigma s} = L_{\sigma S} - L_m \left(1 - \frac{L_m}{L_{\sigma r} + L_m} \right)$$

$$L_{\sigma s} = L_{\sigma S} - L_m \left(1 - \frac{L_m}{\frac{L_{\sigma s}}{k} + L_m} \right)$$

$$L_{\sigma s} = L_{\sigma S} - L_m \left(1 - \frac{kL_m}{L_{\sigma s} + kL_m} \right)$$

$$L_{\sigma s} = L_{\sigma S} - \frac{L_m L_{\sigma S}}{L_{\sigma s} + kL_m}$$

$$L_{\sigma s} = \frac{L_{\sigma S} L_{\sigma s} + kL_{\sigma S} L_{\sigma m} - L_m L_{\sigma S}}{L_{\sigma s} + kL_m}$$

$$L_{\sigma s}^2 + kL_{\sigma S} L_m = L_{\sigma S} L_{\sigma s} + kL_{\sigma S} L_{\sigma m} - L_m L_{\sigma S}$$

$$L_{\sigma s}^2 + (L_m + kL_m - L_{\sigma S}) L_{\sigma s} - kL_{\sigma S} L_m = 0$$

$$L_{\sigma s}^2 + ((1+k)L_m - L_{\sigma S}) L_{\sigma s} - kL_{\sigma S} L_m = 0$$

$$L_{\sigma s}^2 + ((1+k)(L_s - L_{\sigma s}) - L_{\sigma S}) L_{\sigma s} - kL_{\sigma S} (L_s - L_{\sigma s}) = 0$$

$$L_{\sigma s}^2 + (L_s - L_{\sigma s} + kL_s - kL_{\sigma s} - L_{\sigma S}) L_{\sigma s} - kL_{\sigma S} L_s + kL_{\sigma S} L_{\sigma s} = 0$$

$$kL_{\sigma s}^2 + ((1-k)L_{\sigma S} - (1+k)L_s) L_{\sigma s} + kL_{\sigma S} L_s = 0$$

$$L_{\sigma s} = \frac{(1+k)L_s - (1-k)L_{\sigma S} - \sqrt{[(1-k)L_{\sigma S} - (1-k)L_s]^2 - 4k^2L_{\sigma S}L_s}}{2k} \quad (4.16)$$

with $k = \frac{L_{\sigma s}}{L_{\sigma r}} \simeq 1.56$

Finally, considering this parameter and the system written before, then, is possible to calculate easily also $L_{\sigma r}$ and L_m .

$$L_{\sigma r} = \frac{L_{\sigma s}}{k} \quad (4.17)$$

$$L_m = L_s - L_{\sigma s} \quad (4.18)$$

The interesting feature of this innovative test is that is possible to estimate completely the inductances above all the working area of the motor including their dependence from current exploiting one test and elaborating the measurements with simple calculation. In fact the motor during the test is not forced to work in particular conditions as was for example in the No Load test, with any load on the shaft and in Short Circuit test at standstill; therefore the motor operates on all the working area and in this case we can include in the estimation also the dependence from the load conditions.

Once the test is conducted we get the complete map with the measured points in an excel file and elaborating the measurements we can display with several graphs all the pictures we need for example the trend of the stator current, the temperature in the stator and rotor side, the efficiency above all the d-q map and also the torque measured. In particular is possible to compare the measured torque and the calculated torque from the software: those two variables are the most important signal regarding the parameter identification, in fact if the parameters are well identified, the error between the two torque is supposed to be close to zero. Analyzing those maps and all the results got from the test bench has been decided to exploit further this kind of test for get other information about the machine parameter. Considering what has been showed in the *chapter 3* about the torque error due to the parameters deviation, we can directly deduce that the error at low d-current and high q-current is mostly created by a wrong parametrization of the rotor resistance, instead an error at high d-current is caused mainly by a not correct value of the main inductance. The trend of slip frequency shown in *Fig. 3.5*, is high just at low d-current, decreasing heavily in the right part of the map.

Taking into account this deductive reasoning the idea is to try an optimization of the torque error locally considering the different part of the maps: we are going to optimize the rotor resistance from the torque error in the upper left part of the map and the main inductance considering the torque error in the rest of the map. In *Fig. 4.8* is showed the algorithm for optimizing the rotor resistance; this algorithm considers the slip frequency as fixed and starting from the initial error searches for the correct angle of the stator current vector which call off the torque error and with that angle the rotor resistance is calculated. With

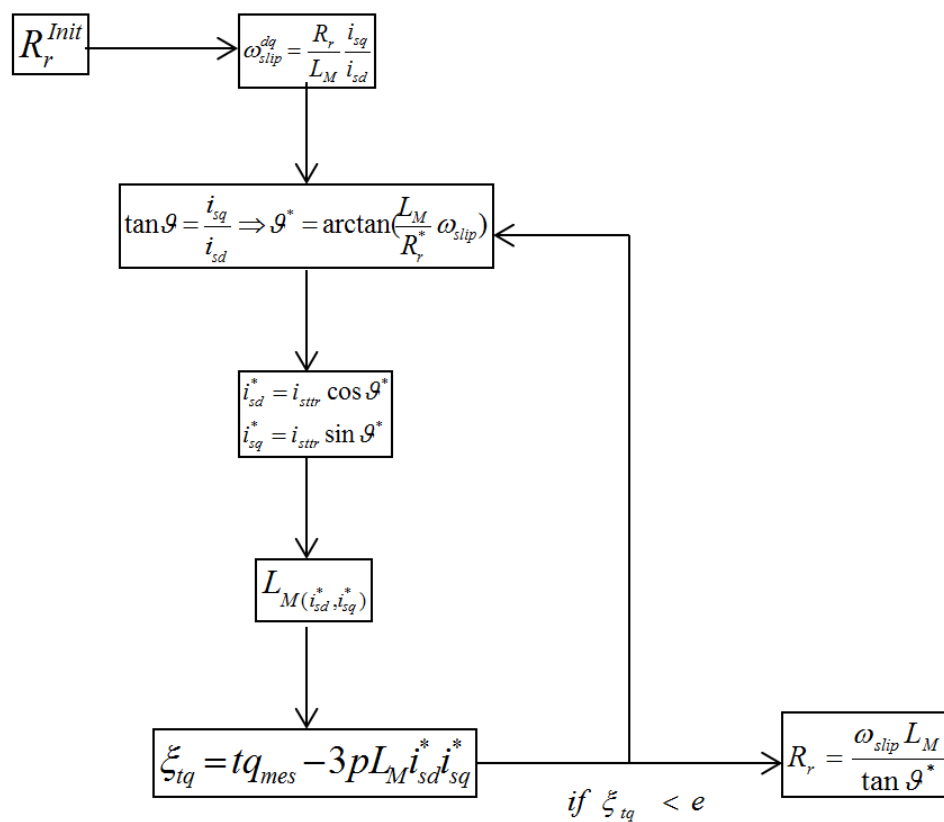


Figure 4.8: Optimization algorithm for the rotor resistance.

this method the hope is to get a new and more correct parametrization for the skin effect, in fact the optimized area corresponds to the area with highest slip frequency. The same approach, then, is used for calculate and optimize the main inductance in the other part of the map, using directly the torque equation and searching for the correct inductance values. This procedure will be tested and showed in detail in the last chapter.

4.6 Rotor resistance detection

For the direct detection of the rotor resistance it is exploited another method that is based on the comparison of two signals: the set q voltage and the calculated q voltage by parameters from *ASMfeldor*. It means that the model exploited for this test is still the *rotor flux oriented*. The idea is to supply the motor with an impulse of current on d -axis, while q current is kept to zero, and the voltage signals are displayed on the software which processes the oscilloscope signals. In these operative conditions, considering the equation 2.37, count:

$$u_{sq} = \omega_s \cdot \psi_{sd}$$

If the set voltage and the calculated depending on stator frequency and rotor flux have not a similar response to the impulse, means that there is a wrong definition of parameters inside the software and in particular they afflict the rotor time constant, in fact the measured q voltage response is strictly linked to this parameter.

$$\tau_r = \frac{R_r}{L_r}$$

This can be shown taking the equation 2.32-2.33, expressing the rotor flux linkage space vector $\vec{\psi}_R$ in terms of the magnetizing vector ψ_M along the d -axis (since that they are aligned as seen in *Fig. 2.9*):

$$\begin{aligned} \frac{d\psi_M}{dt} &= L_{\sigma R} \frac{di_{Rd}}{dt} - (\omega_s - \omega_m) L_{\sigma R} i_{Rq} + R_R i_{Rd} \\ \frac{\psi_M}{L_M} &= i_{sd} - i_{Rd} \end{aligned}$$

and developing it, we obtain

$$\frac{L_R}{L_M} \frac{d\psi_M}{dt} + \frac{R_R}{L_M} \psi_M = R_R i_{sd} + L_{\sigma R} \frac{di_{sd}}{dt} - (\omega_s - \omega_m) L_{\sigma R} i_{sq}$$

Finally this equation can be simplified, considering the *rotor flux oriented model* and the test conditions, that means:

$$\begin{aligned} a &= \frac{L_m}{L_r} \\ L_{\sigma R} &= 0 \\ i_{sq} &= 0 \end{aligned}$$

Writing it in the form:

$$\frac{d\psi_M}{dt} + \frac{R_R}{L_R}\psi_M = R_R i_{sd}$$

This is a simple differential equation of first order where all the variables are time dependent and a general solution can be written as:

$$\psi_{M(t)} = K(e^{-\frac{t}{\tau_r}} - 1)$$

where:

$$K = aL_m i_{sd}$$

$$\tau_r = \frac{R_r}{L_r}$$

So, basically we tune manually the value of rotor resistance, considering constant and correct the value of rotor inductance inside the software, till we are able to see a similar response displayed on the screen. In *Fig. 4.9* is showed the dynamic of the phenomenon here described. The aim is to understand if this procedure is more accurate then the calculation of

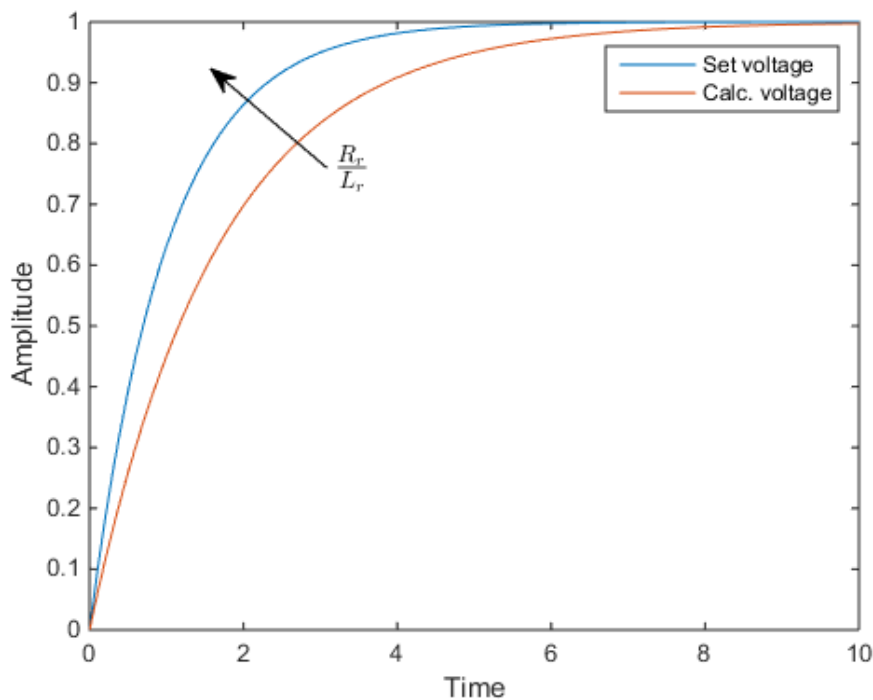


Figure 4.9: Trend of the voltages response.

the rotor resistance from the short circuit test.

4.7 nTq-map

This final test is created for analyze completely the motor above its working region. Is created in input a speed (n) and torque (tq) map which is then feed to the motor and after measurements is possible to display each kind of parameter of the motor and its trend on the map; for example the efficiency, the losses of the system and the power. Also the creation of the *nTq-map* has to consider the maximum power, given a maximum voltage level on the DC bus, in fact normally the motor is tested with 180, 250 and 350 V above all the range of speed; but is clear that for the minimum voltage level is not possible to work with the motor at maximum speed and maximum torque, because the voltage supplied from the source is not enough; in *Fig. 4.10* is possible to see the dependency of the torque constrain from the voltage. This is, normally, the last test conducted on the test bench and allowed

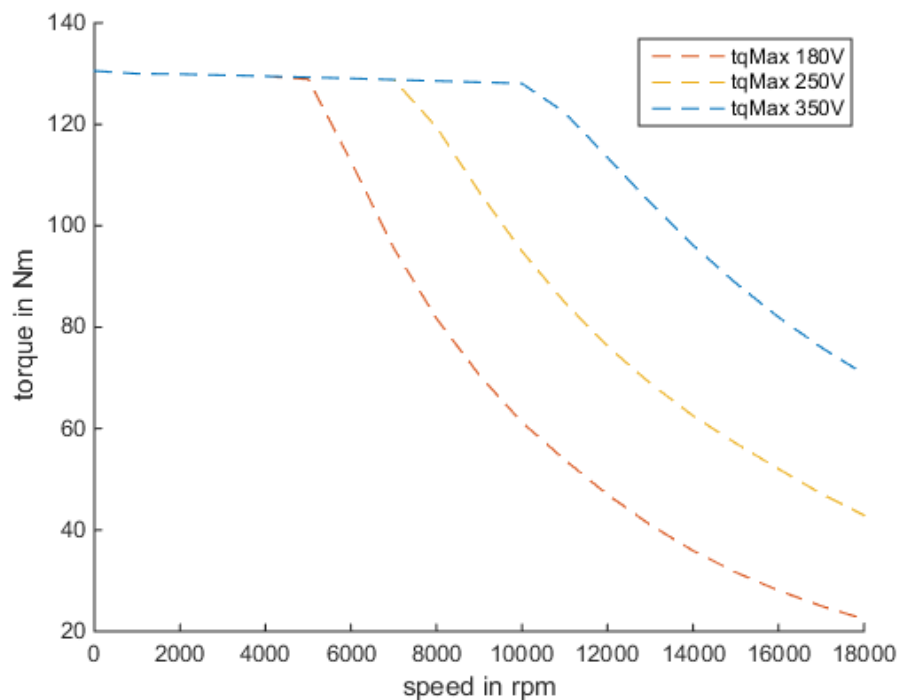


Figure 4.10: Dependency of maximum torque available from voltage.

to have a direct feedback of the motor's performance; in particular is verified the goodness of the *field oriented control* implemented in the inverter, which is supposed to have all the look up tables updated with values taken out from the previous test.

5 Test Bench automated measurement system

In this chapter is presented the basic idea that has been developed for the automation of all the measurement process. In the introduction has been claimed the benefits of this improvement, but the development of an automated system needs care, because when it is operative it must not occur any error during its procedures. At the beginning has to be defined the system and for what is been showed till now in the previous chapter, the analysis procedure can be divided in three phases:

1. pre-processing;
2. measurements;
3. post-processing.

The first phase concerns the definition of the set points for each test. As we have already seen, attention has to be kept about physical constrains, in order to not damage the electrical systems. For achieve this point, has to be developed an automated algorithm, which, after has received in input all the desired characteristics for the setting of the test, is able to elaborate the data and give in output an excel file in which are saved all the points divided for each kind of test. The algorithm reads from the server the simulated data of the motor, which are contained inside a class and filter the created set points with the physical boundaries, creating a valid set point. The latter is very important for the creation of the *dq-map* and *nTq-map*. Therefore the algorithm takes into account these constrains and creates valid set points ready to be applied to the Test Bench.

The second phase consists in the sending of the input data to the Test Bench, which tests the motor following the order of the analysis presented in the previous chapter and makes available the measurements.

Finally in the last phase all the results from the measurements on the Test Bench are picked up and elaborated with several Matlab scripts and following the theory exposed in *Chap. 4* the resistances and inductances are estimated in order to update the values in the software and verified finally the accuracy of the torque control. As far the procedure here described is conduced without a standard protocol and official documentation about those kind of test, creating not less confusion when several people have to work on it. But the biggest problem is about time and failure, in fact when a test is conduced on the Test Bench there are no feedback about measurements and then, only after the test is ended, when the data are available, is possible to understand if there were failures during the test

or if the measurements are valid. In the negative case, the test has to be repeated wasting much time, considering that the test procedures take from 1-2 hours to one entirely day. Therefore, the idea for increase the speed and the automation of the motor analysis is to create something which tries to solve those problems. In *Fig. 5.1* is showed the global analysis process that has to be automated. Looking at the picture upon, it appears evident

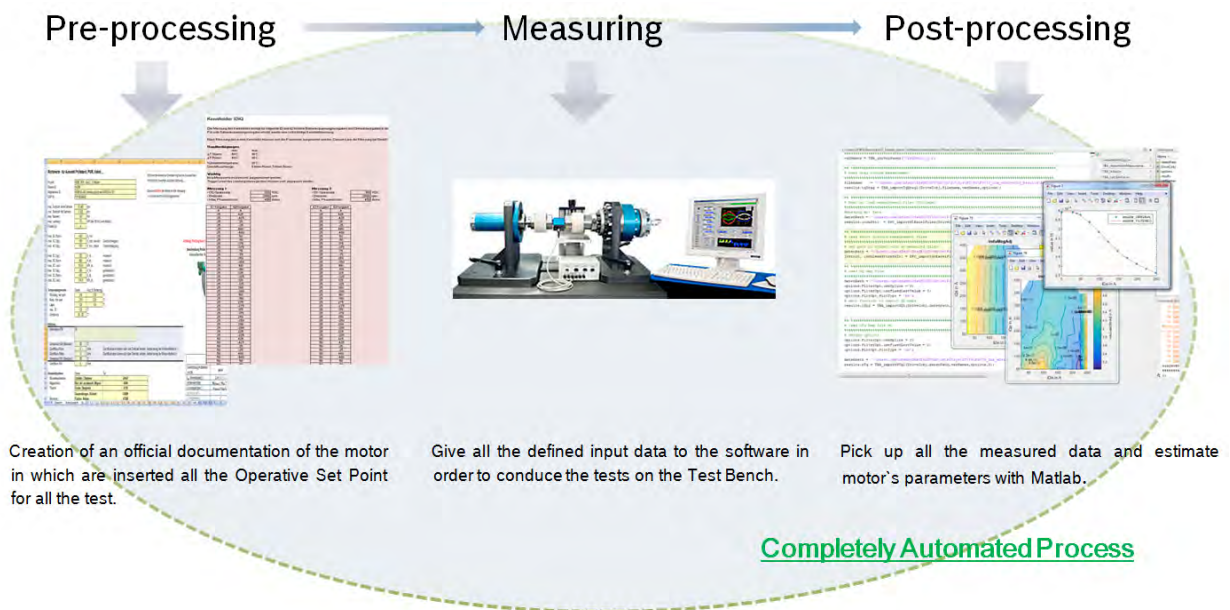


Figure 5.1: Automation system development.

that there is a sort of communication between the Test Bench and the software and in fact what has been developed is an interface which allows the interaction between the Test Bench and Matlab; more details about this interface will be given later. This interface is very primitive, but it is enough to create this connection towards the parts and implement the automation: when the Test Bench makes a measurement, it saves the data inside a long array, which, by the interface, is sent to Matlab. At this point a new feature is introduced, which is the *real time plotting* of the measurements. This feature allows to obtain a direct visual feedback of the values after each measured point in order to understand if there are failures in the procedure or the measurements are valid. This is important, because as we have said previously, it would allow to save time during the analysis of the samples. The last feature that has been developed, but which is still far to be completed, is a sort of Graphical User Interface: it is supposed to be the conjunction of all the 3 phases showed in *Fig. 4.6*, in order to reach the total automation of the procedure.

5.1 Interface

The interface that has been developed for this kind of application it is very simple and is based on the well-known model of *server-client*. With this framework is possible to identify a device which is the *server* and another device, which is called *client*; both are connected to the computer network and can be defined an algorithm able to communicate data automatically from the client to the server. The principle is shown in *Fig. 5.2* For

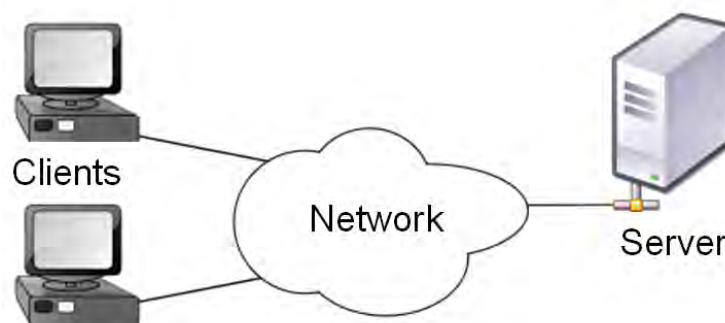


Figure 5.2: A computer network diagram of clients communicating with a server via network.

computing this procedure the important thing is to define a protocol and a common language between the two devices in order to recognize each other during the data exchange. The structure developed for our issue is minimal and briefly let the server recognize the IP address of the client which asks for data sending; after it has established the connection between the two systems, the client sends a string to the server which contains all the relevant information and calls the properly function in the server for managing the string: in this case it will be all the names of the variables and the corresponding measured value. The client is the test bench software and the server is the pc which has got Matlab and all the functions able to recognize the data and process them.

The procedure is divided in two main steps:

1. The initialization procedure in which the test bench asks to the server PC a connection, open Matlab and sends all the variables names in order to prepare the PC for receiving the measurements in exactly the same order while the test bench is going to measure.
2. The measurement step, repeated cyclically for each measured point, in which the test bench sends the values and calls the function on the server for checking and plotting correctly the points at screen.

The system has been tested and the synergy between the test bench, the interface and Matlab seems to be well-performing and the results in terms of automation of the process is on the expectation. In *Fig. 5.3* is showed the Server interface.



Figure 5.3: Server interface receiving measurements by the client.[Bosb]

Future upgrades of this system should include also the possibility from the Server side to send data and command back to the Client and get the completely automation of the measurement procedure by remote interface. In the next paragraph this project is described in detail.

5.2 Real time plotting

For what concern the real time feedback during measurements, exploiting the *interface*, the test bench should be able to call a Matlab’s script which takes the measured data and checks their validity, displaying on screen the values. During the development of this project it has been created this feature for the test seen in *Sec. 4.5* and first of all it has been experimented virtually in Matlab. In order to try this system, to the main script has been added a part which simulates the data’s sending from the Test Bench.

The requirements for this task mainly are:

- Check the physical constrains on the values and give a feedback to the user if they are not validated;
- Compare the measured values with the simulated values and highlight higher deviation between the values;
- Display in real time the measured points in the reference system for the most critical variables in the system in order to get immediately a feedback about failure of sensors.

For this requirements it has to be developed a good and robust structure of function in Matlab which is also flexible for future upgrades as for example the adding of a new variables to be checked in the procedure. The script is able to validate the measurements, plot the measured points of the main variables (in this case *speed, torque, power, DC current, DC voltage* and *efficiency*) and calculate the inductances using *Eq. 4.11-4.16-4.17-4.18*. In *Fig. 5.4* it is possible to see a simulation of the results for several measured points.

Moreover the user has the possibility to interact with the graphs, having lots of measured point on the screen at the end of the test: it has been implemented a feature which gives the possibility to identify immediately in the table the value of a failed measurement for example, by clicking on the cross point in the graph. The result is the highlight of the corresponding row in the table.

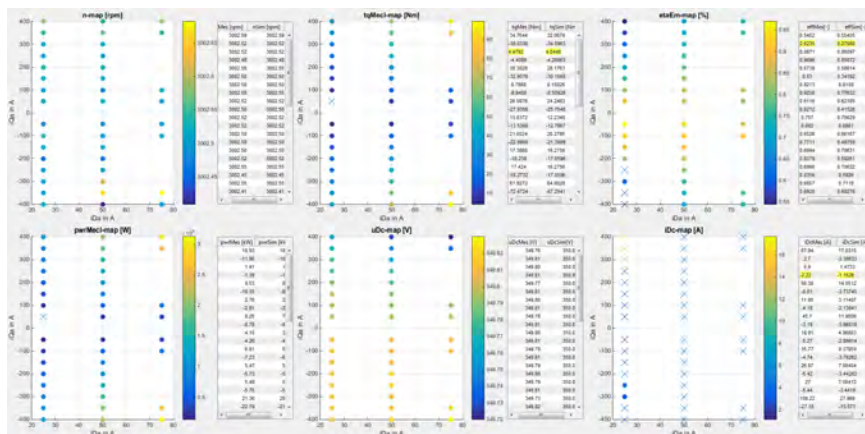


Figure 5.4: Real time plotting example.

5.3 Gui development

This *gui* has been developed entirely in Matlab [The14] and the requirements are:

- Manage all the input set point for each kind of test;
- Generate the official excel file which contains the documentation about the test and the machine;
- Check and display the input data before to start the test;
- Communicate with the test bench software in order to send the input data and receive the measurements back during the test;
- Prepare Matlab to receive and display the measurements in real time;
- Visualize the value of parameter detected and compare them if necessary;
- Generate Look Up Tables for update the software's value.

An idea of the framework is showed in *Fig. 5.5*. As far, it has developed the first part for the

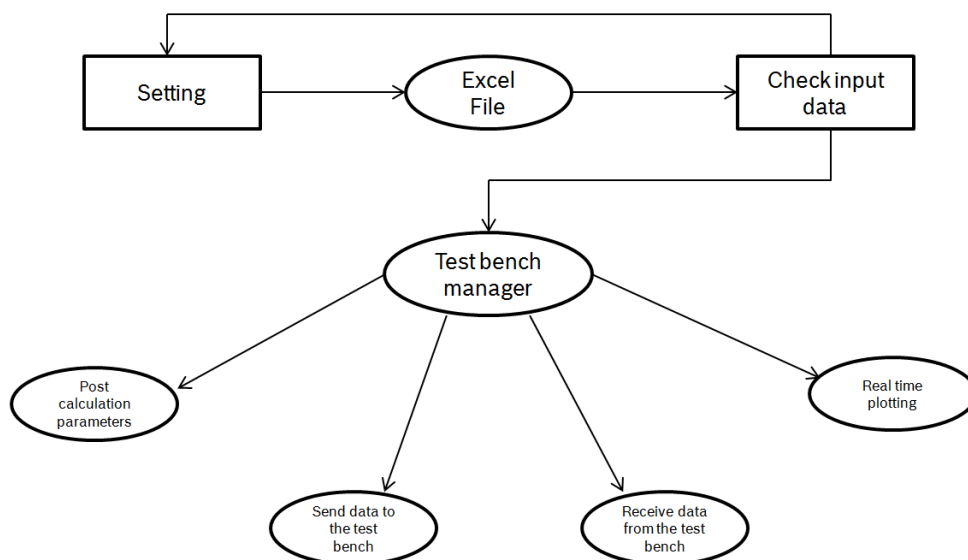


Figure 5.5: Gui framework for the automation system.

generation, management of the set point and a part for analyze the results. The user can upload the data which contains all the information about the motor and can set the options; *Fig. 5.6* shows how is presented the first page of the GUI. Once put all the options, going further the system generate automatically all the set point for the test and prints them in the excel file. In the second stage the user has the possibility to check the generated maps and verify their feasibility with the requirements for the test; for example in *Fig. 5.7* the set point

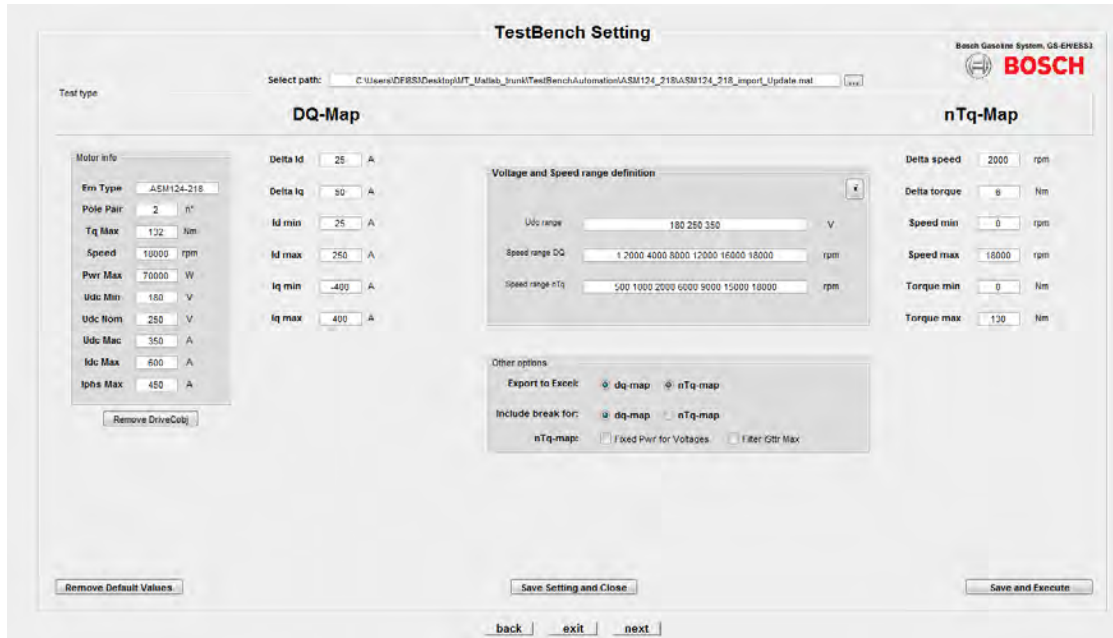


Figure 5.6: Abstract of the GUI.

for the dq-map test can be displayed and if is necessary an options called ‘tighten’ allows to add more points if the physical constrains are too hard in certain operative conditions. The same features are implemented for the managing of the nTq-maps, considering the power limits. Finally, it is developed also a tool for the post-processing which allowed to load all the results and analyze the measurements. The most important feature is a panel called ‘options’ which contains all the plot setting for display three-dimensional or bi-dimensional data. Moreover is possible also to plot with different plot options inside the same figure, in order to understand the quality of the interpolation of the measured points and this can be seen also in *Fig. 5.8*, where the interface is presented. A last option permits to compare quickly two different measured variables in order to check the error and the quality.

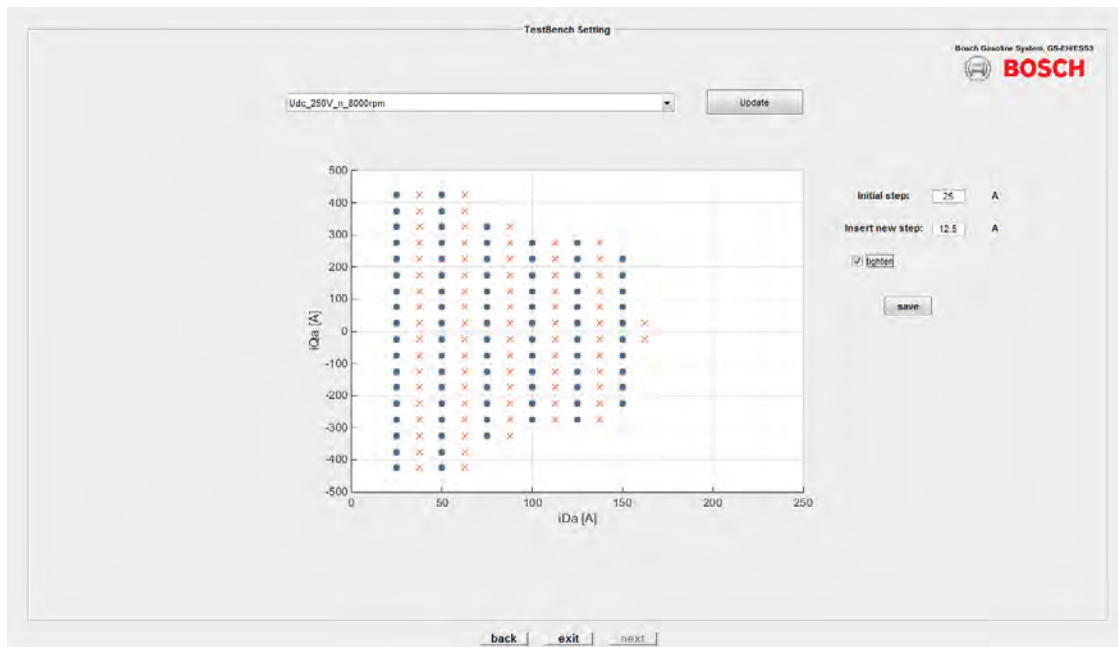


Figure 5.7: Check set points through the gui.

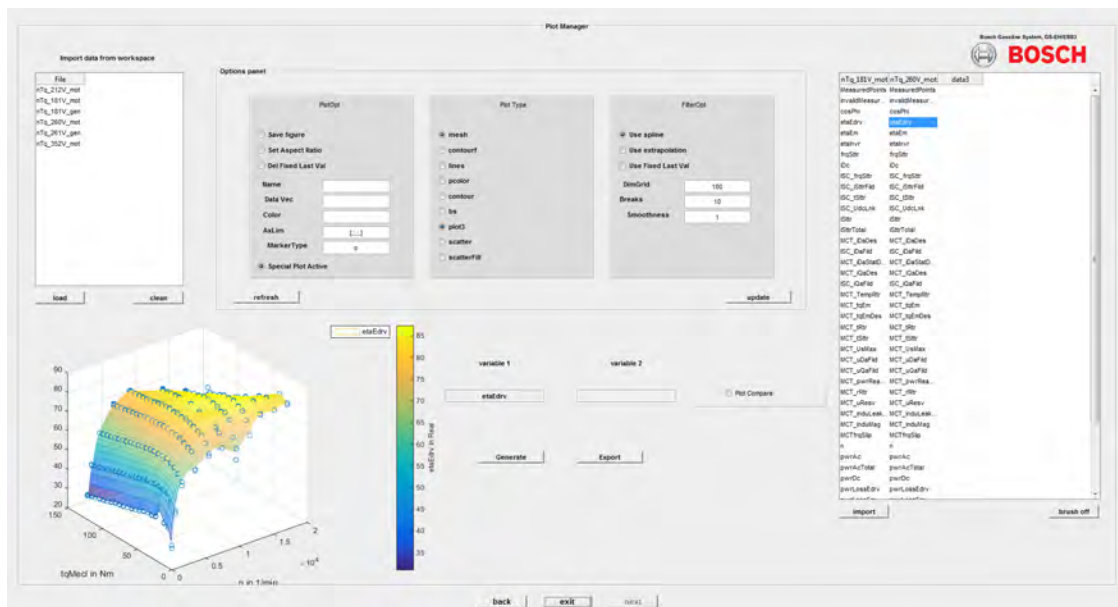


Figure 5.8: Interface for analyze the results in the post-processing.

6 Documentation of the results

In this last chapter are presented all the results of the test conducted at the test bench, following step by step the analytical procedure showed in *Chapter 4*. The motor is a classical induction machine designed by the Company and the plate data can be found in the *Appendix*. Once the motor is mounted on the test bench, the first thing to do is to check and validate the correct operation of all the devices seen in *Fig. 4.2*, included the controller. Moreover, for manage all the results of the test, is created a class with Matlab, exploiting the object-oriented programming theory, which has a very robust structure and inside this class are stored all the information about the motor and all the simulated and measured results. In this way it is possible to:

- Have easy access to all the motor data including the simulated values from *ASMfeldor*, the calibrated values and the measured values during the test;
- Upload the values in the test bench software;
- Use the variables stored inside for making all the calculation in Matlab.

The class is called *DriveC*.

Volt-Ampere measurements

The first step for the motor analysis is the measurement of resistances on the stator side, considering also the cables; this is a simple and manual operation which can be done with a multimeter. The results and their conversion to the reference temperature of 20° by *Eq. 3.1* are showed in *Tab. 6.1*. After the measurement the values are stored in the *DriveC* of the motor and in the software of the test bench. Beside the updating of the software model parameters, those values are necessary at a later stage for calculating the rotor resistance from the short circuit test, subtracting the resistances of the stator side in according with the *Eq. 4.9*.

$[m\Omega]$	$T_{mes} [21.9^\circ]$	$T_{ref} [20^\circ]$
R_{Sttr}	9.625	9.554
R_{Cbl}	1.650	1.630

Table 6.1: Volt-ampere measurements.

Drag torque measurements

The second test concern the analysis of the losses caused by the friction on the machine and the gears. The torque sensor stores in an excel file the measurements for different step of speed, in our case we have brought the speed from 0 rpm to 12000 rpm. In the measurements normally has to be taken into account the noise and for this reason for each speed step are picked up several measurements and in the calculation the trend of the drag torque is evaluated considering the average value. *Fig. 6.1* displays the real measured points and their interpolation. The values are relative low in fact the maximum torque loss we get due to the gear is about 0.9 Nm at high speed. With those results we simply update in the software the look up table for the drag torque correction, according with *Eq. 4.1*. As it was already said, this test goes to find out the torque losses due to the friction without considering load condition which is not accurate enough when the motor is running at random load conditions, in fact it is a reason of torque error in the torque control mode.

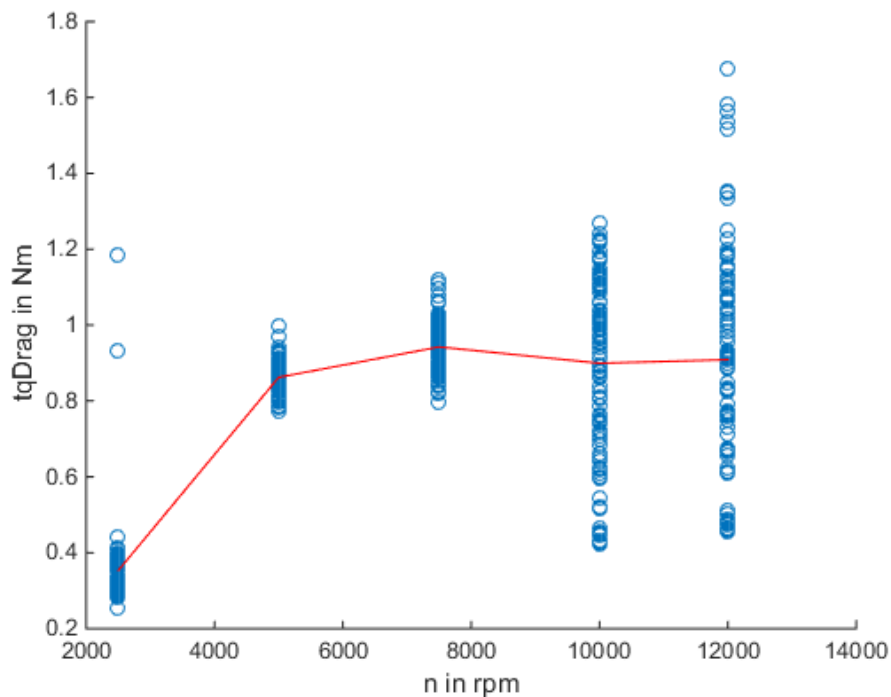


Figure 6.1: Results of drag torque measurements with the data fitting.

No load measurements

Once the drag torque has been measured it is possible to proceed with the test for starting the estimation of the machine's parameter. The first one is the test with the motor at no load and in order to achieve this, the slip frequency is set to zero, using the load machine attached to the shaft which can control the speed of the test bench. This test is conducted to a relative high constant speed of 6000 rpm and several points are captured and stored in an excel file. The test is conducted increasing the current from 25 A to 300 A. Looking to *Fig. 2.12* and *Fig. 2.13*, in according to the *rotor flux oriented model*, the range of the current is controlled setting the d-current, in fact in no load condition there is not any current on the q-axis. The reason why we are interested to measure several points over all the current range is because we want to identify the trend of the saturation in the main inductance. Once the test is done the data are imported in Matlab and elaborated using equation 4.5 for calculating the total inductance of the stator. In *Fig. 6.2* it is possible to see the magnetizing curve evaluating the ratio between the stator voltage and current. Importing the excel file, the values are also filtered taking into account some constrains as the torque, supposed to be always zero, the voltage and current value supposed to be comparable with the simulated one and other signals of sensor failure in the measuring process; those points are plotted in red in the figure. In *Fig. 6.3*, instead is showed the trend of the calculated

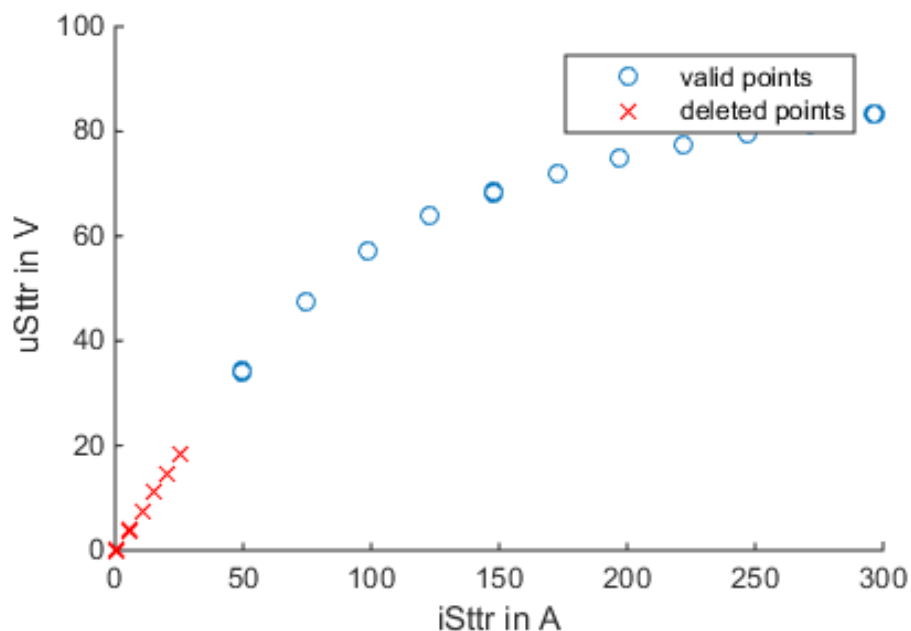


Figure 6.2: Magnetizing curve from No Load test.

stator inductance.

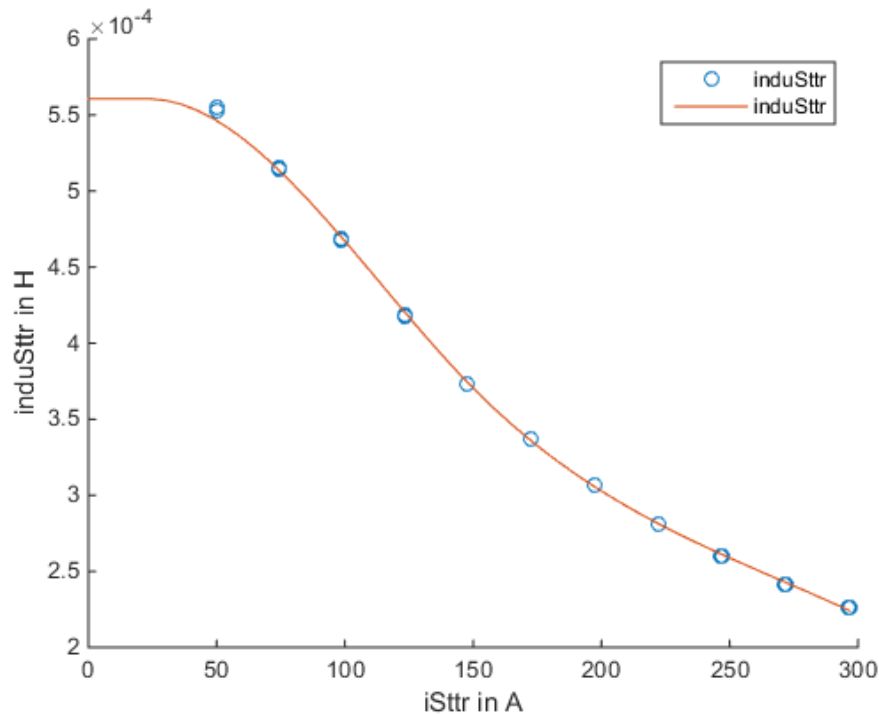


Figure 6.3: Stator inductance calculated from No Load test.

Short circuit analysis

For this test the motor is kept in standstill fixing the speed at the shaft to zero. The two control parameters are the current and the frequency. Changing the current is still possible to take into account the saturation, instead with the frequency is controlled the current which flows in the branch of the main inductance, thus for understand the influence of the frequency on the quality measurements, the test is conducted with different set frequencies: 10.5 - 25 - 50 - 125 Hz. Once all the four measurements are done, the excel files with the results are imported together and elaborated referring to the equations seen in 4.4 for calculating the rotor resistance and the stator-rotor stray inductance. In *Fig. 6.4* and *Fig. 6.5* are showed the results with the measured points at the different frequencies. As is possible to notice in *Fig. 6.4*, the measured leakage inductance varies much depending on the frequency and for example at the lowest frequency we get high influence of the main inductance on the value of the stator and rotor leakage one. On the other side in *Fig. 6.5* at the highest frequency we get a very high deviation of the rotor resistance value from the simulated one, because emerge the skin effect on the bars. This is properly the weakness of the short circuit test, which is not able to identify correctly the parameters. In order to balance the effect of the main inductance and the frequency inside the bar, we decide to choose the results at 50 Hz in order to go further with the analysis; also because the value at that frequency is the closest to the simulated value, which is highlighted in the Figure

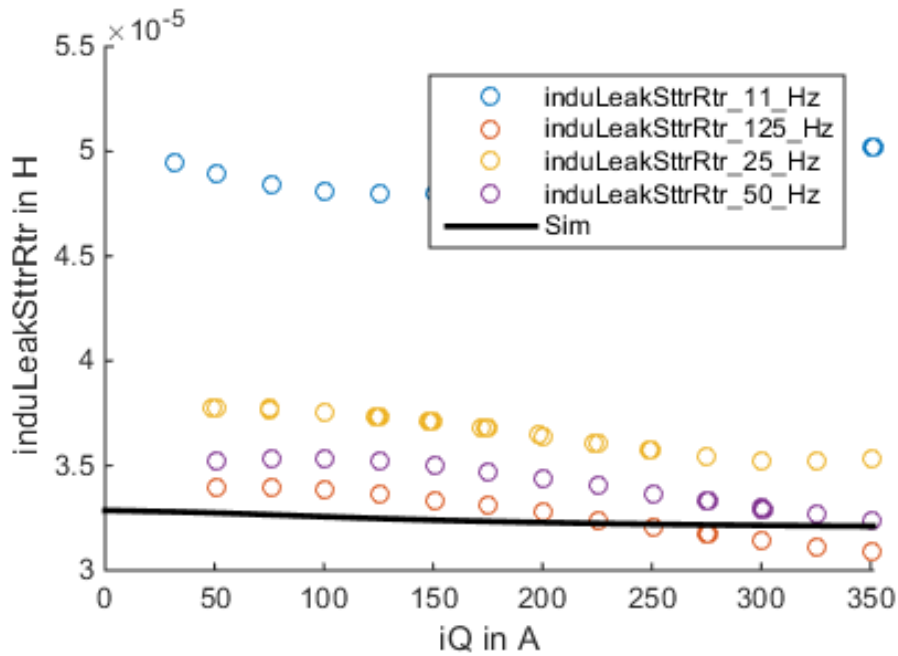


Figure 6.4: Stator-rotor stray inductance calculated from Short Circuit test.

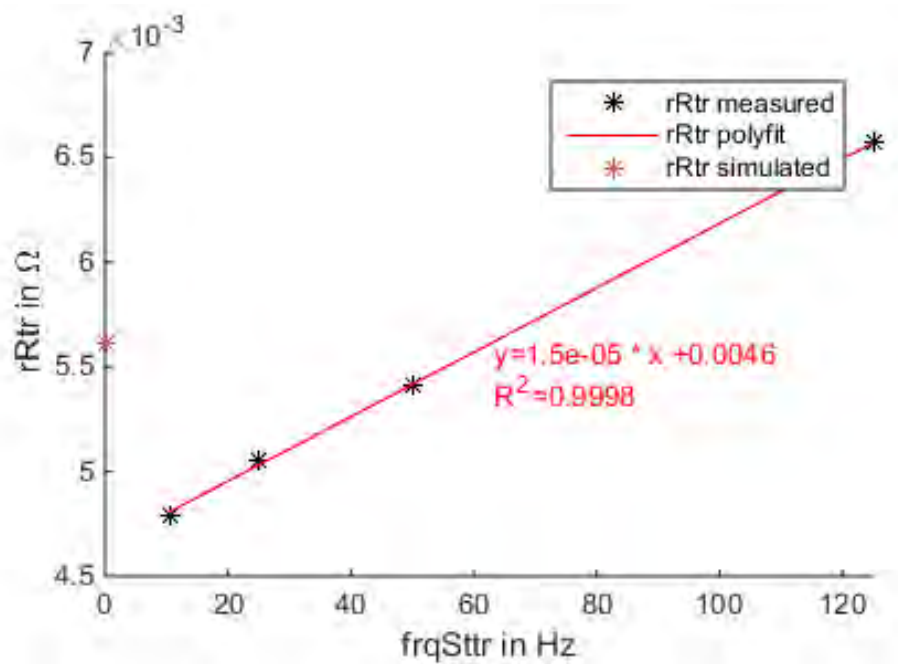


Figure 6.5: Rotor resistance calculated from Short Circuit test.

with a red star at 0 Hz. The value of the rotor resistance, thus, is:

$$R_r = 0.005416 \, \Omega \quad (6.1)$$

and in *Fig. 6.6* is isolated the stray inductance at corresponding frequency.

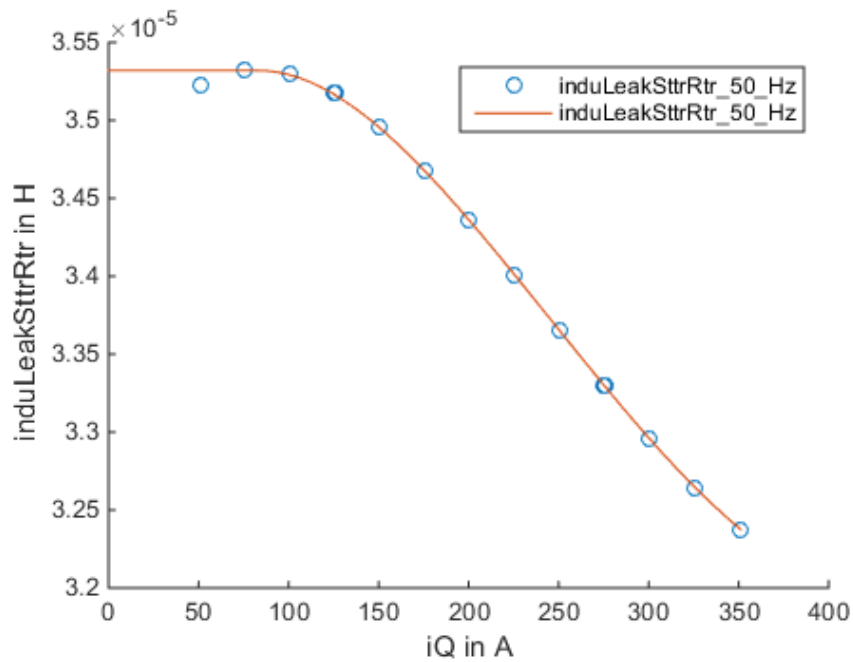


Figure 6.6: Stator-rotor stray inductance at 50Hz.

No load and Short Circuit parameters calculation

After have picked up all the results from the first two test and have imported them in Matlab we are ready to elaborate them in order to extrapolate the three inductances of the machine: this procedure is just a matter of model transformation, in fact we have got the sum stator inductance and the stray inductances, therefore imposing a third condition is possible to calculate the model's parameters independently. In *Fig. 6.7* is showed the difference between the No Load and Short Circuit parameters and the real parameters. The leakage inductance of rotor is called $L'_{\sigma r}$ simply because is the real rotor inductance brought back to the stator side. If we define the equation set for the grouped parameters as

$$L_s = L_{\sigma s} + L_m \quad (6.2)$$

$$L_\sigma = L_{\sigma s} + L'_{\sigma r} \quad (6.3)$$

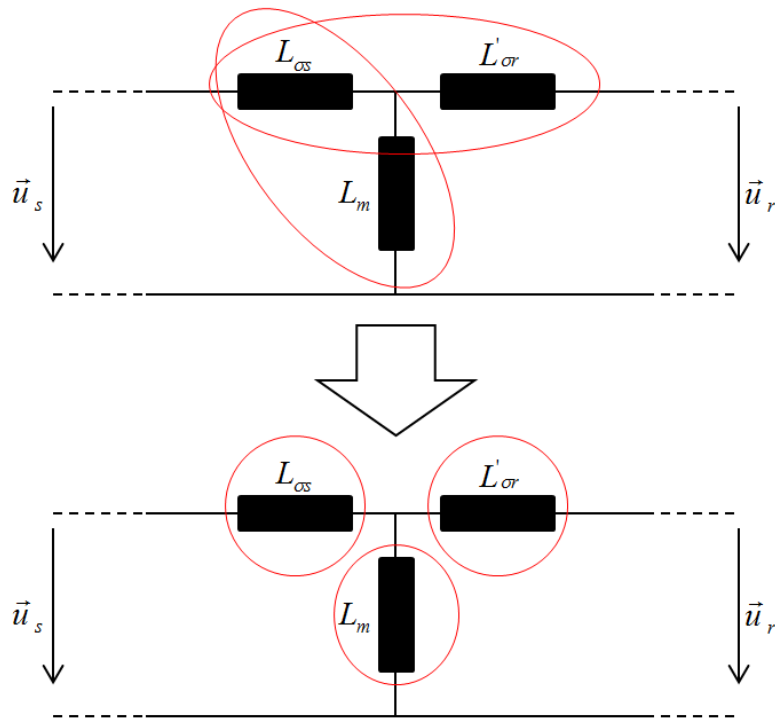


Figure 6.7: Different views of parameter set in the machine's model.

and define also a factor for the stray inductances as

$$c_{\sigma_s/\sigma_r} = \frac{L_{\sigma_s}}{L'_{\sigma_r}} \quad (6.4)$$

The system is complete and it is possible to calculate the three separate parameters solving the equations. The results is

$$L_{\sigma_s} = \frac{c_{\sigma_s/\sigma_r}}{1 + c_{\sigma_s/\sigma_r}} L_{\sigma} \quad (6.5)$$

$$L'_{\sigma_r} = \frac{L_{\sigma}}{1 + c_{\sigma_s/\sigma_r}} \quad (6.6)$$

$$L_m = L_s - \frac{L_{\sigma} \cdot c_{\sigma_s/\sigma_r}}{1 + c_{\sigma_s/\sigma_r}} \quad (6.7)$$

The factor c_{σ_s/σ_r} is estimated from the simulation.

Finally, *Fig. 6.8* shows the extrapolation of the main inductance identified by No Load and Short Circuit test compared also with the value from the simulation; the saturation is equal but we have a little difference at low d-current, about 5%.

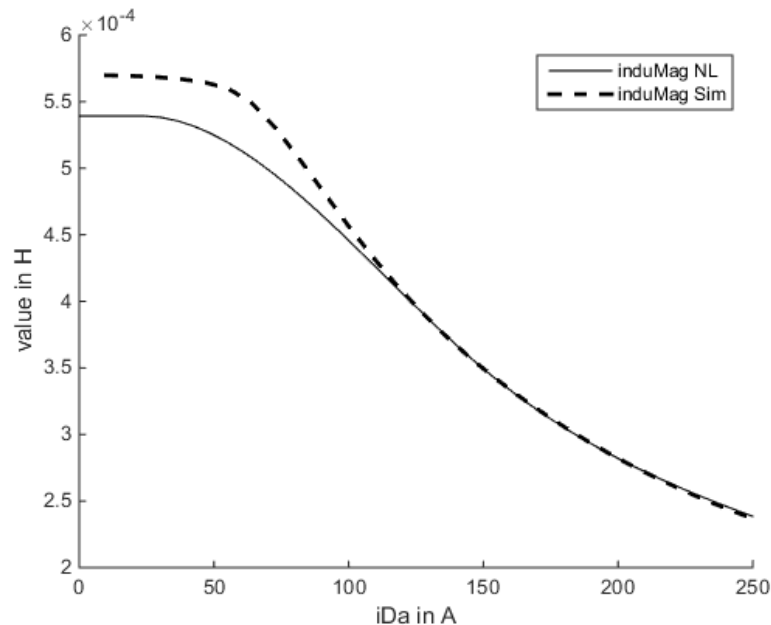


Figure 6.8: Main inductance identified from No Load and Short Circuit test.

As we have seen in Sec. 3.3, the identification of this parameter is much relevant for the control of the motor, however in this case we are able to find out only a dependence from the d-current and we are obliged to save those values as constant for each level of q-current inside

the look up table of the software at the test bench. We expect to get a good comprehension of the dependency from the next procedure we have introduced in Sec. 4.5.

DQ map analysis

So far, the test done are state of the art; thus it is allowed to go further and try to test the proposed procedures and compare the results. The first map supplied on the test bench is at 3000 rpm and it is created using the tool presented in *Fig. 5.7*, taking into account the physical constrains at high d-current. The testbench has about two hundred points to measure and since the stator and rotor temperature has to be kept inside a defined range of 60°C - 100°C it is necessary to insert a break every couple of points measured in order to allowe the cooling system to decrease the temperature, because we have current peak over 400 A supplied to the motor and the thermal power due to the joule losses in the windings is very high. In *Fig. 6.9* there is showed an example of the complete map generated for the test.

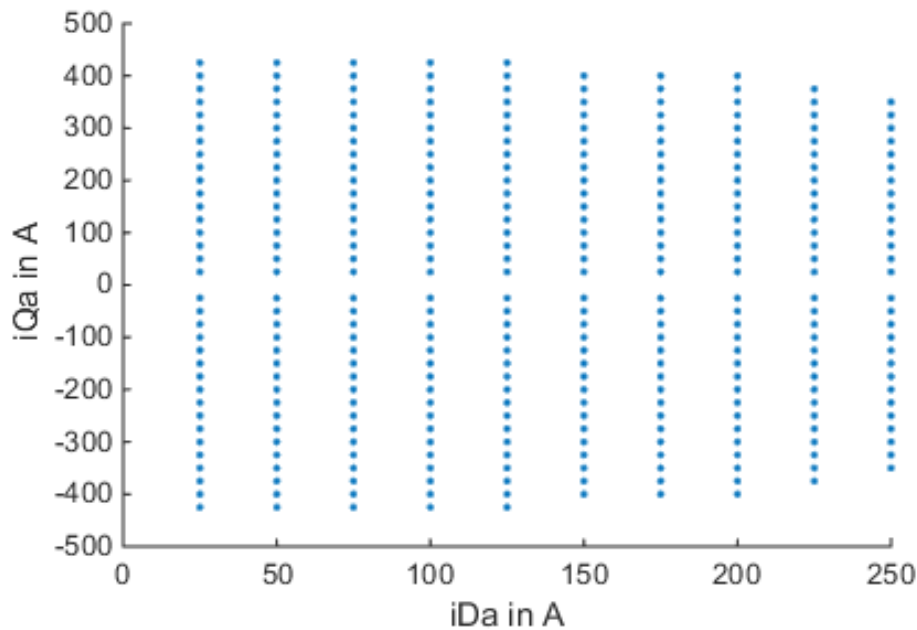


Figure 6.9: Example of DQ set points at 3000 rpm generated by the tool.

The test takes about one hour. After the first test it was found out that the oscilloscope was not well calibrated and the measurements had lot of noise inside. This is the example of how the automation could help the procedure of analysis in fact, instead to make the test twice, if we were able to have a real-time feedback of the test measurements, we can notice immediately the problems with the oscilloscope and we can interrupt the test and solve the problem.

After the oscilloscope was correctly calibrated and the test has been repeated, we got all the results stored in the excel file. Through Matlab scripts we have imported all the map and picked up the measurements in order to get the correct values and axis values for each variable we need to analyze. During the importing the scripts apply a sort of filter for each

point measured twice, so at the end only valid points are imported and *Fig. 6.10* shows the same map after the test with the not valid points. After this phase it is possible to

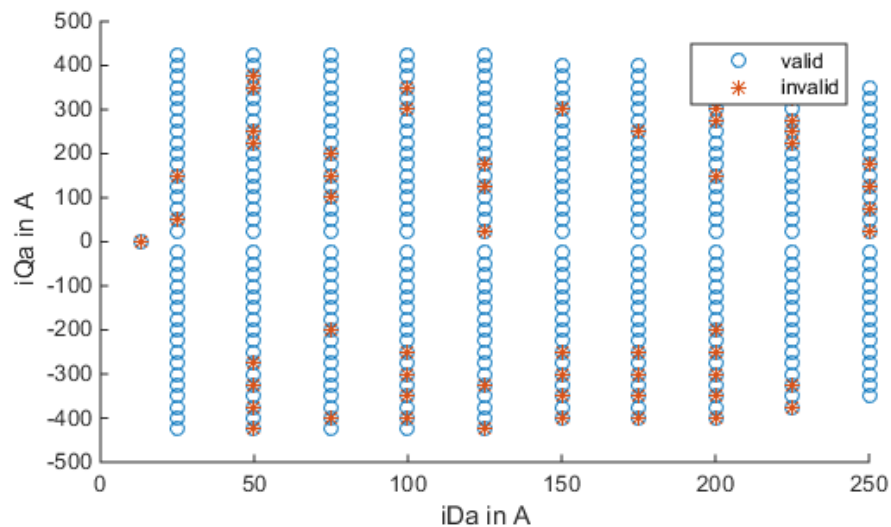


Figure 6.10: Measured DQ-map at 3000 rpm after importing and filtering invalid values.

proceed with the calculation of the parameters by the Eq. 4.11-4.16-4.17-4.18. the scripts recognize all the couples measured values and elaborate the equations. In this case we get the inductances in function of d and q-current and we expect a modified shape of the main inductance compared to the one showed in *Fig. 6.8*. *Fig. 6.12* shows the main inductance calculated from the DQ-map for different constant value of q-current: as is possible to see, the values tend to saturate in the same way and they are feasible with the calculation from No Load and Short Circuit, but at low d-current there is a little variation towards different values of q-current and the overall value of the inductance in general is higher than the inductance of the No Load test and the simulation. The difference in the results that we have got, introduce us to consider an interesting problem: the not linearity of the inverter. The issue consists in a distortion of the input signal to the inverter and its output which is supplied to the machine and the reason of this signal mutation is mainly due to two well known phenomenon (cmp. [ML99]):

1. IGBT voltage drop;
2. Dead time.

The first problem is itself defined by the hardware components of the power electronics, while the second one is caused by the time shifting, necessary imposed in order to avoid short circuits between the bridges of the same phase inside the inverter. Both the effects lead, however, to a phase shift and an amplitude drop of the reference signals feed to the inverter, as shows in *Fig. 6.11*.

Therefore, aware of this existing issue, when we exploit measurements in the synchronous

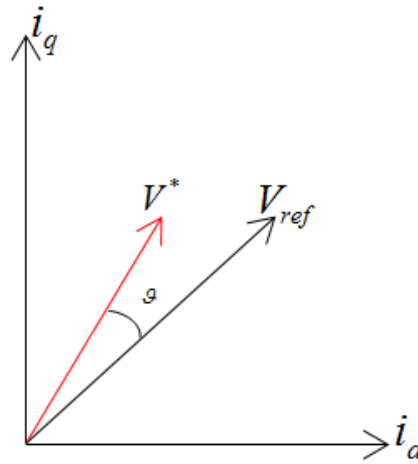


Figure 6.11: Effect of the non linearity of the inverter on the reference signal.

reference frame for the parameter identification, the results are affected by the error due to the inverter and this is the reason of the high value of the main inductance. Developing a script, which simulates the voltage and time shift compensation, it is possible to notice which is the sensitivity of the main inductance to this issue. *Fig. 6.14* shows the results. It is clear how the error due to the inverter affects considerably the shape of the inductance in the not saturated area, where the voltages are very low and is possible to find a combination of both the compensation factor which makes the main inductance calculated from the dq-map very similar to the simulated one. Finally, *Fig. 6.13* presents the trend of the stray inductance of rotor calculated from the map. This parameter is not much sensitive to the problems given by the inverter as is the main inductance, however, as it is possible to see the value is much smaller at low d-current and this can be due to the skin effect, in according with *Fig. 3.4*. The results from the calculations are picked up and collected in look up tables ready for be loaded inside the testbench software; but before to procede with the measurement of new dq-maps and check the quality of the calculation, we try to validate the rotor resistance tuning explained in Sec. 4.6.

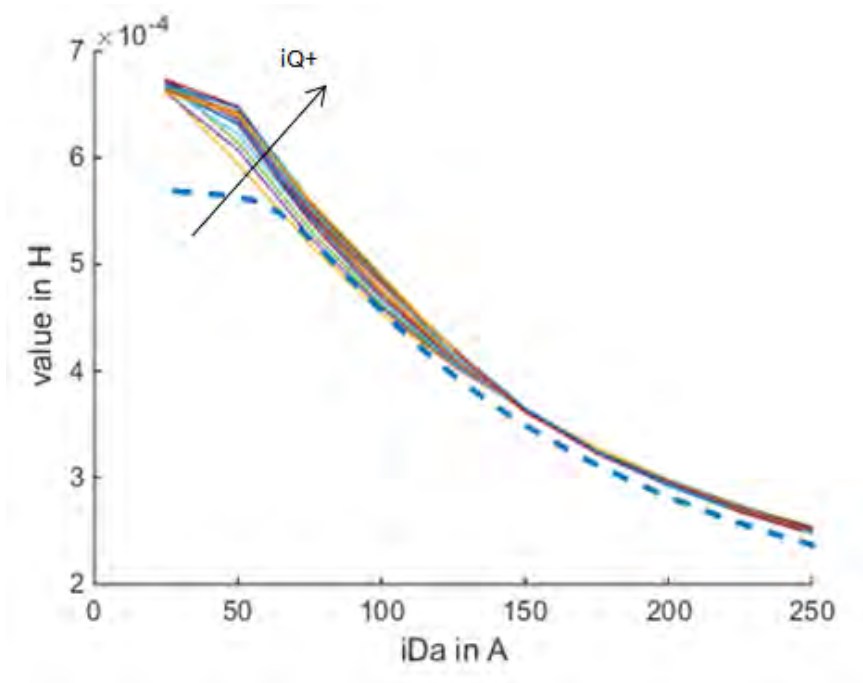


Figure 6.12: Main inductance calculated from the DQ-map.

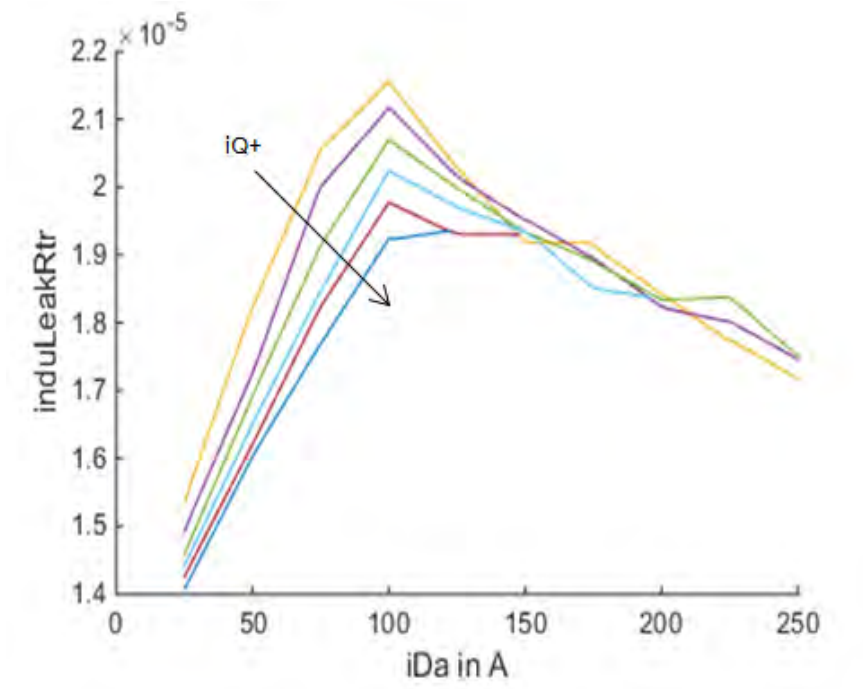


Figure 6.13: Leakage inductance of rotor calculated from the DQ-map.

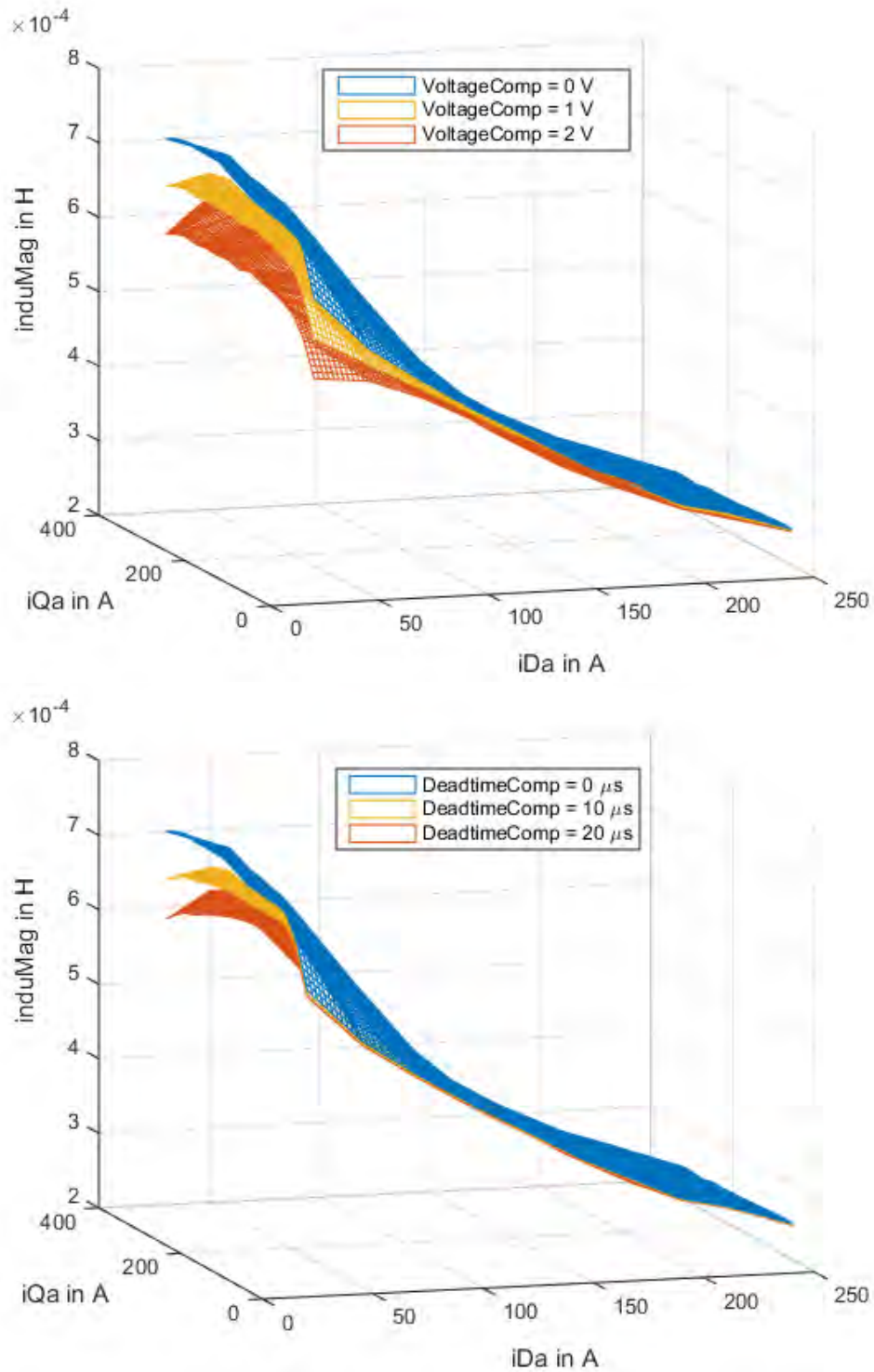


Figure 6.14: Simulated compensation of the inverter voltage drop and time shifting.

Rotor resistance detection

This test is very fast and is done manually on the test bench controlling the current input. On a screen is prepared the oscilloscope analyzer ready to display the set and estimated in the controller q-voltages. Varying the value of the rotor resistance from $5.6 \text{ m}\Omega$ to $7 \text{ m}\Omega$, the comparison between two signals is stored at each d-current impulse and at the end all the images are analyzed in order to see for which value of rotor resistance the trend of the two voltages is completely equal. In *Fig. 6.15* is showed a chain of impulses supplied to the motor with the relative voltages response and in *Fig. 6.16*, *Fig. 6.17*, *Fig. 6.18* is showed the detail of three responses: the first one is with a too low rotor resistance value, the second one is with a too high rotor resistance value and the third is the most accurate voltage response in which the trends are almost completely overlapped. The value of the corresponding rotor resistance is $6.4 \text{ m}\Omega$: the value is much higher compared to the value identified from the Short Circuit test, but in order to understand the validity of the procedure is necessary to upload this value in the software as the value of rotor resistance at $20 \text{ }^\circ\text{C}$ and measure a new map.

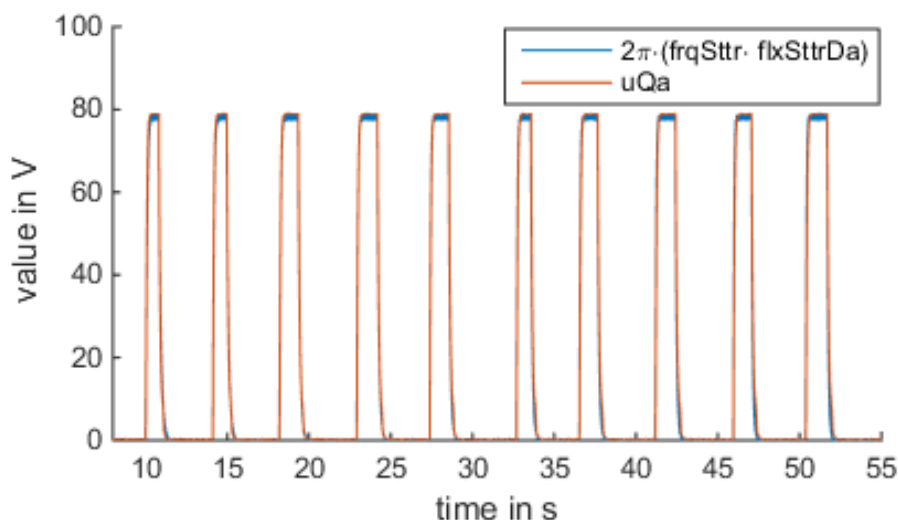
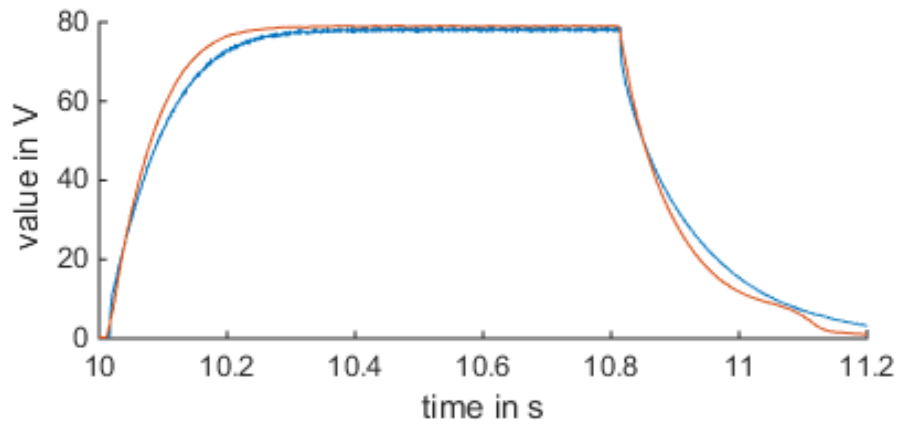
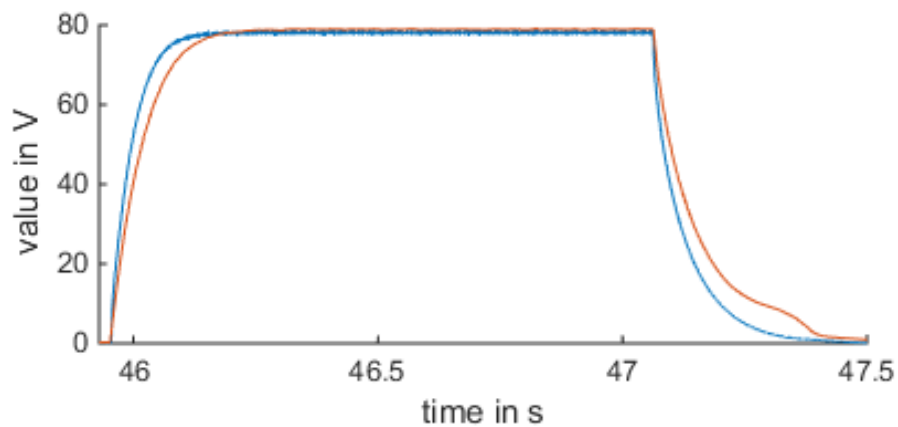
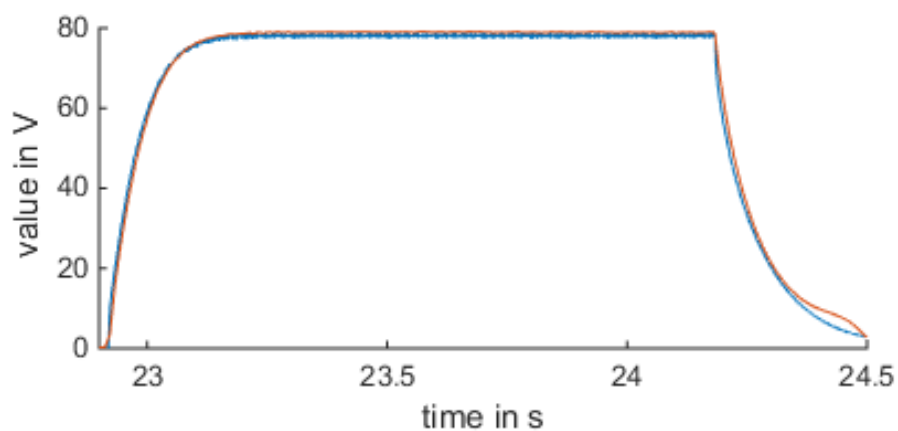


Figure 6.15: Voltage responses to the impulses for the rotor resistance identification.

In order to minimize also the potentially error due to the gear box, the new map is measured at 500 rpm, considering that at that speed the gear losses are very low and do not affect much the controller; in fact one has to be aware about the fact that between the machine and the torque sensor there is the gear box and it produces losses not predicted and compensated by the controller, as it has been explained in Sec. 4.2.

Unfortunately the quality of the measured map is not high in fact after filtering we have much invalid points and they are deleted from the imported results; however is still possible to analyze the data and understand the effect of the changes done in the software'parameters. *Fig. 6.19* shows the comparison between the measured torque at the shaft and the torque

Figure 6.16: Zoom for the response with $R_r = 5.6 \text{ m}\Omega$.Figure 6.17: Zoom for the response with $R_r = 7 \text{ m}\Omega$.Figure 6.18: Zoom for the response with $R_r = 6.4 \text{ m}\Omega$.

estimated in the controller over the map and the results are pretty bad; in particular at low d-current on the q-current range the two torque diverge much. Definitely those divergence in that part of the map, in according to the trend of slip frequency showed in *Fig. 3.5* is caused by a wrong rotor resistance identification. The error reach the 15% in the upper part of the map. It can be explained looking to the rotor resistance test has been described in this section: when the inverter generate an impulse on d-current it also produces a certain quantity of harmonics at high frequency and thus this harmonic content inside the signal, distorts the real value of the rotor resistance because of the skin effect produced.

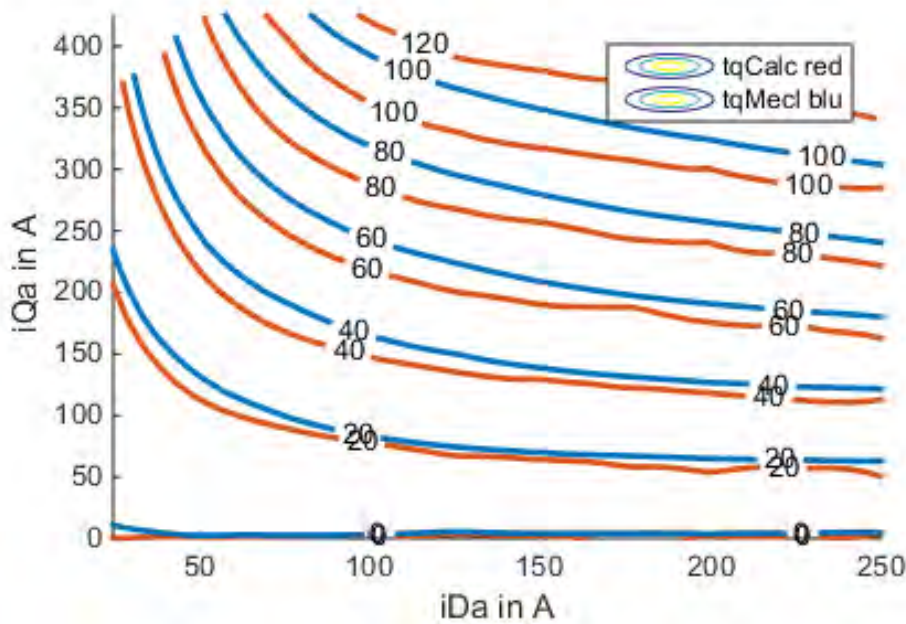


Figure 6.19: Comparison between measured and calculated torque at 500 rpm with $R_r = 6.4 \text{ m}\Omega$.

Parameters optimization and final validation of the procedure

Once the rotor resistance detection test has been discarded from the procedure of analysis, we have implemented the optimization method exposed in Sec. 4.5 and showed, for what concern the rotor resistance, in *Fig. 4.8*. The input data refers to the first measured dq-map presented in *Fig. 6.9*. First the torque error looking in the range of 25-50 A on d-current and 25-400 A for the q-current has to be optimized, because in that range we get the rotor resistance with its complete parametrization of the skin effect and thereafter is optimized the saturation of the main inductance in the range of 75 - 250 A for the d-current. The algorithm are written in Matlab and they elaborate all the results automatically giving as an output the new shapes and values.

For the rotor resistance we get the trend showed in *Fig. 6.20*; as is possible to notice, the optimization algorithm has some problems with the first measured values, because the slip frequency is very low and it runs into some numerical errors which brings the solution to not correct points, but when the slip frequency increases the optimization stabilizes itself and produces an interesting result.

Fitting the points with a least squares method we get a very good parametrization of the rotor resistance and the value considered at 0 Hz, that is the dc value of the rotor resistance, is of 5.6 mΩ, which is perfectly feasible with the results from the No Load and Short Circuit test and also with the simulated one, seen in *Fig. 6.5*. The most important feature of this

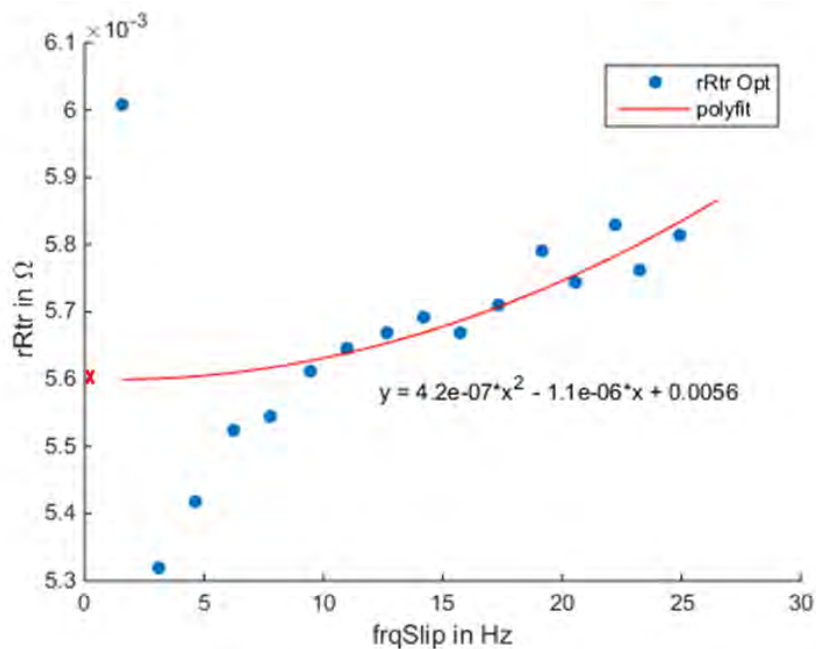


Figure 6.20: Results of the rotor resistance optimization.

optimization algorithm is about its capability to find out a parametrization of the skin effect from the measurements, in fact the gain on the rotor resistance can be directly extrapolated

by the Figure. As far, in the software the skin effect gain was stored as a linear gain function of the frequency, taken out from analytical equations, as the study-case described in Sec. 3.2, but it has never been measured tentatively as the purpose of this method.

Finally, in *Fig. 6.21* is compared the skin effect parametrization estimated from the optimization and the one calculated theoretically, the gain at the maximum slip frequency is incremented to about 3.8%, against the 1.6% of the previous trend, which can be considered plausible since that the theoretical calculation takes into account several approximation in order to get an analytical function for determining the skin effect (see Sec. 3.2).

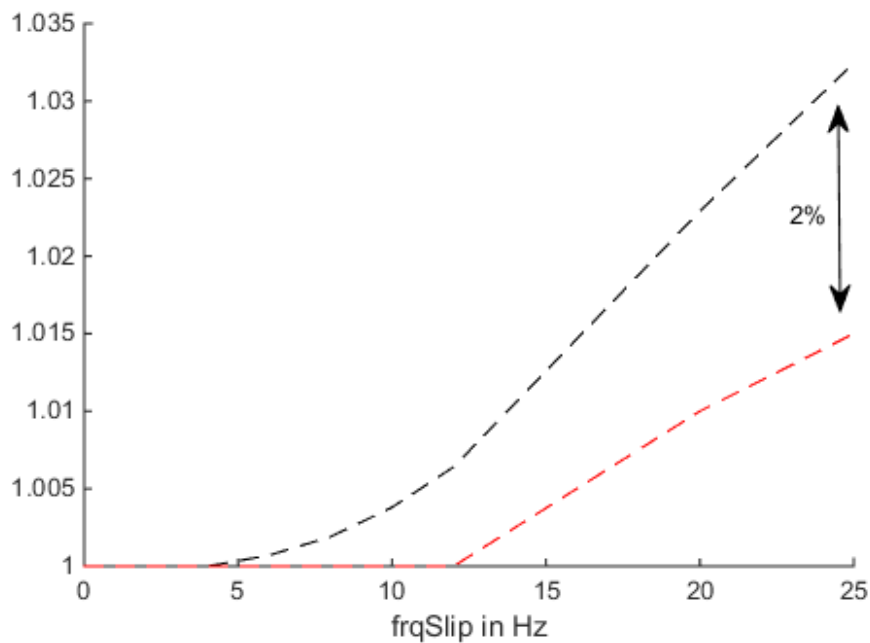


Figure 6.21: Comparison between skin effect parametrization optimized from measurements (black) and analytical (red).

Considering equation 3.13 and the torque error in the right part of the measured map, the main inductance has been optimized iteratively point by point with an algorithm, searching for the value which leads to zero error and the result is presented in *Fig. 6.22*. The difference between the two lines shows that the saturation is about 5% deeper then the previous main inductance (*Fig. 6.12*). After that the optimized piece of main inductance has been merged

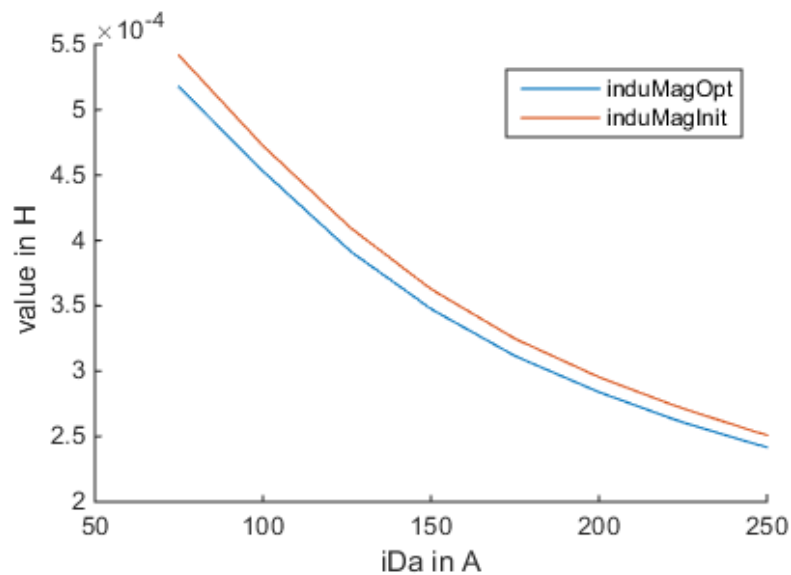


Figure 6.22: Main inductance after optimization.

through a linear overlapping to the original one in order to get a complete identification of the parameter above all the map and the final result is showed in *Fig. 6.23* compared to the original. Once all the operations are completed the main inductance, the rotor resistance value and the new skin effect parametrization are exported from Matlab and updated in the software of the test bench.

At the end, in order to validate all the works done on the parameter identification, new maps are measured on the test bench; in particular is measured the first map at 500 rpm and the second at 3000 rpm, in order to make the measurements as free as possible from the effect of gear losses. However, is also possible to completely delete the effect of the gears evaluating the average torque from both motor and generator motor's operation, since that the losses when the torque is positive, subtract themselves from the calculated torque in the software, instead when the torque is negative, sum themselves on the torque produced. The scheme showed in *Fig. 6.24* explains the concept. Anyway we are going to show also the behavior in both operations in order to see if there are some asymmetry. In *Fig. 6.25* is showed the torque error of the first measurement with all the parameters updated, at 500 rpm. The results are interesting, because we have got a good match between the iso-torque lines of the calculated torque and measured by the transducer; the error is lower then 6% above almost all the map and the map seems to be very symmetric, signal of a valid parameters identification. Even if at 500 rpm the gear losses should be very low, we also try to estimate

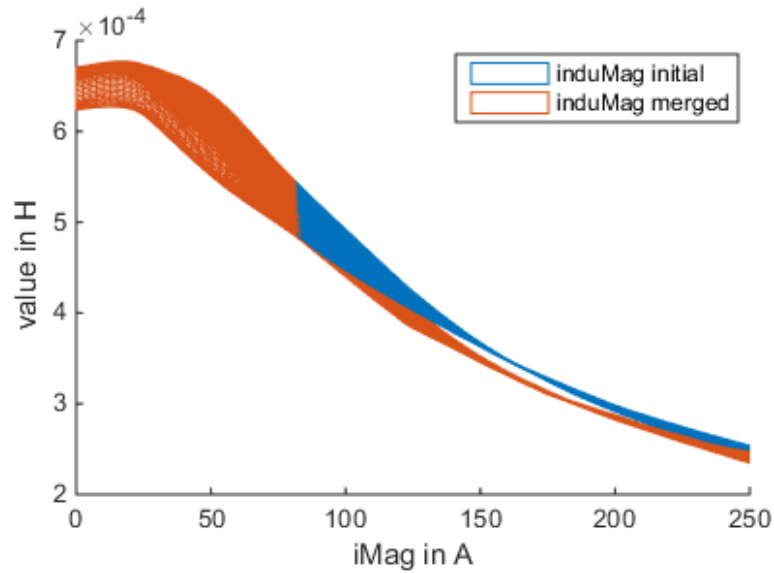


Figure 6.23: Main inductance merged with the original one.

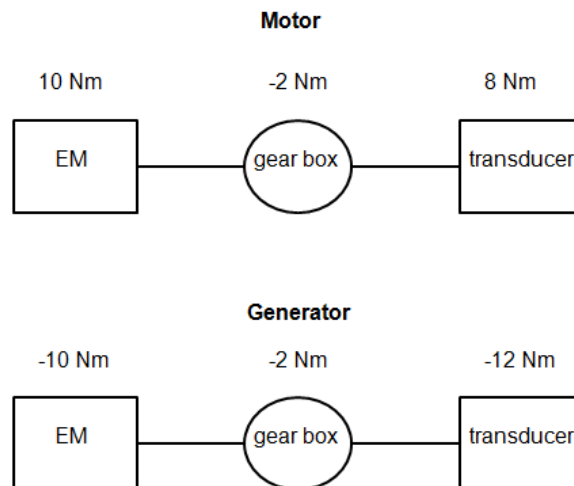


Figure 6.24: Behaviour of the gear losses on the two different operation of the motor.

the torque error considering the average torque error between the two quarter and in *Fig. 6.26* is showed as in the most part of the operative conditions, the error is about 2%.

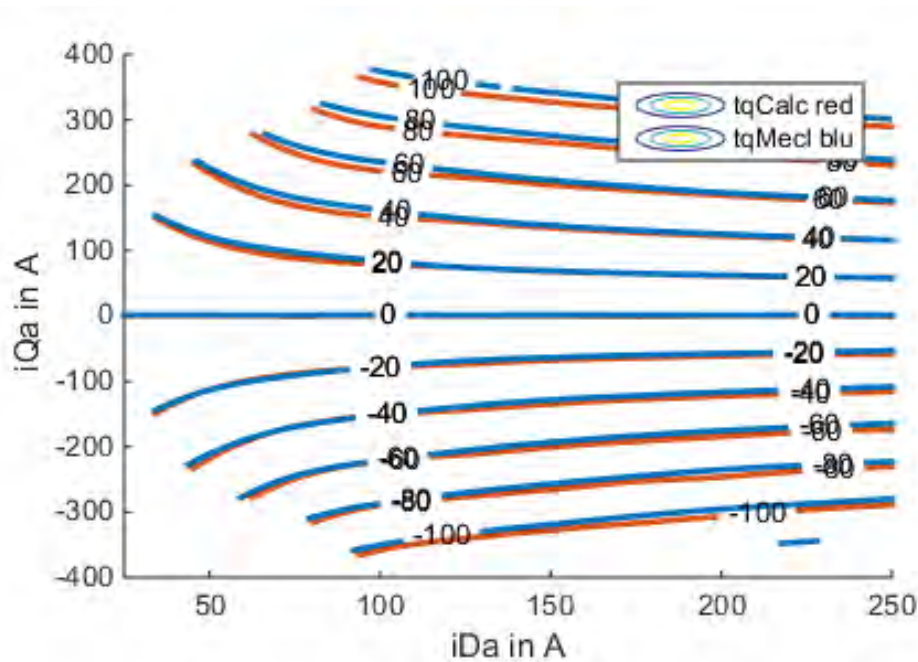


Figure 6.25: Torque error after parameters updating at 500 rpm.

After the first measurement, another at 3000rpm has been done, in order to verify the stability of the parameters increasing the speed and the effect of gear losses. What has been noticed is that the parametrization works well and there is still a good match between the two torque, with an error that do not go over 8% in motor operation, as presented in *Fig. 6.30*, but it creates a sort of asymmetry between the two quadrants and this is much probably caused by the gear losses. Therefore, proceeding with the calculation of the error trying to neglecting the effect of the gear we can see in *Fig. 6.27* how the torque is compensated and more stable, reducing the error of several percentage points; in fact the error is comparable with the other estimated from the map at 500 rpm.

Finally has been measured two last maps at 6000 rpm and 9000 rpm always with the same procedure, but it is clear that increasing the speed the number of point to measure at high d-current are reduced because of the maximum flux constrain (*Eq. 4.10*). However the results have a good quality and they can be analyzed. For shortness we have reported in *Fig. 6.28* the comparison of the average torque and its error at 6000 rpm and in *Fig. 6.29* at 9000 rpm. Still another time, neglecting the gear losses that afflict the mechanical torque, we got a good torque control response, in fact the error does not go over 6%. Even if the error is limited and in a good range, we can observe that it tends to increase with the speed, the reason can be due to many factors as the current sensors error, or temperature variations in the two operation. In any case the method has been validated through all those test and

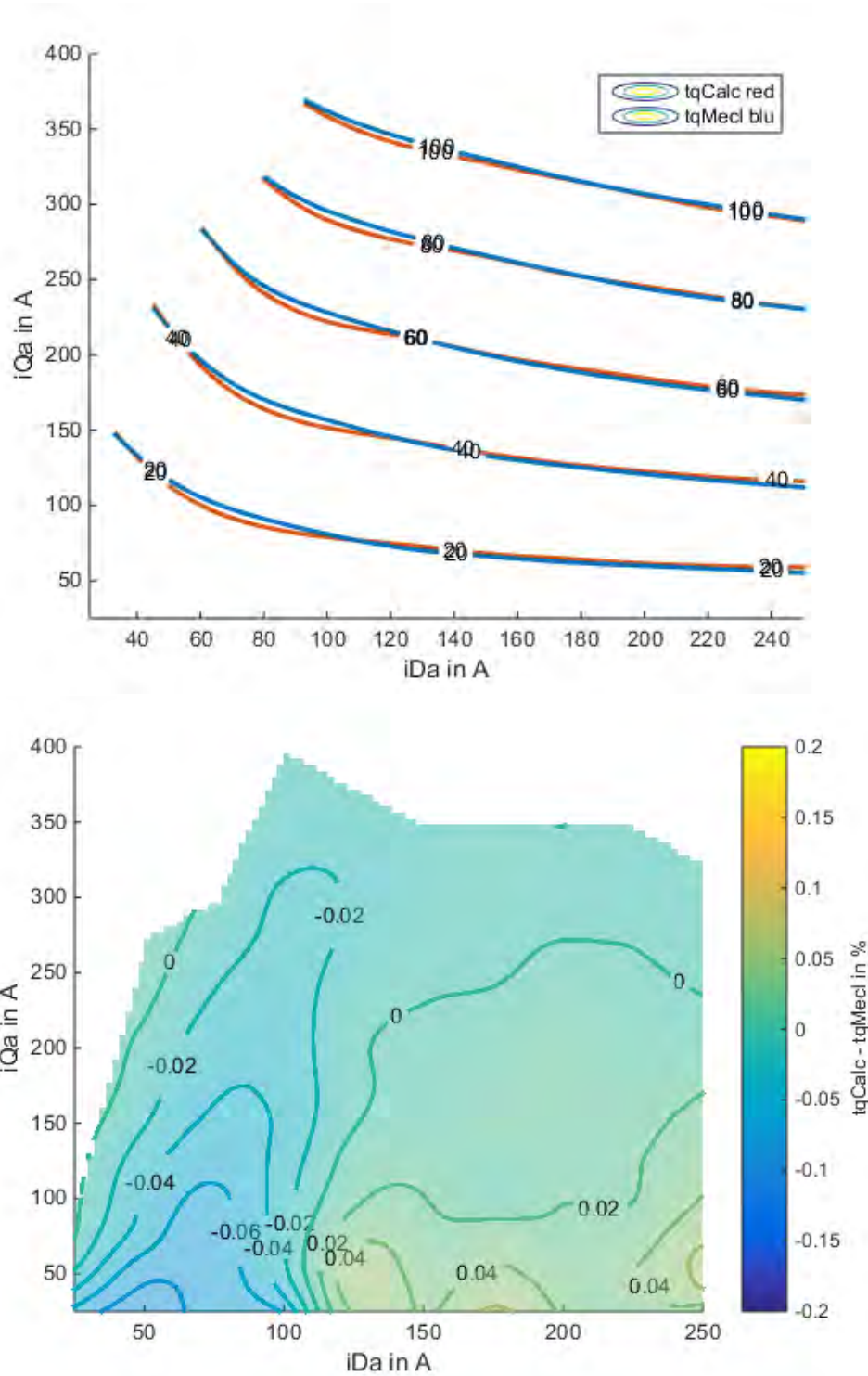


Figure 6.26: Map of the torque error neglecting the gear losses taking into account the average value between motoring and generating at 500 rpm.

the results can be considered positive for what concern the parameter identification, in fact the torque control seems to be stable and robust in a large range of speed.

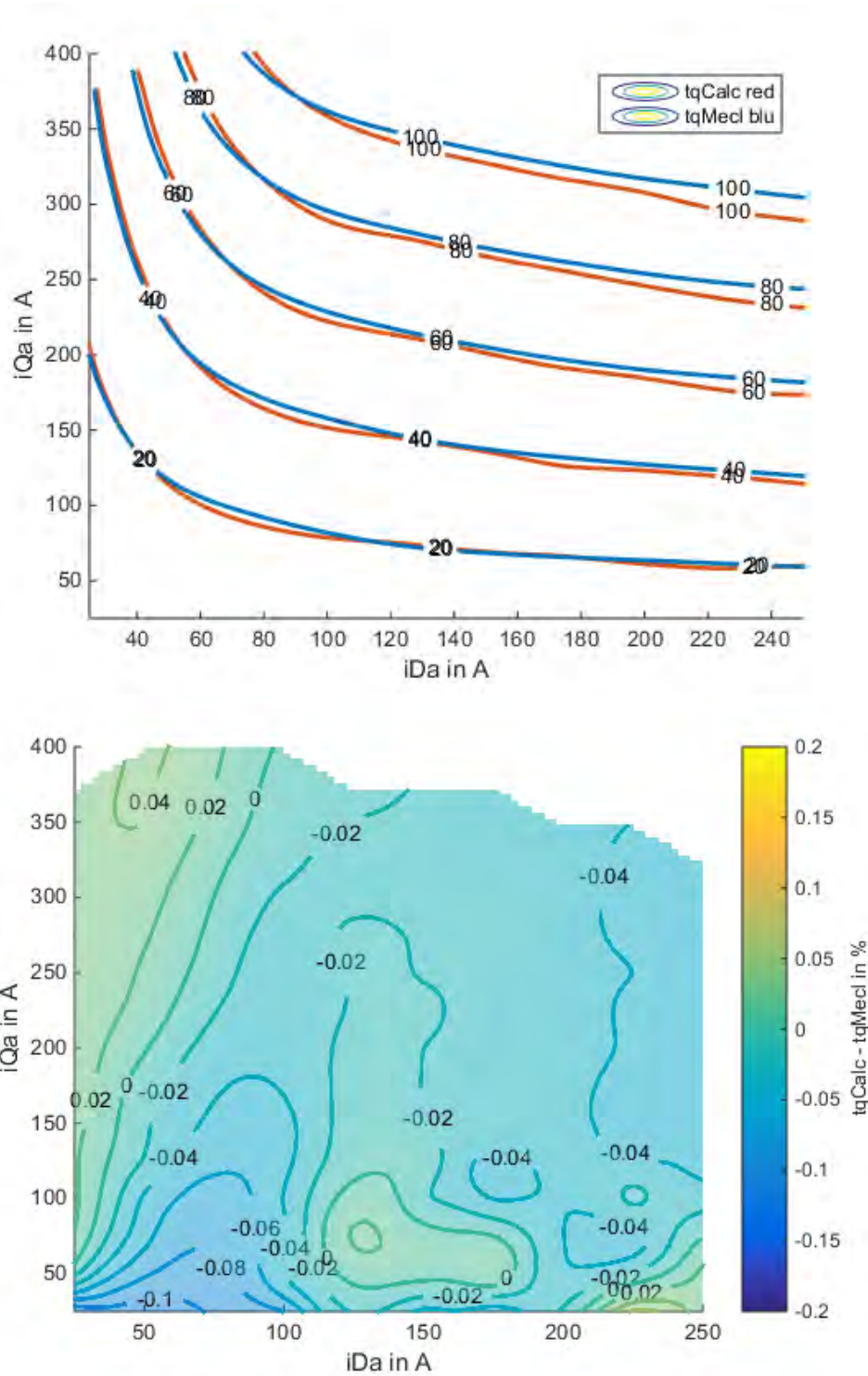


Figure 6.27: Map of the torque error taking into account the average value between motoring and generating at 3000 rpm.

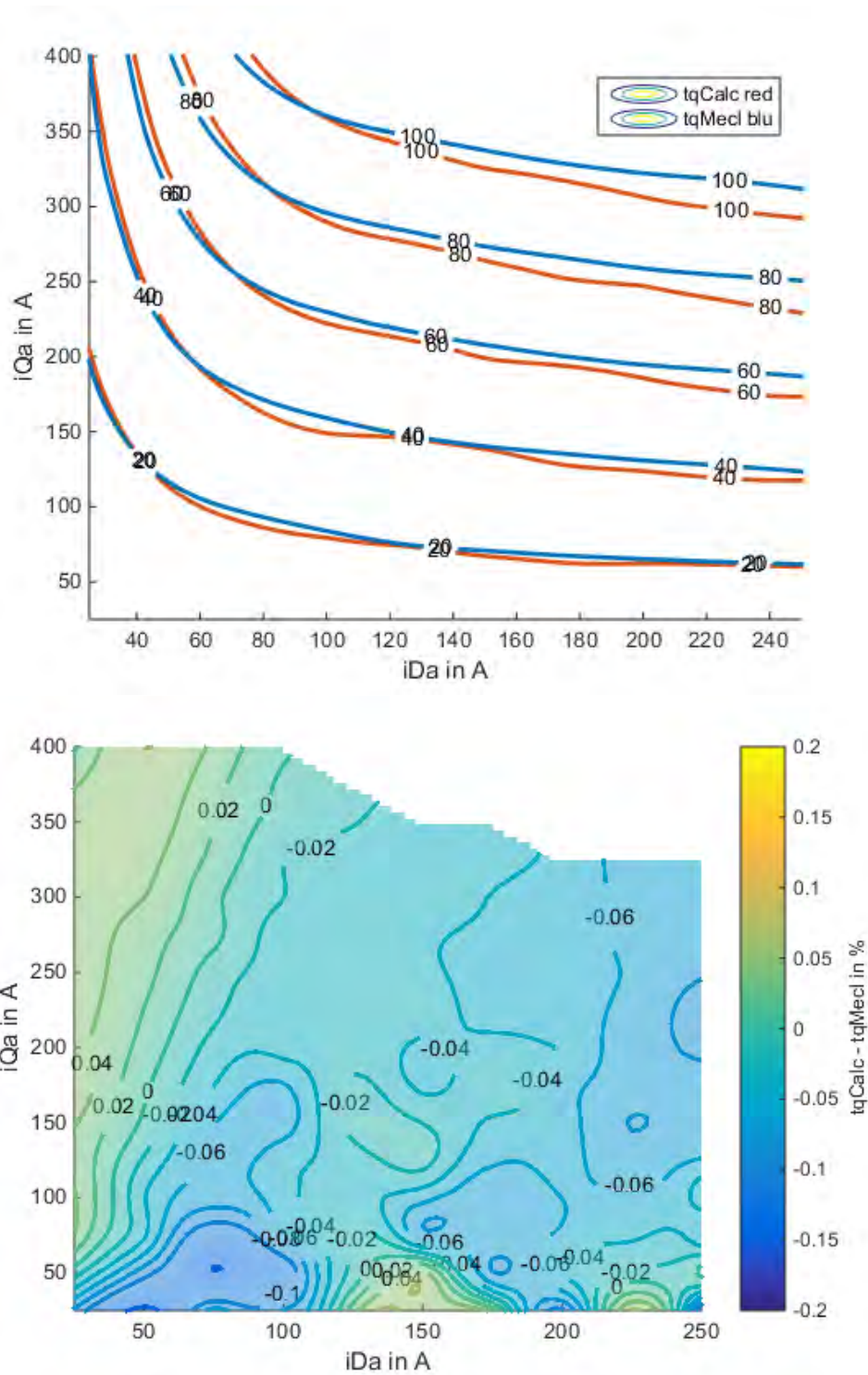


Figure 6.28: Torque error at 6000 rpm with mean values.

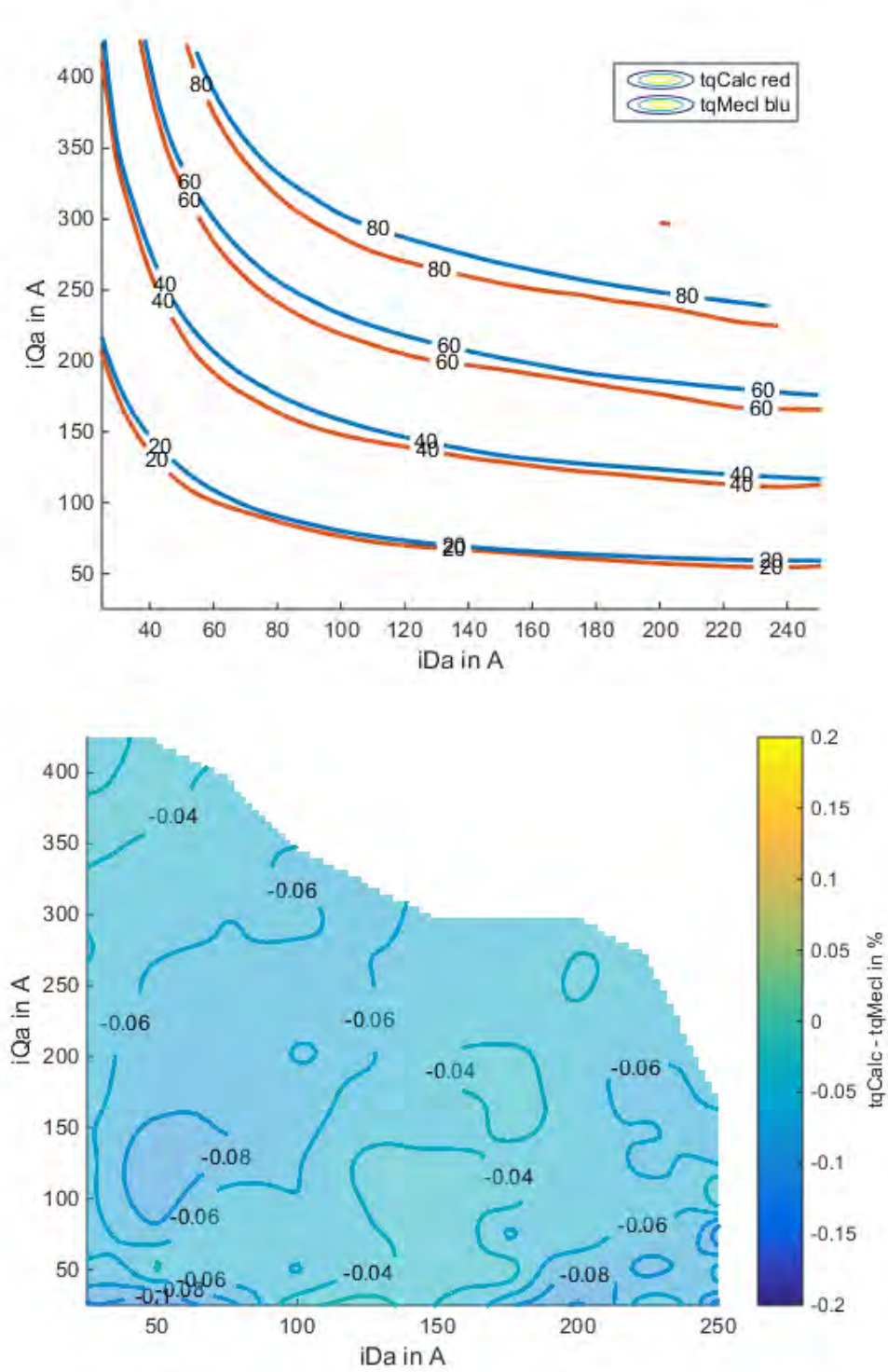


Figure 6.29: Torque error at 9000 rpm with mean values.

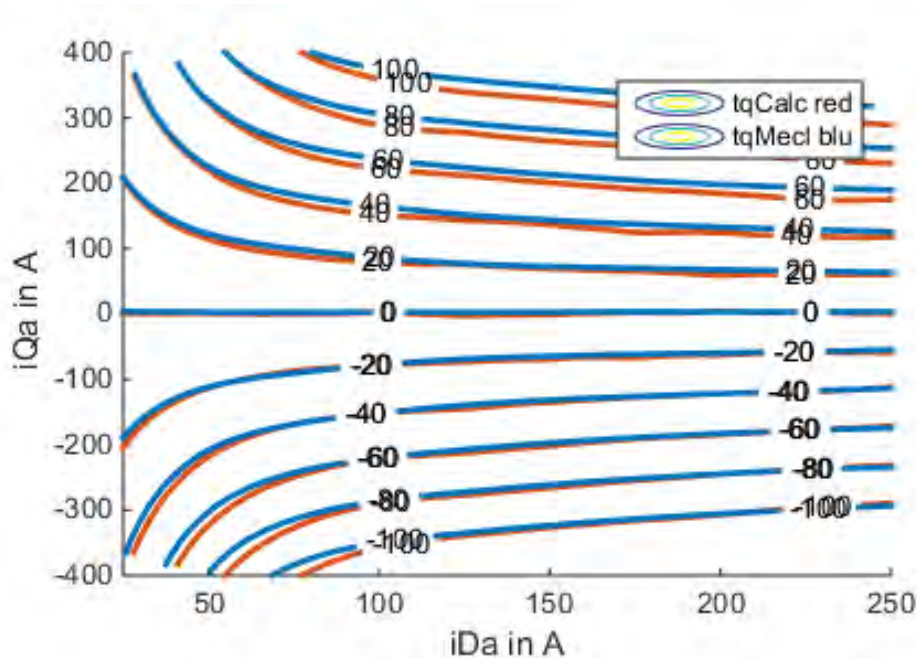


Figure 6.30: Torque error at 3000 rpm.

Estimation of the asymmetrical losses

Looking to the results presented in *Fig. 6.30*, also if the error is very low, it is possible to notice an increase with speed and a certain level of asymmetry between motoring and generating side. Therefore, what is happening, is a sum of two not predicted effects which affect the mechanical torque and increase the error compared to the calculated one. We have already spoken about the gear box and if we refer to *Fig. 6.24* is clear as the gears, increasing the speed, generate an opposite effect on the two operation, giving the feeling of this asymmetry, but actually is the torque error due to the gear. The other physical effects which can contribute to the arise of the error are the iron losses; in fact, as we know from the theory, the iron losses have a considerable contribution to the total losses at high speed (cmp. [CCS96]). Since that the controller on the test bench is not optimized for the iron losses compensation, the error is also given by them. We have decided to call the sum of those two effects *asymmetrical losses*. Analyzing the data, thus, it is possible to extrapolate those losses and the idea is to exploit the knowledge of the theoretically iron losses from the simulation for finally find out the contribute to the error given by the gear. The method consists of:

- Subtract the average value of the mechanical torque to both the motoring and generating mechanical torque;
- Multiply the result with the respective speed considering the different speed dq-map;
- Estimate the total iron losses from the simulation;

- Calculate the pure gear losses from the asymmetrical and simulated iron losses.

Accomplishing the first point we discover that the asymmetrical losses are distributed in the same way in the two quarters and this gives a proof that the gear affect the motor identically in motoring and generating as it was expected; in particular in *Fig. 6.31* and *Fig. 6.32* is presented the overall behavior of the asymmetrical losses on the speed-torque map. The calculations come from the dq-map, but they are converted in a torque speed map, which is much more useful in order to understand the influence above speed. As is possible to notice, it has been added a new dq-map at 12000 rpm which allowed to calculate the losses till that speed. At maximum speed we get about 5 kW of losses and this power is split as

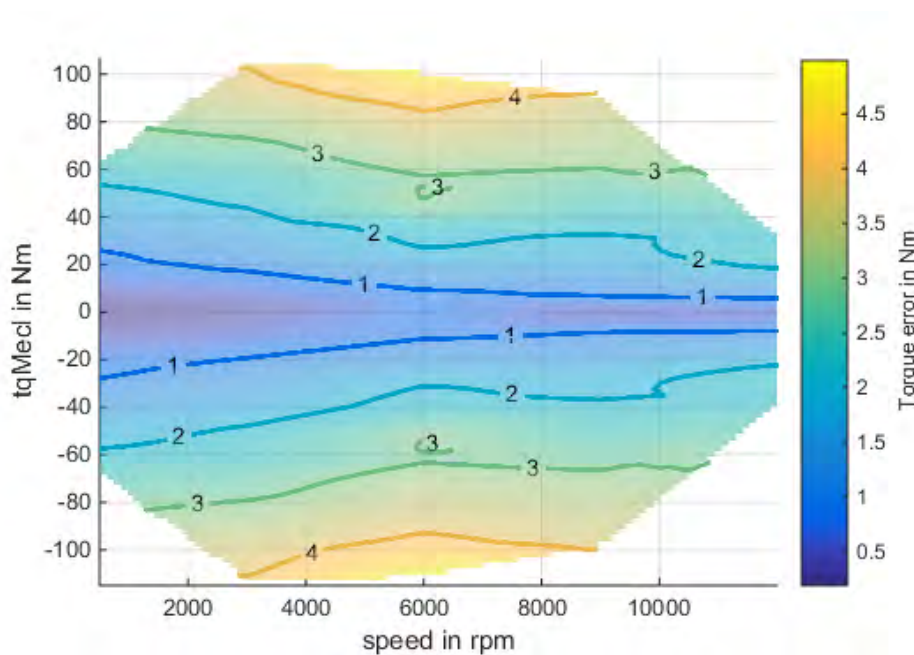


Figure 6.31: Torque error due to the asymmetrical losses.

follow:

$$P_{Loss}^{asym} = P_{Loss}^{gear} + P_{Loss}^{Fe}$$

Therefore, calculating the simulated iron losses in each measured point we can subtract the power and obtain the losses due to the gear; *Fig. 6.33* shows the theoretically iron losses and *Fig. 6.34* shows the estimated gear losses. We recognize that at high speed in this case the gears generate more losses than the iron, at about 20% more; but we cannot be sure about this because the iron losses are not measured directly on the sample. For validating the calculation we can, moreover, estimate the overall gear efficiency taking into account the

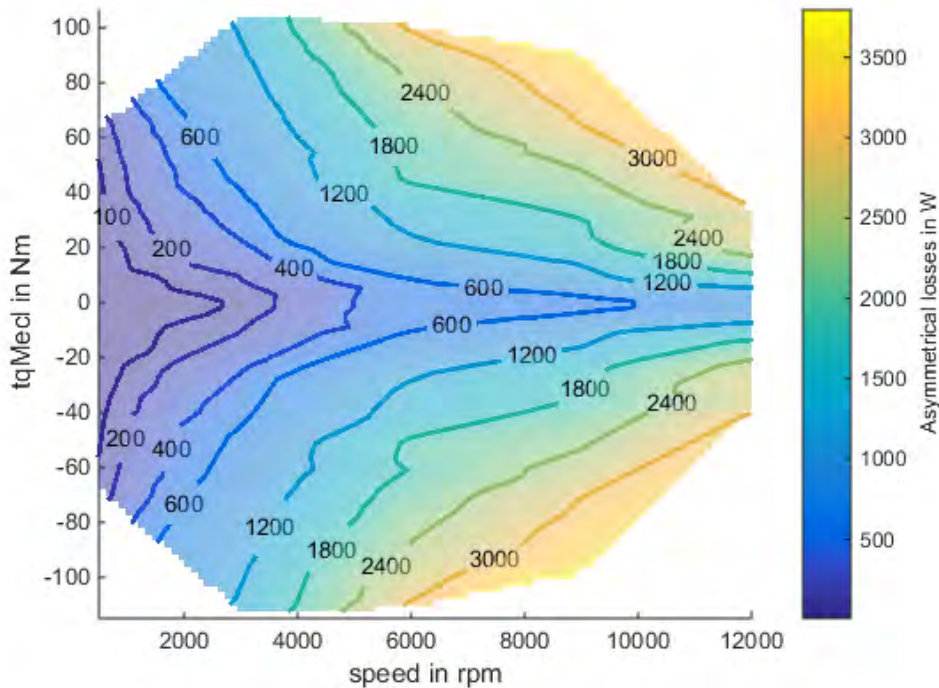


Figure 6.32: Asymmetrical losses in terms of Watt.

mechanical power, in fact

$$\eta_{gear} = \frac{P_{mecl}}{P_{mecl} + P_{gear}}$$

As result we get a mean efficiency over the map in the range of 97% (*Fig. 6.36*), which is compatible with the real performance of the gear box.

Perhaps in the future this map can be exploited for create a more accurate torque compensation, compared to the drag torque test showed in Sec. 4.2. As far, all the information we got and have documented here come from an unique test, the dq-map; thus, if this procedure will be validated further with other motor samples, it can substitute the classic test and gives much more information and feedback to the user, compared to No Load and Short Circuit test. In the next section the motor is going to be tested completely in order to check the overall performance.

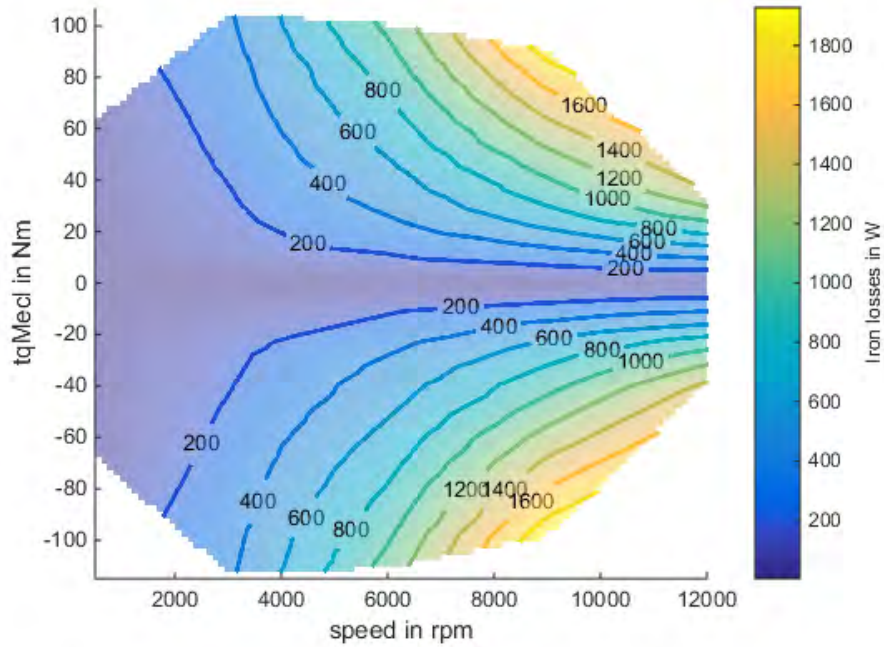


Figure 6.33: Estimation of total iron losses from simulation.

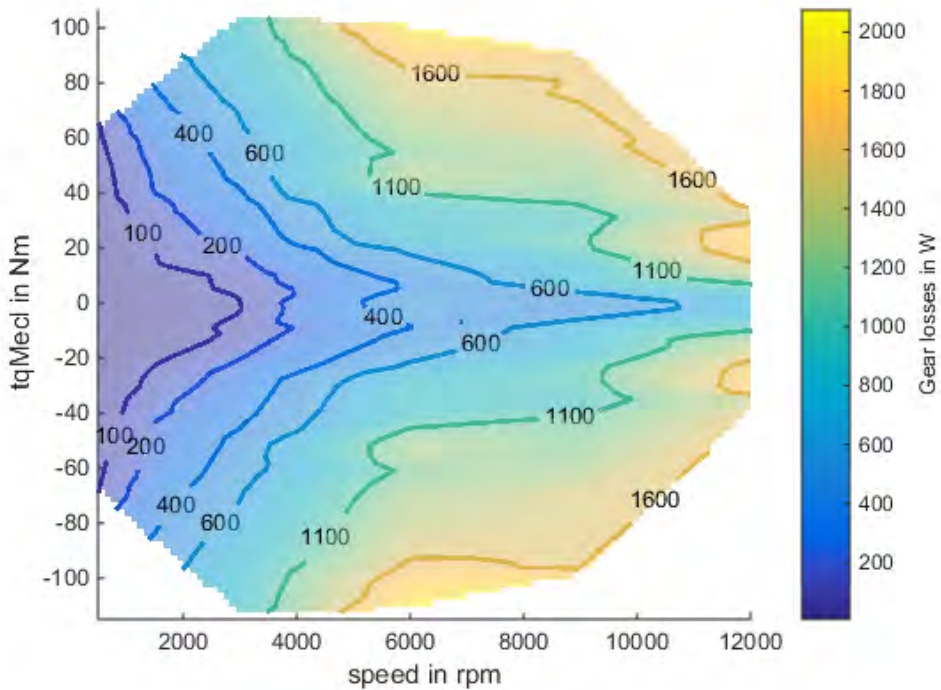


Figure 6.34: Calculation of pure gear losses.

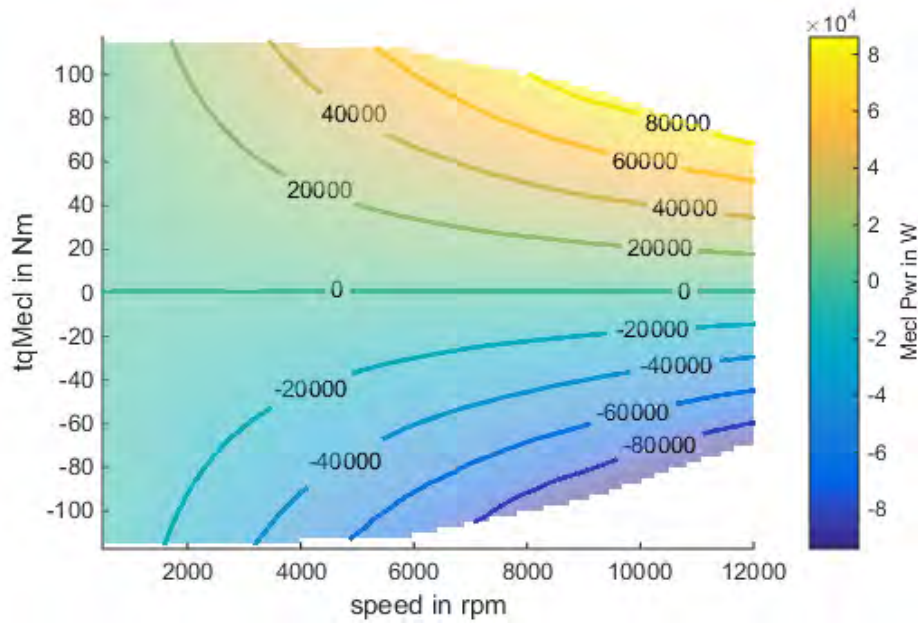


Figure 6.35: Mechanical power above the map.

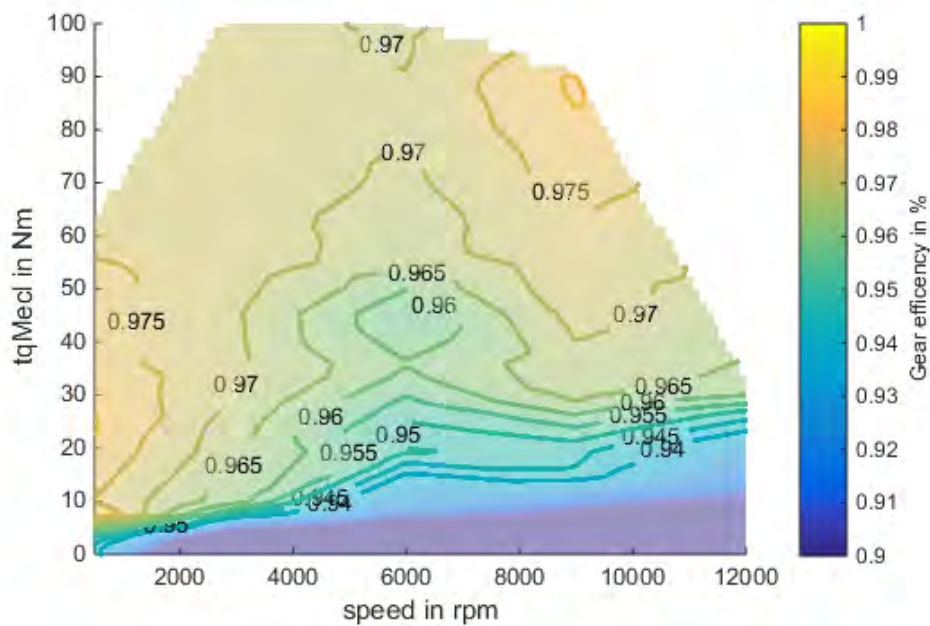


Figure 6.36: Overall gear efficiency.

nTq measurements and E-drive performance validation

As a final measurements we are going to document the nTq-maps and evaluate the overall performance of the complete E-drive comprehending the inverter and the machine. Also for this kind of test, the set point are generated with the interface developed but in this case, at the contrary of *Fig. 4.10*, we set the power limit for all three step voltages at 70 kW; this means that also at the maximum voltage, at high speed the test bench is not allowed to increase the power over the threshold, although it would be able. From this measurements, basically, it is possible to get as results complete maps about efficiency, torque, currents, voltages, flux of the motor over torque and speed, in fact the set points are maps similar to the one presented in *Fig. 6.37*. In general this test is done for the motor operation and

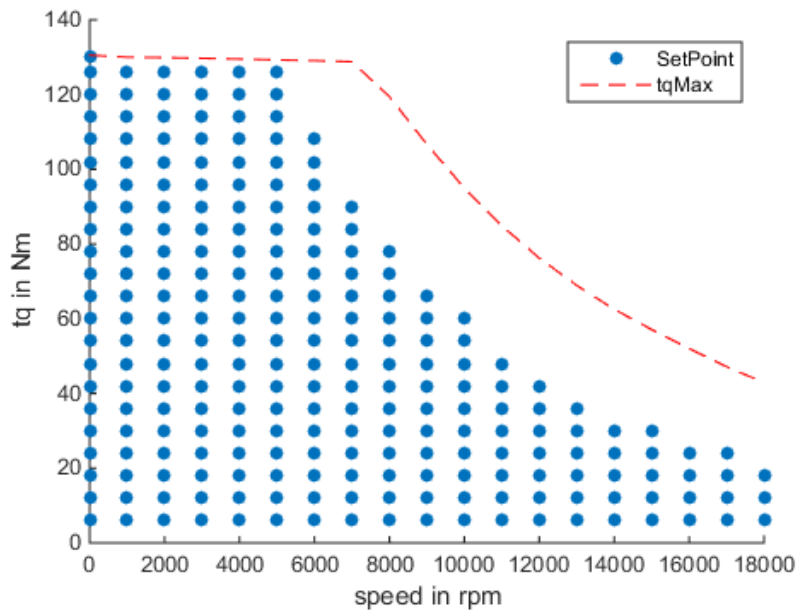


Figure 6.37: Example of a nTq-map generated by the gui.

generator operation in order to analyze the different behavior. Unfortunately, we were able to get a complete map only for the positive quarter; anyway the behavior of the machine has been well analyzed with the dq-map, thus we do not expect any surprise from this test. Finally, as an example of the results, in *Fig. 6.38* and *Fig. 6.39* we present the efficiency of the power train and the torque comparison above the speed. In the figure of the efficiency is interesting to notice the interpolation and the real measured point; this way to analyze the results is very good because allowed to check the quality of the test and the reliability of the interpolation. For what concern the torque error, considering only the motor operation, it is feasible with the results got in the dq-map.

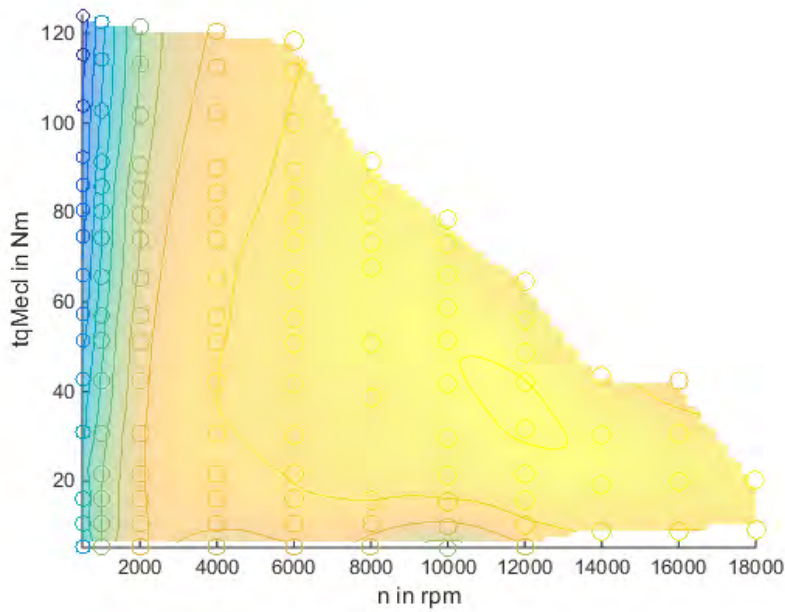


Figure 6.38: Efficiency of the overall E-drive at 260V in motor operation.

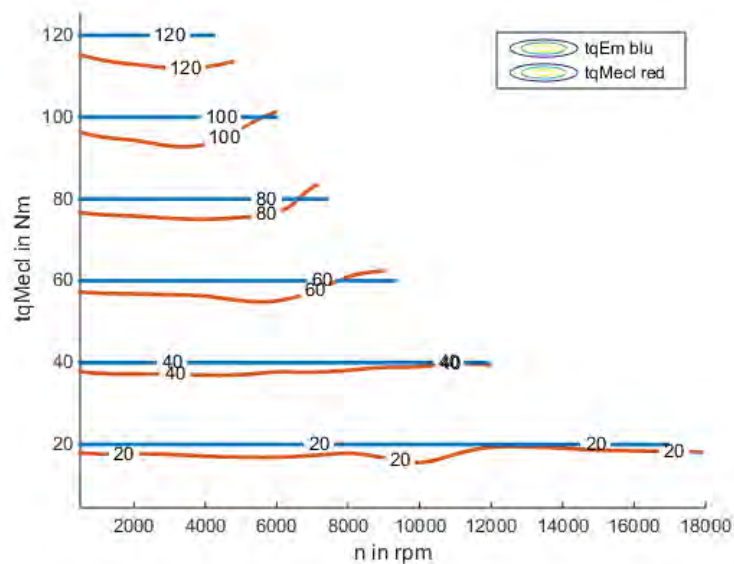


Figure 6.39: Comparison between reference torque and the mechanical response of the motor.

Conclusion

The thesis here developed proposes an interesting analysis of the asynchronous machines for automotive applications, highlighting the most critical issues in the parameters identification on the test bench. The work focuses deeply in regards to the parameters sensitivity and the dependencies which have to be correctly identified in order to get a robust motor control over a wide speed range.

After the analysis it has set up a procedure on the test bench which returns a complete analysis of the motor and its parameters. From the validation of the method we got good responses and we can consider the procedure globally correct, even if there are some limits, as for example the choice of a fixed factor for the ratio between measured stray inductances, taken by simulations and the non linearity of the inverter which causes distortion of the main inductance; however we get a match of parameters with their sensitivities which gives a reliable output torque. Moreover, this procedure is compatible with the requirements of automated measurements concept and therefore, we get benefits also in this way.

Finally, the offline method of calculation offers an alternative procedure to the parameters identification on the test bench and our expectation is that it will be possible to repeat this on other samples getting the same accuracy in order to validate it as a general procedure for the parameters determination.

Summary

- Development of automated setpoint generation for the test (GUI);
- Creation of the Matlab interface for the online measurements validation;
- Sensitivity analysis of the induction machines;
- Development of an automated procedure for induction machine parameters identification.

Appendix

A Motor plate data

Squirrel cage induction machine

- Maximum torque: 133 Nm
- Maximum speed: 18000 U/min
- Power: ca. 65 kW
- N° of stator slots: 48
- N° of rotor slots: 36
- Maximum stator current: 450A
- Rotor winding: cage
- Rotor skewing: no
- Cooling: forced
- Coolant: oil

Nomenclature

a	Scaling factor
\vec{B}	Induction magnetic vector
B_x, B_y, B_z	Induction magnetic component in the three dimensional directions
$c1$	Constant term of differential equation solution
$c2$	Constant term of differential equation solution
c_{σ_s/σ_r}	Ratio between stray inductances of stator and rotor
\vec{H}	Magnetic field vector
H_x, H_y, H_z	Magnetic field component in the three dimensional directions
h	Rotor slot length
i_d	D current component in the synchronous reference
\vec{i}_M	Scaled magnetizing current
i_q	Q current component in the synchronous reference
\vec{i}_R^{dq}	Scaled rotor current vector in the synchronous reference
i_R	Scaled Rotor current vector
i_{Rd}	D rotor scaled current component
i_{Rq}	Q rotor scaled current component
\vec{i}_r^{xy}	Rotor current in a generic reference system
i_r	Rotor current
i_s	Stator current
\vec{i}_s^{dq}	Stator current in the synchronous reference
i_{sd}	D stator current component
i_{sq}	Q stator current component
\vec{i}_μ	Real magnetizing current
\vec{J}	Current density vector
J_x, J_y, J_z	Current density component in the three dimensional directions
K	Constant factor in the homogeneous solution of a differential equation
k	Ratio between stray inductances of stator and rotor
L_M	Scaled main inductance
L_m	Real main inductance
L_R	Real stator inductance

L_r	Real stator inductance
L_s	Real stator inductance
$L'_{\sigma r}$	Rotor leakage inductance on the stator side
$L_{\sigma r}$	Rotor leakage inductance
$L_{\sigma R}$	Scaled Rotor leakage inductance
$L_{\sigma S}$	Scaled Stator leakage inductance
$L_{\sigma s}$	Stator leakage inductance
$L_{\sigma sr}$	Stator and rotor leakage inductance
L_{σ}	Sum of the stator and rotor stray inductances
n	rotor speed in rpm
P_{Loss}^{asym}	Asymmetrical losses
P_{Loss}^{Fe}	Iron losses
P_{Loss}^{gear}	Mechanical losses due to the gears
P_m	Magnetic power
P_{me}	Converted power from electrical to mechanical
P_{mecl}	Mechanical power produced at the shaft
P_j	Power losses for joule effect
p	pole pairs
R_R	Scaled rotor resistance
R_r	Rotor resistance
R_s	Stator resistance
s	Rotor slot height
t	time
tq	torque produced from the machine
u_{DC}	Voltage at the DC source
\vec{u}_s^{dq}	Stator voltage vector in the synchronous reference
\vec{u}_s	Stator voltage vector
u_s^{max}	Maximum stator voltage
u_s	Stator voltage
u_{sd}	D component of the stator voltage
u_{sq}	Q component of the stator voltage
ω	Generic pulse
ω_s	Stator electrical pulse
ω_m	Mechanical pulse
ω_{slip}	Electrical pulse of slip
x	Generic length

$\vec{\psi}_M$	Scaled Magnetizing flux
$\vec{\psi}_m$	Magnetizing flux
$\vec{\psi}_R$	Scaled rotor flux
$\vec{\psi}_r$	Rotor flux
$\vec{\psi}_s^{max}$	Maximum stator flux
$\vec{\psi}_s$	Stator flux
θ	Stator current phase in the synchronous reference
ϵ	dielectric strength
ξ	Ratio between rotor slot length and penetration thickness
ξ_{tq}	Torque error
τ_r	Rotor time constant
μ	Magnetic permeability
σ	Electrical charge density
δ	Penetration thickness
η_{gear}	Gears efficiency

Bibliography

- [Bosa] Bosch GmbH, R. ‘Internal documentation’. GS-EH/ESS3 (cit. on p. 31).
- [Bosb] Bosch GmbH, R. ‘Internal documentation’. GS-EH/EVT (cit. on p. 52).
- [CCS96] Choi, J.-W., Chung, D.-W., and Sul, S.-K. ‘Implementation of field oriented induction machine considering iron losses’. In: 1 (Mar. 1996), 375–379 vol.1. DOI: 10.1109/APEC.1996.500469 (cit. on p. 84).
- [DDPV07] De Doncker, R., Pulle, D. W., and Veltman, A. *Fundamentals of Electrical Drives*. 1st ed. Springer Science+Business Media B.V., 2007, 356 p. (Cit. on p. 3).
- [DDPV11] De Doncker, R., Pulle, D. W., and Veltman, A. *Advanced Electrical Drives - Analysis, Modeling, Control*. 1st ed. Springer Science+Business Media B.V., 2011, 462 p. (Cit. on pp. 3, 4).
- [Kab+97] Kabbaj, H., Roboam, X., Lefevre, Y., and Faucher, J. ‘Skin effect characterization in a squirrel cage induction machine’. In: *Industrial Electronics, 1997. ISIE '97., Proceedings of the IEEE International Symposium on*. Vol. 2. July 1997, 532–536 vol.2. DOI: 10.1109/ISIE.1997.649011 (cit. on p. 22).
- [ML99] Munoz, A. and Lipo, T. ‘On-line dead-time compensation technique for open-loop PWM-VSI drives’. In: *Power Electronics, IEEE Transactions on* 14.4 (July 1999), pp. 683–689. ISSN: 0885-8993. DOI: 10.1109/63.774205 (cit. on p. 67).
- [The14] The MathWorks, I. *MATLAB®*, *Creating Graphical User Interfaces*. R2014b. 3 Apple Hill Drive Natick, MA 01760-2098, Oct. 2014 (cit. on p. 54).

